2008

AN INVESTIGATION OF SIZE EFFECTS ON THIN SHEET FORMABILITY FOR MICROFORMING APPLICATIONS

Nasr AbdelRahman Shuaib
University of Kentucky, nshuaib@uky.edu

ABSTRACT OF DISSERTATION

Nasr AbdelRahman Shuaib

The Graduate School

University of Kentucky

2008

AN INVESTIGATION OF SIZE EFFECTS ON THIN SHEET FORMABILITY FOR MICROFORMING APPLICATIONS

ABSTRACT OF DISSERTATION

A dissertation submitted in partial fulfillment of the requirements
for the degree of Doctor of Philosophy in
the College of Engineering at the
University of Kentucky

By
Nasr AbdelRahman Shuaib

Lexington, Kentucky

Director: Marwan Khraisheh, Professor of Mechanical Engineering
Co-Director: I.S. Jawahir, Professor of Mechanical Engineering

Lexington, Kentucky

2008

ABSTRACT OF DISSERTATION

AN INVESTIGATION OF SIZE EFFECTS ON THIN SHEET FORMABILITY FOR MICROFORMING APPLICATIONS

The increasing demand for powerful miniaturized products for all industrial applications has prompted the industry to develop new and innovative manufacturing processes to fabricate miniature parts. One of the major challenges facing the industry is the dynamic market which requires continuous improvements in design and fabrication techniques. This means providing products with complex features while sustaining high functionality. As a result, microfabrication has gained a wide interest as the technology of the future, where tabletop machine systems exist. Microforming processes have the capability of achieving mass production while minimizing material waste. Microforming techniques can produce net-shape products with intricacy in fewer steps than most conventional microfabrication processes. Despite the potential advantages, the industrial utilization of microforming technology is limited. The deformation and failure modes of materials during microforming is not yet well understood and varies significantly from the behavior of materials in conventional forming operations. In order to advance the microforming technology and enable the effective fabrication of microparts, more studies on the deformation and failure of materials during microforming are needed.

In this research work, an effort to advance the current status of microforming processes for technologies of modern day essentials, is presented. The main contribution from this research is the development of a novel method for characterizing thin sheet formability by introducing a micro-mechanical bulge-forming setup. Various aspects of analyzing microscale formability, in the form of limiting strains and applied forces, along with addressing the well known size effects on miniaturization, were considered through the newly developed method. A high temperature testing method of microformed thin sheets was also developed. The aim of high temperature microforming is to study the material behavior of microformed thin sheets at elevated temperatures and to explore the capability of the known enhancement in formability at the macroscale level. The focus of this work was to develop a better understanding of tool-sheet metal interactions in microforming applications. This new knowledge would provide a predictive capability that will eliminate the current time-consuming and empirical techniques that, and this in

turn would be expected to significantly lower the overall manufacturing cost and improve product quality.

KEYWORDS: Microforming, size effects, thin sheet formability, strain limits, forming limit diagram.

Nasr A. Shuaib

November 12, 2008

AN INVESTIGATION OF SIZE EFFECTS ON THIN SHEET FORMABILITY FOR MICROFORMING APPLICATIONS

By

Nasr AbdelRahman Shuaib

Dr. Marwan Khraisheh
Director of Dissertation

Dr. I.S. Jawahir
Co-Director of Dissertation

Dr. L. Scott Stephens
Director of Graduate Studies

November 12, 2008

RULES FOR THE USE OF DISSERTATIONS

Unpublished dissertations submitted for the Doctor's degree and deposited in the University of Kentucky Library are as a rule open for inspection, but are to be used only with due regard to the rights of the authors. Bibliographical references may be noted, but quotations or summaries of parts may be published only with the permission of the author, and with the usual scholarly acknowledgments.

Extensive copying or publication of the dissertation in whole or in part also requires the consent of the Dean of the Graduate School of the University of Kentucky.

A library that borrows this dissertation for use by its patrons is expected to secure the signature of each user.

Name	Date

DISSERTATION

Nasr AbdelRahman Shuaib

The Graduate School

University of Kentucky

2008

AN INVESTIGATION OF SIZE EFFECTS ON THIN SHEET FORMABILITY FOR MICROFORMING APPLICATIONS

DISSERTATION

A dissertation submitted in partial fulfillment of the requirements
for the degree of Doctor of Philosophy in
the College of Engineering at the
University of Kentucky

By
Nasr AbdelRahman Shuaib

Lexington, Kentucky

Director: Marwan Khraisheh, Professor of Mechanical Engineering
Co-Director: I.S. Jawahir, Professor of Mechanical Engineering

Lexington, Kentucky

2008

Dedicated to

My father (Professor AbdelRahman Shuaib) who paved the way for me;

My mother and siblings who provided continuous moral support; and

All of you who put a mark in my wonderful life.

ACKNOWLEDGEMENTS

I would like to acknowledge and express my thanks to all who assisted in the accomplishment of this work: Professor Marwan Khraisheh, my advisor and teacher, for his support, guidance and patience during my graduate studies. Professor Keith Rouch for his continuous support while being a GAANN Fellowship recipient. Professor I.S. Jawahir for his guidance, technically and morally, during my stay at the University of Kentucky. The U.S. Department of Education for providing me with financial assistance through the GAANN Fellowship for Areas in Assisted Needs. Dr. Liu at SECAT for his technical support and training in my research relater work. Larry Crocket and Richard Anderson for their assistance in critical machining tasks including experimental setups. Dr. Osama Rawashdeh and Phillip Profitt for assisting in control aspects of my experimental setups. Mohannad Shuaib for assisting in designing and assembling my high temperature microforming setup. The staff of the Center for Manufacturing for their assistance, support, and kindness. My research team (Fadi, Mohammed, Basil, and Firas) for helping me pull it through.

TABLE OF CONTENETS

CHAPTER SIX

CHARACTERIZATION OF THIN SHEET FORMABILITY AT THE MICROSCALE LEVEL

CHAPTER SEVEN

HIGH TEMPERATURE MICROFORMING AND ANALYSIS OF MATERIAL BEHAVIOR AT ELEVATED TEMPERATURES

CHAPTER EIGHT

SUMMARY AND FUTURE RECOMMENDATIONS

LIST OF TABLES

LIST OF FIGURES

LIST OF FILES

Nasr_Shuaib_Dissertation.pdf……4.4 MB

CHAPTER ONE

INTRODUCTION

1.1 Statement of the Problem

The increasing demand for powerful miniaturized products in almost all industrial applications has prompted the industry to develop new and innovative manufacturing processes to fabricate miniature parts and structures. One of the major challenges facing the industry is the dynamic market which requires continuous improvements and changes to the design and fabrication techniques, as can be seen in cellular phone technology. The reason for this is the ongoing demand by consumers for smaller and more efficient products. This means providing more complex features in electronic devices, for example, while sustaining the same, if not better, performance. As a result, **microfabrication**, which is the fabrication of parts with at least two dimensions in the submillimeter range, has gained a wide interest as the technology of the future, where tabletop machine systems exist and less space is utilized for production.

Micro parts are defined as parts that have at least two dimensions in the sub-millimeter range [1]. There are two major categories in the manufacturing industry that are dominating in the fabrication of micro parts: micromachining and microforming. So far, there is no standard of comparison to favor one type over the other. Most fabrication processes are conducted from previous knowledge of a certain material behavior. Until recently micromachining techniques had more share in the microfabrication industry than microforming techniques. To optimize microfabrication processes we have to consider the production rate and amount of material used for such a process. Microforming processes have the capability of achieving mass production as well as minimizing material waste. Microforming techniques can produce net shape products with intricate details in fewer steps than most conventional microfabrication processes. Despite the

potential advantages, the industrial utilization of microforming technology is limited. The deformation and failure of materials during microforming is not yet well understood and varies significantly from the behavior of materials during conventional macroscale forming operations. In order to advance the microforming technology and enable the effective fabrication of microparts, more studies on the deformation and failure of materials during microforming are needed.

Although microforming processes seem to be a promising alternative for some existing microfabrication processes from a mass production point of view, the application of these processes have been restricted by the know-how of process parameters that are usually scaled down from conventional macroscale operations. Along with the lack of standard procedures to efficiently perform existing microforming processes, previous research shows that scaling forming processes from macroscale to microscale level will yield different material deformation; contradicting with expected calculated scaling of deformation characteristics which is expected to follow the applied geometrical scaling. Therefore, research related to **size effects**, which is the phenomenon which in our current work accompanies microforming applications by causing deviation in expected material behavior as a result of geometrical scaling of the tool, workpiece, and die in the microforming process, is the main focus of research related to investigations in the field of microforming processes.

1.2 Motivations

Micro parts and products go hand in hand with future industrial applications that are being applied in the consumers markets nowadays. Small devices that contain tiny

parts such as miniature screws and springs, connector pins that can be seen in CD players, mp3 players, IC units, and microprocessors are all examples of micro-electro-mechanical systems (MEMS) parts that are applied in the electronic industry. In biomedical applications, micro parts and products are utilized by applying integrated devices in the form of human implants that can replace vital organic processes. To stay competitive, industries must utilize advanced concepts to improve their production rate of such products and minimize their dependence on costly trial and error approaches.

So far, very little is known about the formability of materials at the microscale level. Understanding the formability at such a scale is essential for successful forming operations. It is also essential to develop predictive models that can be used to optimize microforming processes and to accurately simulate the effect of various parameters on the integrity of manufactured parts.

1.3 Objective and Methodology

The long term goal for this research area is to ***advance the current status of microfabrication processes, particularly microforming, in order to advance the technologies of modern day essentials that require mass production of effective miniature parts***. The focus of this research is to develop innovative concepts for understanding the tool-sheet metal interactions in microforming applications. This will supply related industries with proper predictability tools that will eliminate the time consuming and empirical techniques that are currently employed, and this in turn would be expected to significantly lower the overall manufacturing cost and improve the product quality. To achieve this objective, the following stages were carried:

1. Investigating the characterization of sheet formability at the macroscale level: Formability testing at the macroscale level was performed on the conventional Olsen cup test machine. Formability ranking of tested material on forming limits diagrams (FLDs) were compared according to grain-structure related process parameters.
2. Due to the lack of testing equipment die microsclae testing, a testing setup for thin sheet formability testing at the microscale level was designed and developed for characterizing thin sheet formability. The microforming setup exhibits the high precision and tight tolerances required for such a significantly small scale.
3. Studying the influence of process parameters on thin sheet formability in an effort to identify size effects on thin sheet formability, and consequently, optimize thin sheet formability techniques. A new state of the art technique was introduced for providing surface strain measurement at the microscale level; which has not been accomplished in a scientific way so far. Formability limits of tested material will ultimately be used in constructing FLDs for ranking thin sheets according to its formability.
4. Expanding the capabilities of the microforming setup to accommodate high temperature testing and investigating the effect of high temperature testing on thin sheet formability at the microscale and then determining if high temperature microforming utilizes the advantage of superior forming characteristics at higher forming temperatures similar to the macroscale level.

1.4 Dissertation Layout

After identifying the long term goal behind this research work and specifying the tasks and stages that will be undertaken within the required investigation, the layout of the dissertation was constructed. In Chapter Two, a thorough literature review is presented to highlight the significance of micromanufacturing in our daily life necessities and to show what impact it produces from a technological point of view. Since this work is related to microforming, currently applied microforming techniques will be introduced and related discoveries of the well known *size effects* will be referenced. Current investigations on high temperature microforming testing will also be presented. In order to acquire a better understanding of the characterization of sheet formability, sheet formability testing at the macroscale using conventional testing apparatus was investigated and the results are presented in Chapter Three. The effect of microstructure, or average grain size in particular, on sheet formability ranking in forming limit diagrams (FLDs) was the main focus of the study, which is also generally regarded as an important part of size effects on sheet formability. In Chapter Four, a newly developed microforming setup for thin sheet testing was introduced to replace the current inaccurate and unreliable testing methods that are present when performing microscale testing on conventional macroscale setups and apparatus. The effect of varying process parameters on thin sheet formability at the microscale level was investigated in Chapter Five. This study was initiated to develop a better understanding of material behavior of thin sheets for microscale applications. Subsequently, an investigation on formability characterization at the microscale was initiated and results are presented in Chapter Six by introducing a method for calculating surface strain limits of microformed thin sheets.

The state of the art method that was developed and employed enabled the construction of strain limits for tested sheets, which ultimately allowed the investigation of size effects on formability at the microscale level. Size effect on friction form lubrication testing was also investigated. In Chapter Seven, the capabilities of the developed microforming setup were expanded to exhibit a high temperature microforming module. This module allowed for thin sheet testing at elevated temperatures, which ultimately enables the determination of whether or not high temperature forming offers an advantage at such a scale similar to the superplastic forming application at the macroscale level. Finally, a summary of conclusions and major contributions resulting from this work, as well as recommendations for future work, are presented in Chapter Eight.

CHAPTER TWO

BACKGROUND

2.1 Microscale Fabrication

Microfabrication of parts and components has been the focus of research in advanced material processes and technologies for the last twenty years. Though microfabrication processes and techniques are widely implemented in the production sectors of most modern technologies, most of these processes are based on empirical understanding of these processes. Miniaturization of existing larger scale techniques, which demonstrates a top-down method, defines the design of microfabrication processes. Micro-machining, blanking, bending, drawing, forging, extrusion, rolling, and many similar fabrication processes are currently utilized in related industries. The two major branches of microfabrication processes are micromachining and microforming. Micromachining processes are based on material removal of existing raw material, while microforming processes are material forming techniques which are divided into micro-bulk metal forming and micro-thin sheet forming. Most microfabrication processes are based on geometrical scaling of existing macroscale fabrication processes. However, it is not an easy task to perform manufacturing processes at such a small scale without taking in consideration the effect of these processes on the final product. Accurate dimensions, surface finish, mass production, and more crucial parameters have to be considered upon choosing a suitable process in order to obtain the desired characteristics and quantity of the final product.

Currently, micromachining processes are the dominant branch among utilized microfabrication techniques. In the past, micromachining processes were defined by applying photolithography and chemical etching techniques on silicon wafers for mechanical applications such as miniature sensors and actuators. Recently, a wide variety

of machining processes are performed at the microscale such as laser machining, electron-beam machining, wire electric charge machining, and micro-CNC machining, as seen in *Figure 2-1*.

Figure 2- 1 Illustration of micromachined components [2]

Since manufacturers of microparts continuously favor microfabrication processes at high production rates while maintaining reasonable manufacturing cost, the need for alternative techniques, which would save time and cost, is needed. This is where microforming processes started gaining it significance.

2.2 Microforming Processes

Microforming processes have their share in the production of microparts in the form of critically produced micro components of many existing products. *Figure 2-2* shows parts that are microformed for modern day essentials such as TVs and computers. Micromolding of microscale components and structures holds a major part in this branch; facilitating product requirements for manufacturing various micro-fluid and chemical parts and components. *Figure 2-3* shows a micro molded centrifugal pump and a micro-flow sensor.

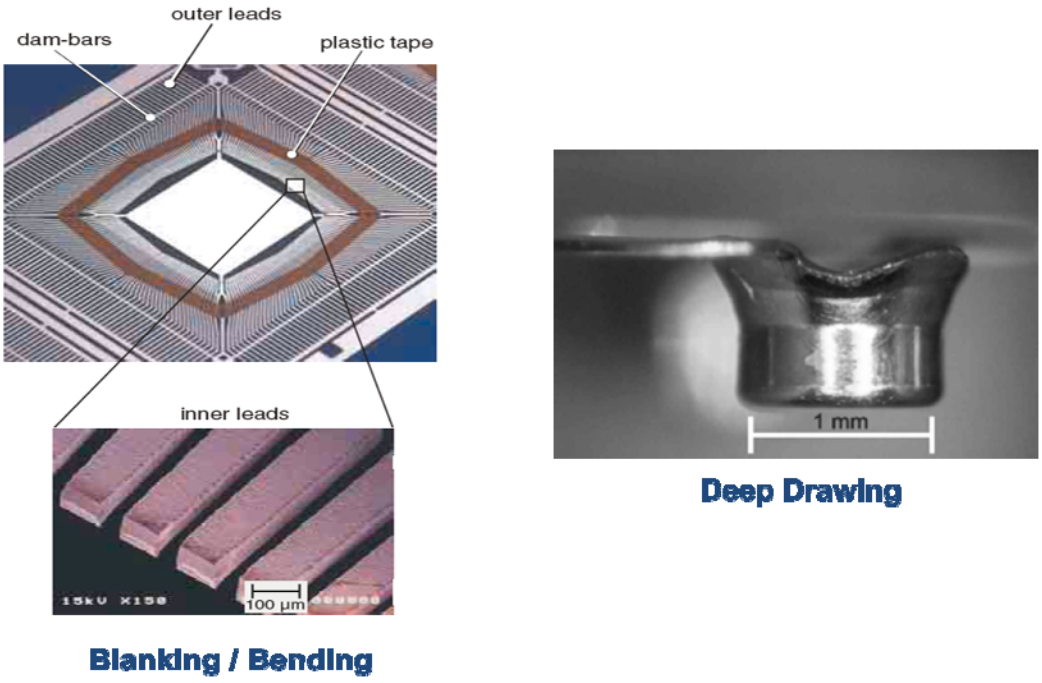

Figure 2- 2 Microformed (a) lead frame for microprocessors and (b) electron gun for TVs [1]

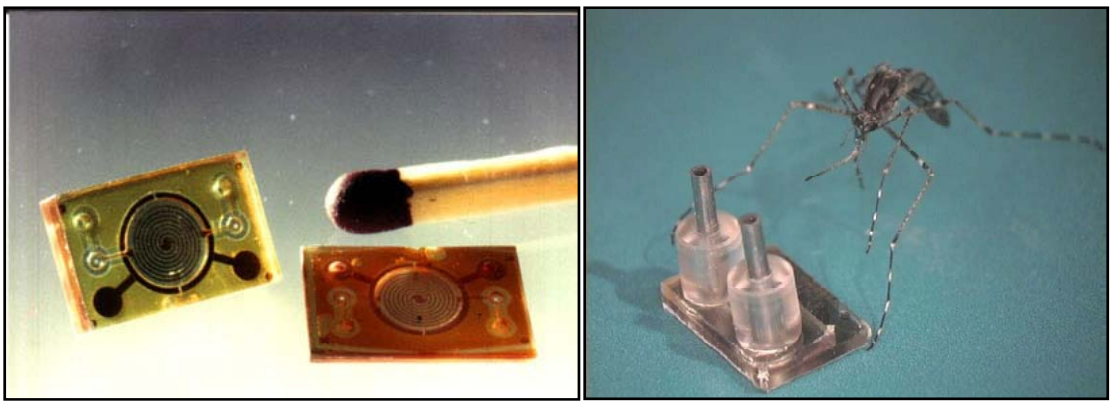

Figure 2- 3 Micro-molded (a) centrifugal pump and (b) fluid flow sensor [2]

Metal forming is known to be an efficient manufacturing technique which satisfies mass production along with enhanced product performance and minimal waste. In other words, metal forming processes display high productivity and better material utilization than many of the alternative manufacturing processes, which enables it to satisfy the continuous demand by consumers as well as industries that are relying more on smaller products with diverse applications [1, 3-4]. In the forming process, unlike machining and casting, the amount of raw material used in the process is almost fully consumed to process the final product with a very small percentage of material losses. Some machining processes, such as chemical machining and laser beam machining, can produce high grade micro components, but manufacturing cost and material losses could be of significant concern. This shows why machining cannot overcome the economical aspect of mass production. Microforming gives controlled mechanical properties of parts. This gives the ability to obtain products in near-net shape, which means less finishing operations.

Considering the aforementioned advantages, along with the fact that micro parts are usually consumed at high rates to supply the continuous demand for commercial

products, and applying them at the microscale level, microforming processes will enable the micro-components manufacturers to produce parts and components with intricate geometries and configurations in fewer steps than the currently applied multi-stage techniques. Furthermore, since high precision and tight tolerances are mandatory aspects in micromanufacturing, microforming processes can be suitable to replace many of the costly existing micromanufacturing processes. It is not an easy task to achieve the desired shape of a product using other processes. Intricate details of some products require the use of specific processes to obtain the accuracy in shape and dimensions of the final product. Microforming enables manufacturers to design die molds with a high level of detail and complexity to produce micro parts with complex shapes, as can be seen in micro deep drawing.

So far, applications of microforming have covered a wide range of industrial applications such as micro-electromechanical systems (MEMS), medical and biomedical, micro-fluidic, and chemical applications [1-4]. More emphasis is placed on electronics and biomedical applications due to their convergence with modern day essentials. The products of such applications are the core of leading technological applications. The major microforming processes currently applied are extrusion, bending, drawing, rolling, and forging processes for both bulk and sheet materials. As discussed, these processes have the capability of producing parts with intricate details; similar to what is known about them in the macro scale processes. Raw materials are in the form of billets, produced by wire drawing, or thin sheet rolls, produced by sheet rolling. The major challenge in the field of utilizing microforming processes is to be able to understand the process at the microscale level. This means that what is known about forming processes

in the macroscale, in terms of tool, die, and workpiece, will be scaled down geometrically and functionally. For this reason, a better understanding in material behavior and related parameters is needed in order to achieve the desired utilization of such valuable acquisitions.

2.3 Size Effects in Microforming Processes

In order to utilize the advantages of microforming processes, material behavior during forming must be well understood. Expected material behavior at the macroscale level cannot be simply scaled down along with geometrical scaling of the process to describe material flow during microforming. The deviations and unpredicted material behavior from these expected scaled behaviors in microforming processes are known as the "***size effects***" or "***scaling effects***" [1]. These size effects influence the process, material behavior, tools, and equipment of the microforming process. Many researchers focused on identifying size effects in commonly implemented microforming processes. Their work was divided into micro-bulk forming and micro-sheet metal forming. The experimental work conducted towards identifying size effects was carried out by scaling down the geometry of current techniques and test apparatus applied at the conventional macroscale level nowadays. The materials that were tested presented a wide range of industrial materials that are being implemented in current microfabrication practices, mainly the electronics and biomedical industries.

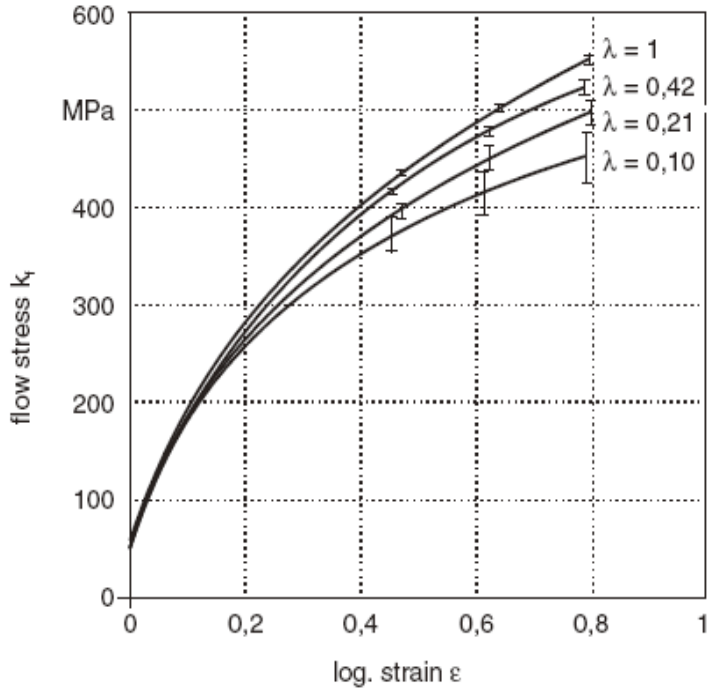

Figure 2- 4 Miniaturization effects on flow stress of compressed CuZn15 (λ: scaling factor) [1]

Geiger et al. [1, 5-8] investigated the effect of miniaturization on microforming considering various material properties. By performing compression tests on *CuZn15*, they were able to show that with increasing miniaturization, by scaling down the geometry of the tensile specimen, the flow stress of the specimen decreased while maintaining a fixed cross section for tested specimens as shown in *Figure 2-4*. This phenomenon was explained later by the so called surface layer model demonstrated in *Figure 2-5*, where the microstructure of materials consists of inner grains and surface grains. Since more miniaturization gives more share of surface grains, which are less restricted than inner grains, less force is needed in order to obtain the same amount of deformation at such a scale.

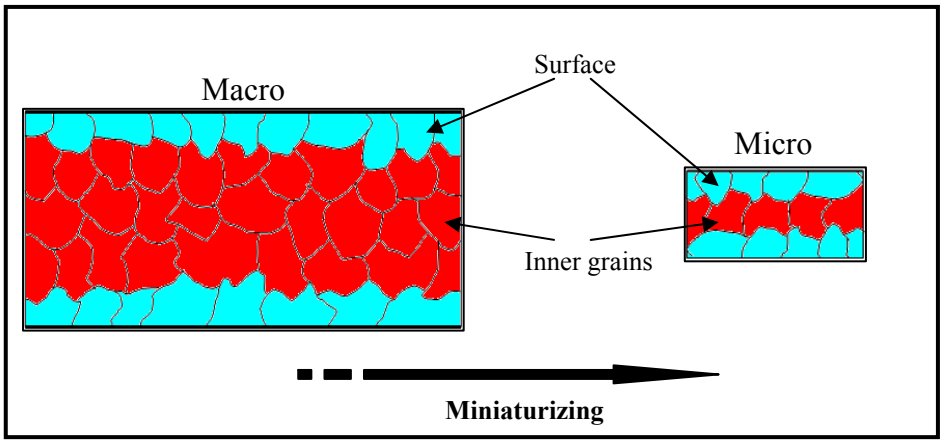

Figure 2- 5 Microstructure of a specimen in both macro and micro scale

Kals and Eckstein [1, 9] investigated size effects on material ductility. They conducted simple tension experiments on *CuNi18Zn20* and *CuZn15* brass alloys with different grain sizes and thicknesses. Scaling down the dimensions of the specimen led to an increasingly brittle-like behavior and a worsening in the ductility in air bending tests that were performed on 0.5mm thin *CuZn15* sheets, which resulted in almost zero ductility at the scale factor of 0.1; defying the well-known high ductility of such an alloy. Raulea et al. [10] discovered an interesting transition that occurred in flow stress while bending *Al 1xxx* series at the microscale level. The result of this bending process showed that although more miniaturization resulted in a decreasing yield stress, the yield stress increased as the miniaturization increased when the thickness of the specimen was less than the size of one grain of the specimen material; contradicting the famous Hall-Petch relation which regards a decreasing flow stress with increasing grain size [10]. This effect was accounted for in microforming processes that presented free deformation on the workpiece such as blanking and forging processes. Similar results were obtained by Gau et al [11]. They performed three-point bending tests on Al 1100 and brass 26000 and

concluded that the yield strength for both alloys decreases with increasing miniaturization, or thickness to grain-size ratio until this ratio equals 1, where the yield strength as well as the deviation start to increase and reverse the previous trend.

Since friction has a major influence on most forming processes, many researchers addressed the effect of friction on microforming processes using different techniques. The first technique was proposed by Messner [12] by implementing the conventional ring compression test at the microscale level for micro forging applications. The results showed an increasing friction with increasing miniaturization. To accommodate for extrusion processes, which have more related applications than forging processes at the microscale level, the double cup extrusion test was conducted by Tiesler and Engel [13, 14]. In this test, a cylindrical billet was deformed by penetrating a punch from one side while another stationary punch would penetrate from the other side. The higher the friction gets, the more the flow is prevented at the lower punch. By testing *CuZn15* with different diameters and grain sizes, they concluded that friction increased with decreasing specimen size. The frictional behavior was explained by the "open and closed lubricant pockets" model. Closed lubricant pockets tend to distribute pressure evenly across the surface, contrary to the high pressure needed for open pockets that tend to concentrate loading on hill tips. Since miniaturization comes along with more share of open pockets, the friction effect was ascertained to be more dominant at such a scale. Krishnan et al. [15, 16] and Cao [17] et al. investigated the friction effects in microextrusion. They conducted extrusion tests of *CuZn30* pins having various grain sizes and dimensions. They also used different dies with different surface roughness in order to vary the frictional effect. They showed out the variation of flow stress of specimens that had the

same size with different grain structure. They indicated that the size, orientation, and distribution of grains play an important part in the extrusion process, and that the use of coatings will reduce extrusion forces and frictional effects, and therefore will increase the length of extruded pins.

Research on the size effects on micro-sheet metal forming has not emerged until the last few years. Most of it covered bulging and drawing tests for investigating size effects on flow stress. Vollertsen et al. [18, 19] performed drawing tests in thin sheets of Al 99.5 using a 1mm diameter punch as well as thick sheets of the same material using a 50mm diameter punch for comparison, with scaled process parameters and conditions. Due to the limited surface area of the small punch, blank holder forces could not be applied perfectly onto the blank. The result was a high amount of wrinkling at the microscale when compared to the ones obtains at the macroscale level. They also observed high frictional forces that resulted in failure at the bottom part while deep drawing at the microscale, which were significantly higher than the frictional forces that resulted in the macro-deep drawn sheets. By applying lubrication to the process, the coefficient of friction had a larger decrease at the microscale than that at the macroscale level, which meant that lubrication had a different effect between both scales. Their conclusion was that friction increases in deep drawn cups as miniaturization increases. Michel and Picart [20] introduced technique by which the size effects on flow stress can be verified through two parallel approaches. The first approach was simple tensile testing of thin sheets of *CuZn36*. The second approach was conducting hydraulic-bulge testing of thin sheets of the same material, since biaxial stress was proven to be more accurate than the uniaxial stress obtained through simple tension tests. Effective diameters of the

bulged sheets were 20mm and 50 mm. Hydraulic pressure was supplied by using water as the required fluid. Various sheet thicknesses and widths were tested in order to verify size effects for a range of material characteristics. They ascertained the decreasing flow stress with increasing miniaturization through hydraulic bulging experiments and developed a constitutive model for flow stress. Hoffman and Hong [21] presented similar results by testing pure copper (99.9% Cu) in simple tensile testing and air-bulge testing. Both approached relied on an optical measurement system (ARAMIS) for calculating the flow stress using CCD cameras. Flow stress was calculated at the pole of the bulged thin sheets as it deformed and more accurate results of decreasing flow stress along with increasing miniaturization were presented. The trend of decreasing flow stress with decreasing thickness was verified in both approaches. Mahabunphachai and Koç [22] were able to construct a hydroforming (fluid pressure based) microforming setup for fabricating micro channels on thin sheets of SS304 stainless steel with 51μm thickness. By testing SS304 with varying grain size on dies with varying width and depth grooves, they were not able to correlate between these parameters and size effects. Nevertheless, the impact of changing the parameters on the form and geometry of the formed micro channels was detected.

A different set of investigations on micro-sheet metal forming were initiated by Saotome et al. [23]. They developed an experimental apparatus to conduct microdeep drawing with a 1 mm diameter punch and thin sheets as low as 0.1 mm in thickness. Process scaling was regarded by the relative punch diameter, which is the ratio of the punch diameter to the sheet thickness. Their study showed that the limiting drawing ratio (LDR) decreased with increasing relative punch diameter. Saotome and Okamoto [24]

also performed incremental sheet metal forming of thin sheets using a hammering mechanism. A 10 μm diameter punch directed by a piezoelectric actuator provided incremental deformation of 10 μm thickness sheets. The accuracy of displacement of the hammer was assured by an eddy current displacement sensor. Justinger and Hirt [25] recorded size effects in deep drawing by measuring the peak drawing forces for different blanks of CuZn37 with different annealing conditions. The comparisons of the resulting drawn thin sheets were based on their grain-size-to-thickness ratio. Punch diameters were in the range of 1 mm to 8 mm. The trend of peak forces of the drawn sheets with respect to miniaturization was similar to the one obtained by tensile testing by previous researchers [1, 5]. Their results showed a decreasing peak force which did not depend on the geometrical factor, or scaling factor. It rather depended on the grain size to thickness ratio in a proportional manner.

Since the springback behavior in macroscale sheet bending is a significant issue, this was also investigated at the microscale level. Gau et al. [26] tested brass sheets of thicknesses between 300 μm and 3000 μm and discovered that the trend of increasing springback for thinner sheets at the macroscale is not true for sheets with thicknesses less than 500 μm, and that thickness-to-grain-size ratio does not influence the amount of spring back.

2.4 Microforming at Elevated Temperatures

All the aforementioned investigations were conducted at room temperature. New studies aiming at applying high temperature forming or superplastic forming, at the microscale level have been initiated. The advantage of forming at high temperatures lies

in the fact that at higher temperatures, usually around 0.5 to 0.7 of the melting temperature, all materials demonstrate superior ductility while being formed, regardless of its mechanical characteristics at room temperature. Applying this technique at the microscale level has prompted for studies on applying superplastic microforming processes. By implementing superplastic materials into microforming processes, various testing apparatus and industrial application have been recognized. The following investigations cover the majority of the ongoing effort to supply related industries with net-shape microformed parts. Saotome et al. [27, 28] characterized amorphous alloys as potential candidates for the fabrication of microparts in MEMS applications and even nano-devices. They conducted forging experiments on $Pd_{40}Cu_{30}Ni_{10}P_{20}$ and $La_{60}Al_{20}Ni_{10}Co_5Cu_5$ amorphous alloys. They were able to utilize the viscous flow that these alloys exhibit in the supercooled liquid state, and consequently fabricate fine 2D and 3D structures in the with widths as low as 1μm. Saotome et al. also introduced a technique for fabricating micro-gear shafts by forward extrusion [29] and backward microextrusion [30] of Al-78Zn superplastic alloy. The gear shaft had a module of 10μm for the forward extruded shaft and 20μm for the backward extruded one. They discovered the significant effect of surface roughness and lubrication between the billet and the inner wall of the die, where surface roughness had to be reduced and reasonable lubrication had to be applied in order to obtain a well formed shaft with intricate details at such a scale. Son et al. [31] performed microforging of Al5083 foils in a punch-die configuration at elevated temperatures to employ the well known superplastic behavior of the aluminum alloy. *Al5083* foils of 2.5x2.5x1 mm size were forged into a 100 μm sized v-grooved die. They ascertained the increasing formability of the foils with increasing forming load and

time. However, they pointed to the dependability of the process on the grain size of the tested sheets. Fine grained foils tend to deform in a more accurate manner than coarse grained foils, which need more force and time to deform grains at its preferred orientation. Yeh et al. [32] utilized the conventional hot embossing process to be applied to microforming applications. The material they used was a fine-grained *Zn-22Al* eutectoid alloy which exhibits superplastic behavior at elevated temperatures. They conducted compression tests on the superplastic alloy under different temperatures (150, 175, 200°C) and strain rates (0.0006-0.6s^{-1}) and obtained flow curves based on force vs. distance recordings. They concluded that the flow stress decreases with increasing forming temperature, while the strain sensitivity index increased with increasing forming temperature. Based on comparison, they were able to identify the required parameters for optimum forming conditions. While optimal parameters were held, a micro-hot embossing process for fabricating micro-sized gears was successfully achieved. All fabricated gears did not show any type of internal failures, and a reduction gear train was assembled and operated properly. Furushima and Manabe [33, 34] succeeded in fabricating microtubes by conducting a dieless drawing process on *Zn-22Al* and *AZ31* superplastic materials. Microtubes with outer and inner diameters of 190 μm and 91μm, respectively, were fabricated successfully by a four-pass drawing process. The deformation temperature was 250°C for *Zn-22Al* and 400°C for *AZ31*. The major achievement of this work was presenting the ability to hold the same inner-to-outer-diameter ratio and a homogeneous microstructure, which would hold the superior mechanical properties that these alloys bear. Laser forming has also been introduced as a forming technique for microforming thin metal sheets. Ocaña et al. [35] applied laser-

shock microforming, which is a non-thermal distortion technique, on AISI 304 stainless steel. The obtained results of deformed beam-specimens were suitable for validating a numerical approach for characterizing beam bending of the same alloy with varying pulse energy. Thermal based laser forming was utilized by Cheng et al. [36] by combining the advantages of laser shock peening, laser forming, and metal forming along with an ultra high strain forming rate. They performed thin sheet bulging on thin copper sheets (with thickness of 15 μm) by shock wave propagation of induced laser beams which makes the specimen take the 3D shape of the mold in the bottom. They were able to prove that materials with fine grains demonstrate a significantly higher formability than coarse ones. Eichenhueller et al. [37] investigated size effects on microforming at elevated temperatures, and below recrystallization temperature. They constructed flow curves of *CuZ15* and stainless steel *X4CrNi-18-10* by upsetting, lateral extrusion, and backward extrusion of billets with varying average grain size while maintaining the same specimen size (0.5 mm in diameter) at varying temperatures up to 400˚C. They verified the decrease in flow stress and increase in scatter which accompanies an increasing miniaturization for both alloys. They also found that a moderate increase in the forming temperature for microforming will result in a significant reduction in scatter, which will ultimately lead to more stability and reliability in testing at such a scale.

As noted in the literature above, miniaturization through microforming has its advantages in supplying alternative techniques and methods to the dynamic demand of the market nowadays. However, disadvantages and limitations come along with this emerging technology. Further investigations should be performed in order to develop more understanding of the material behavior during microforming. Although a good

amount of knowledge is deduced in bulk metal forming at the microscale level, very little is known about the formability issue of thin sheets at such a scale. In general, investigations of size effects on ductility and formability of thin sheets in microforming applications are limited to tensile tests of thin sheets and few micro deep drawing and micro bulge forming studies. Formability during tensile tests was simply characterized by elongation to failure [1, 5-9, 20, 21]. For the biaxial experiments, limiting drawing ratio and maximum bulge height were used to characterize the formability during micro deep drawing [18, 19, 22, 24] and micro bulge forming [20, 21] respectively. These limited formability analyses are not sufficient to understand the size effects on deformation and formability at the micro scale. More detailed analysis of strain distributions and limiting strains during microforming of thin sheets is needed to be able to predict the formability limits for thin sheets and minimize trial and errors runs that are conventionally performed to master the know-how of a micro-metal forming process. Thin sheet metals are of extensive use in the field of electronics and MEMS applications and understanding the different aspects of formability at the microscale level is essential in order to advance the use of microforming processes in these fields and many more that can benefit from its advantages. The consequences of such investigations are better optimization of process parameters and reduced overall manufacturing cost in microforming processes.

CHAPTER THREE

CHARACTERIZATION OF SHEET FORMABILITY AT THE MACROSCALE LEVEL WITH VARYING GRAIN SIZE

3.1 Introduction

Since most fabrication processes are initially scaled down from existing macroscale geometries and parameters, as mentioned in the previous literature review, it is essential to initiate research on thin sheet formability by investigating the effect of varying parameters, which influence microscale formability, at the macroscale level. Along this path, the characterization of sheet-metal formability was represented by constructing forming limit diagrams (FLDs). FLDs are valuable diagnostic tools that rank the effectiveness of sheet metal alloys in various industrial applications with respect to their formability. Since formability is influenced by various process parameters, such as tool geometry and material properties, extensive research has been conducted in an effort to identify the parameters that influence the form and position of forming limits curves (FLCs), such as strain hardening exponent n and plastic anisotropy factor r, in formability charts. Nevertheless, few studies concentrated on correlating FLDs of different sheet thicknesses with the microstructure of these formed sheets. In this chapter, formability tests were conducted on a Tinius Olsen cup test machine. The tested batches, which were of a *CuZn30* alloy, were distinguished according to their thickness as well as their average grain size which was varied according to different annealing schemes. The aim of this study is to identify any effects of grain size on formability limits of sheet metal.

3.2 Previous Work

The automotive industry, especially in the U.S., has benefited from the concept of forming limit diagrams since the 1960's, when Keeler [38] emphasized the significance

of applying FLDs as a predictive tool for stamping applications in the automotive industry. Since then, extensive research has been conducted on factors that influence sheet formability in order to achieve better utilization of FLDs for sheet metal forming in general. Since FLDs rank the effectiveness and likeliness of using certain alloys over others according to its ease of formability, mechanical properties were the focus of process factors that affect the formability of sheet metal. Early investigations reported the effect of strain hardening exponent *n*, anisotropy factor *r*, and inhomogeneity on the magnitude of strain limits [38]. Those parameters influenced the ability of deformed sheets to distribute strain more, or less, uniformly which may increase, or decrease strain limits at a certain strain path. Keeler and Backofen [39] stated that strain limits are proportional to the hardening exponent *n*. Marciniak and Kuczynski [40] described the effect of each of the previous properties on sheet formability. They concluded that limiting strains increased rapidly as the inhomogeneity of the material deceased. They also presented theoretical analysis supporting the fact that limiting stains increased as the *n* exponent increased and as the anisotropy factor *r* decreased. Similar results were presented in [41].

Further studies were carried out for optimizing the use of FLDs in the sheet metal forming industry. These studies identified sheet thickness and microstructure as parameters that affect the form and position of FLCs. Yamaguchi and Mellor [42] studied the effect of thickness and microstructure of sheets under biaxial tension and were able to predict the limiting strains of sheets by relating grain size to surface roughness and sheet thickness. This was achieved by modifying the theoretical models that Marciniak and Kuczynski [40, 41] developed for predicting limiting strains of sheet metal. Recent

studies showed the dependability of limiting strains to new parameters such as the amount of heat treatment [43, 44] and thickness to grain size ratio [45]. Although the aforementioned parameters were proven to have a significant influence on the formability of sheets in general, more depth into the characterization of formability based on microstructural features of sheets is needed to utilize the advantage of performing minor modifications in sheets, such as annealing, and consequently obtain different formability limits depending on the desired application for the formed sheets. This way, better material utilization will be achieved and less alteration between different materials will be necessary. This investigation emphasizes on critical properties in sheet forming processes that related industries can benefit from applications where the microstructure of formed sheets has low significance in their post-forming applications.

3.3 Experimental Procedure

In this study, conventional limiting dome height tests were performed on *CuZn30* alloy, in as-received state, with thicknesses of 2mm, 1mm and 200μm. Consequently, FLDs were constructed and the effect of sheet thickness and thickness-to-grain-size ratio on sheet formability was validated based on previous literature. Furthermore, annealing was performed on the same material samples of similar thickness values in order to obtain a reasonable variation in the grain size of same-thickness sheets. Limiting strains and forming limit curves were compared for each case of thickness and annealed state with respect to their thickness-to-grain-size ratio λ as well as their volume-to-grain-size ratio π. In an effort to append more significance to the influence of grain size and position on the formability of sheets, the grains of deformed volumes in the formability tests were

classified into surface grains and inner grains depending on their relative position within the sheet. The ratio of surface-to-inner-grains N_s/N_i was introduced as an additional factor to study the influence of the ratio of surface grains to inner grains on sheet formability. The specific steps taken to initiate the investigation are described as follows:

3.3.1 Grid marking and sheet-formability testing:

Before sheet formability testing, grid marking on sheet surfaces was made by an electro-chemical etching process for facilitating the surface strain measurement of deformed sheets. Circles of 2.54 mm in diameter were printed on all sheet specimens. An illustration of the grid marking process is shown in *Figure 3-1*. The procedure for electro-chemical marking is listed in Appendix I. A Tinius Olsen cup test machine (*Figure 3-2*) was used for applying sheet bulging. *CuZn30* sheets of 2mm, 1mm and 200μm thicknesses were stretched over a hemispherical punch-tip with 60 mm in diameter at a speed of 4 mm/min. To ensure proper clamping and restriction from sheet drawing, a clamping bead mechanism provided sufficient pressure for clamping the tested sheets according to their thickness (*Figure 3-2*). Sheets were provided for testing at various widths to demonstrate a range of strain paths between the balanced biaxial and plane-strain state (*Figure 3-3*). For each test, the punch was stopped at the onset of necking which was detected automatically at a certain level of force drop determined by the machine's force sensor; which is adjusted according to sheet thickness. Tensile specimens with a 50.8 mm gauge length and 12.7 mm width were tested for a negative strain path which represents a uniaxial strain path on the FLD. Circle-grids were printed on the tensile specimens following the same electro-chemical etching procedure. Tensile

samples were upset on an Instron universal testing machine at a speed of 4 mm/min until the onset of necking was detected at a recorded force drop (around 10%).

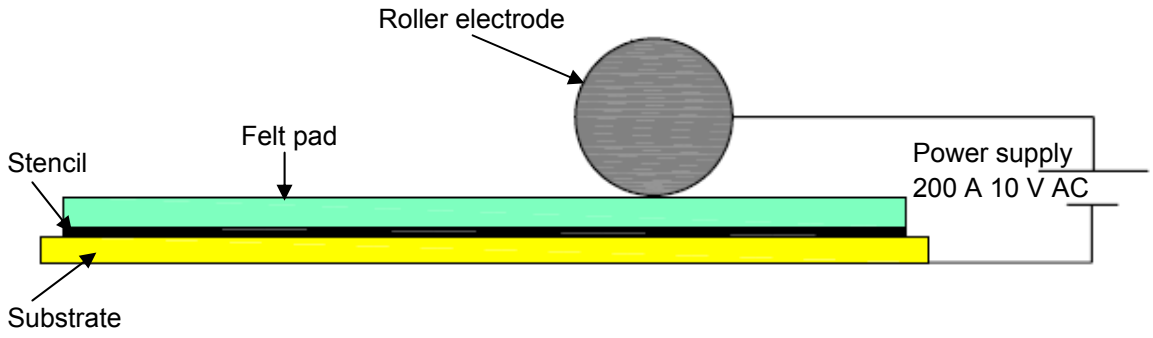

Figure 3- 1 Grid marking process

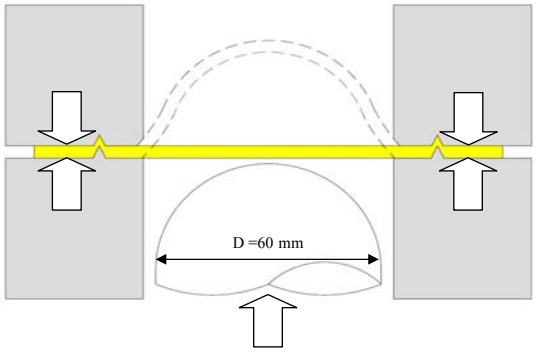

Figure 3- 2 Tinius-Olsen BUP 200 Ductomatic sheet metal testing machine

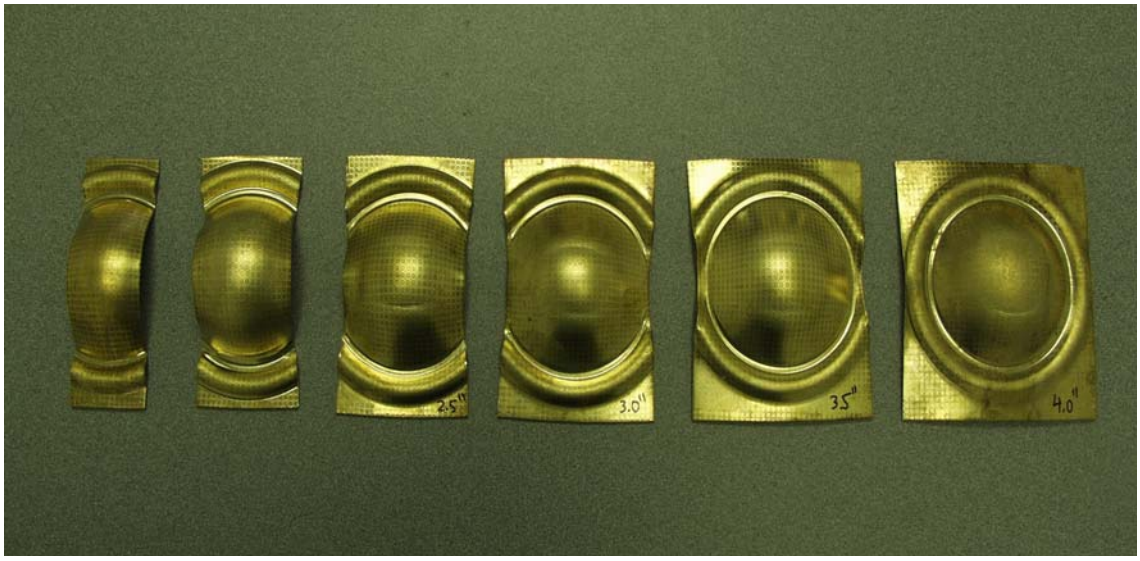

Figure 3- 3 Set of deformed sheet with various strain paths

3.3.2 Strain measurement

Surface strain limits for every strain path were calculated using the ASAME strain measurement software. ASAME (Automatic Strain Analysis and Measurement Environment) is a software package by which surface strains can be calculated automatically from actual photo images of sheets around the vicinity of the crack. In order for the software to measure strain along curved surfaces, a cubic-target element, which enables the software to account for curvature and three-dimensional coordinates, is used. *Figure 3-4* shows a bulged sheet along with the cubic target. Strain limits of failed and safe regions were clearly distinguished in color representation to ensure proper selection of limits on the FLD and plotting FLCs (*Figure 3-5*).

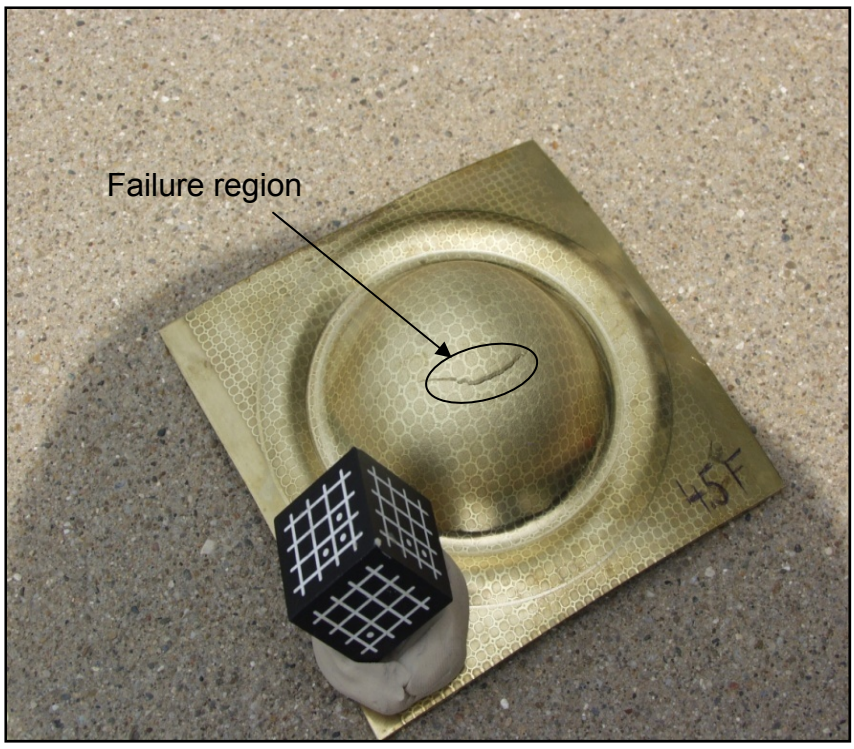

Figure 3- 4 A deformed sheet in biaxial strain path

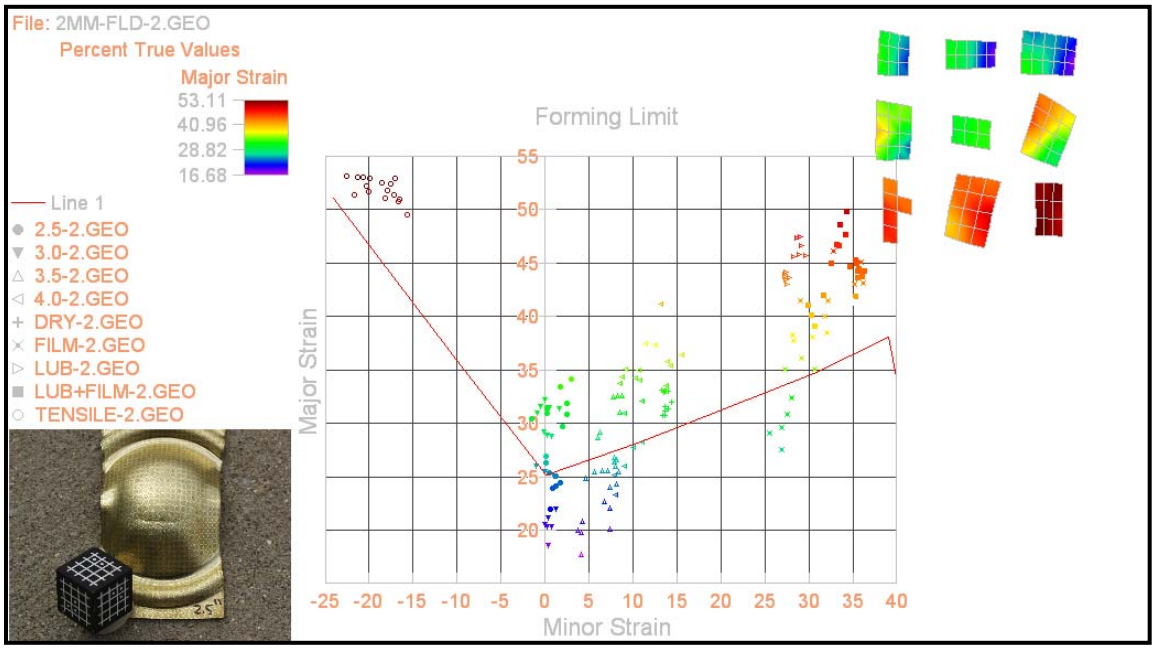

Figure 3- 5 ASAME representation of a FLD

3.3.3 Selective-grain size control

The formed sheets were classified into two batches. The first batch presented all sheet thicknesses in the as-received state. The second batch presented the same sheet thicknesses annealed at different temperatures and durations to demonstrate a reasonable variation in grain size between all tested samples. Microstructural analysis was done on all sheet batches to determine the average grain size d for each sheet thickness. For every sheet thickness and annealing state, samples were polished and then etched to reveal the microstructure for each specimen. Appendix II lists the procedure for sample mounting, polishing, and etching. Optical microscopy was used for determining the average grain size for each sample by applying the conventional linear intercept method; accordingly with ASTM standard E112-96 for determining the average grain size [46]. The calculated grain size for all samples represented the average grain size between surface grains and through-thickness-grains. In order to have a means by which the tested sheet can be compared, ratios between thickness and grain size λ and between deformed volume and grain size π were calculated. Furthermore, after determining the average grain size for each batch, the total number of deformed grains N_t was calculated assuming spherical shaped grains. The volume for each deformed grain was calculated from the determined average grain size which represents the average diameter of the specified grains. From N_t, The total number of surface grains for each case was determined, assuming a total of half a layer on the top surface and another half on the bottom surface of the sheets, as well as half a layer on the sides in the case of plane-strain and tensile samples, assuming unrestricted surfaces on the sides of the samples. The total number of deformed inner grains N_i was then determined. The symbols used in this study are listed in *Table 3-1*.

Table 3-1 Symbols used

Symbol	*Description*
d	Average grain size
λ	Thickness-to-grain-size ratio
π	Deformed volume-to-grain size ratio
N_i	Number of inner grains in deformed volume
N_s	Number of surface grains in deformed volume
N_t	Number of total grains in deformed volume

3.4 Results

The microstructural analysis conducted on *CuZn30* sheets for determining the average grain size d, the thickness-to-grain-size ratio λ, and the volume-to-grain-size-ratio π for the as-received sheets is shown in *Table 3-2*.The same variables were calculated for the annealed sheets and are presented in *Table 3-3*. The required statistical analysis in this investigation is demonstrated in Appendix III. The volume-to-grain-size-ratio π was calculated for samples that represented a strain path for the balanced biaxial, plane-strain, and uniaxial deformation states. The plane-strain path refers to samples that reflect stain limits in the plane-strain region in the FLD. *Figure 3-6* shows microscopic images of surface microstructure for sheets in both as-received as well as annealed sheets for each thickness, which clearly illustrates grain variation between them. For the tested batches, *Figure 3-7* shows the FLDs obtained for the as-received state *AR*, while *Figure 3-8* shows FLDs obtained for the annealed state *AN*.

Table 3-2 Microstructural analysis for as-received state

Thickness (μm)	*d* (μm)	*SD*	*λ*	*π* (μm^2)		
				Biaxial	Plane-strain	Uniaxial
2000	55.5	2.24	36.1	150,824.9	141,691.2	27,027.0
1000	29.9	1.07	33.5	139,979.6	131,502.7	35,535.1
200	16.0	1.03	12.5	52,317.4	49,149.1	13,281.25

Table 3-3 Microstructural analysis for annealed state

Thickness (μm)	Temp. (°C)	Time (Hr)	*d* (μm)	*SD*	*λ*	*π* (μm^2)		
						Biaxial	Plane-strain	Uniaxial
2000	700	7	476.2	0.21	4.2	17,578.3	16,513.8	4,462.4
1000	700	1	238.1	0.26	4.2	17,578.3	16,513.8	4,462.4
200	600	3	48.8	0.06	4.1	17,153.2	16,114.5	4,354.5

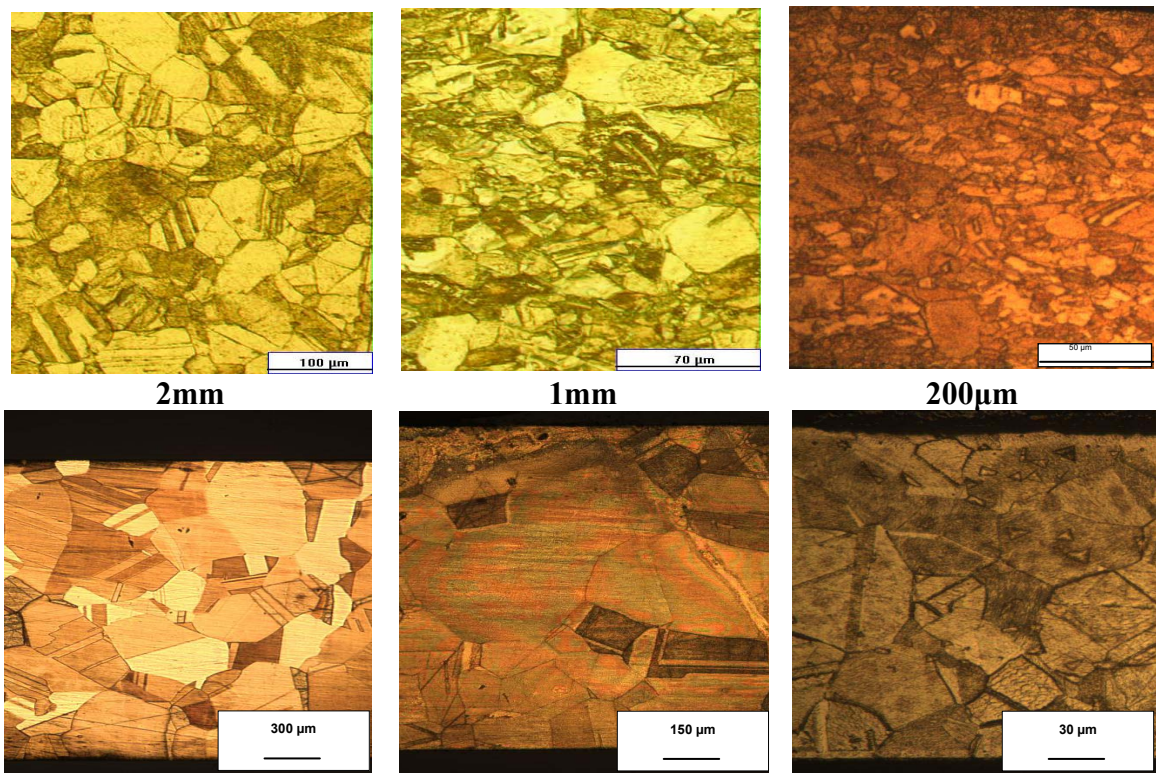

Figure 3- 6 Microstructural images of as-received (top) and annealed (bottom) CuZn30 sheets

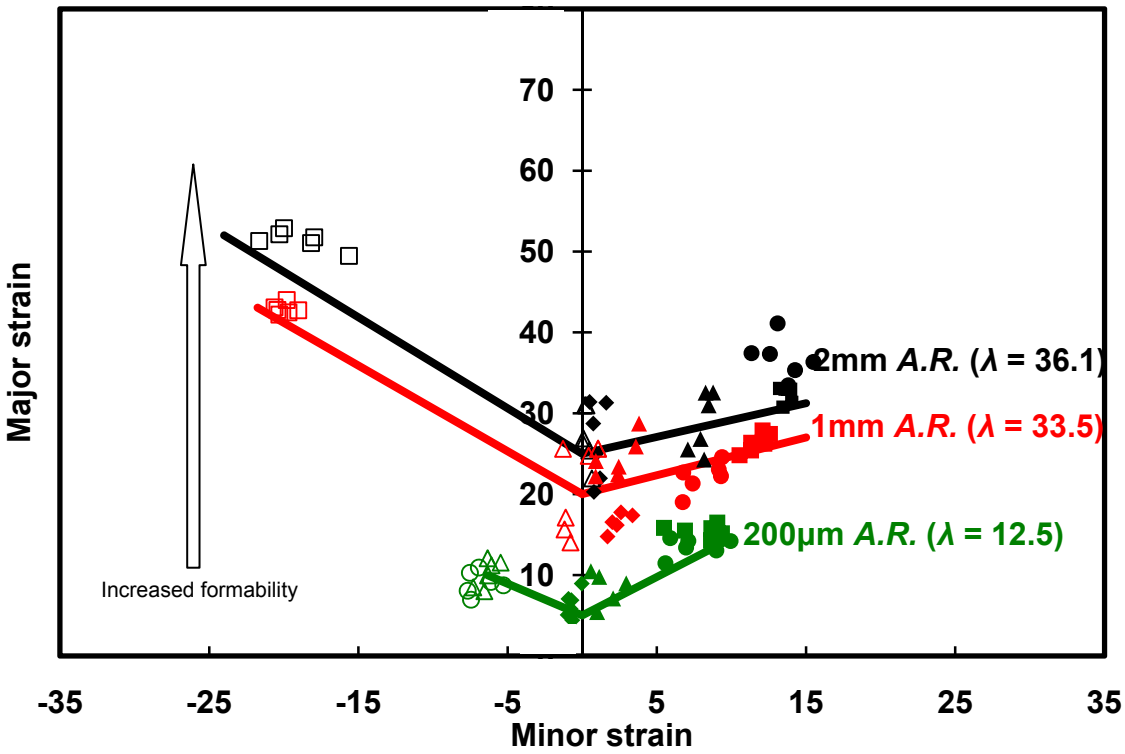

Figure 3- 7 FLDs for as-received state

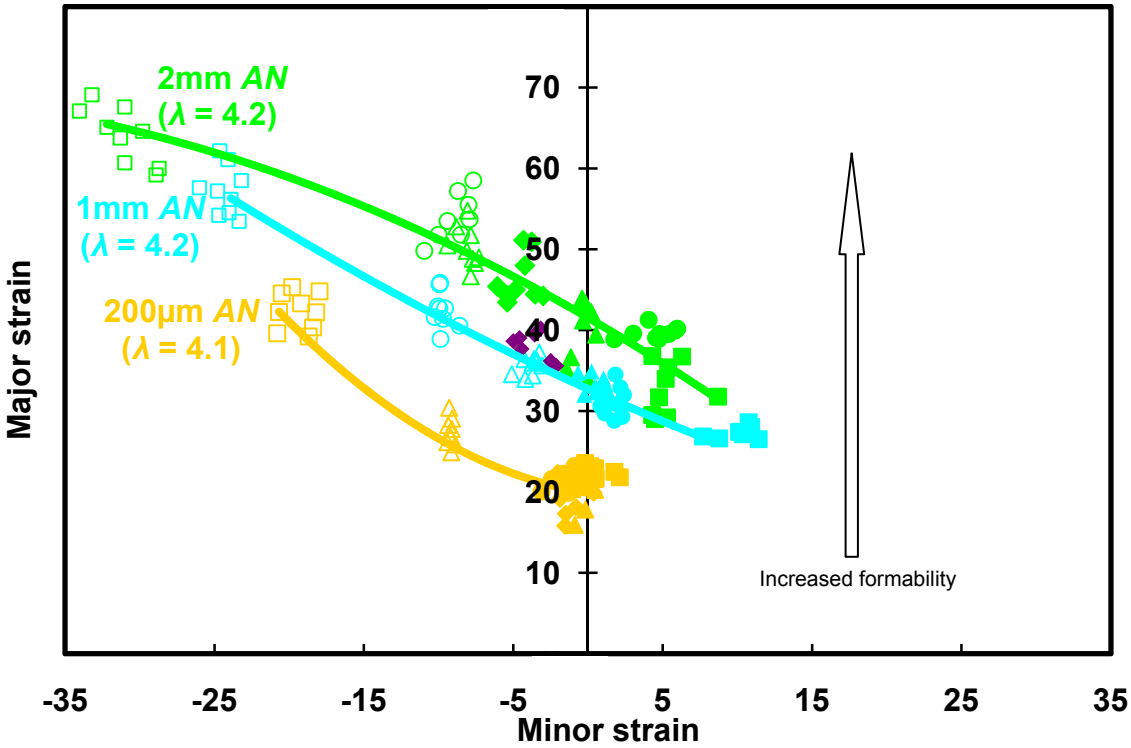

Figure 3- 8 FLDs for annealed state

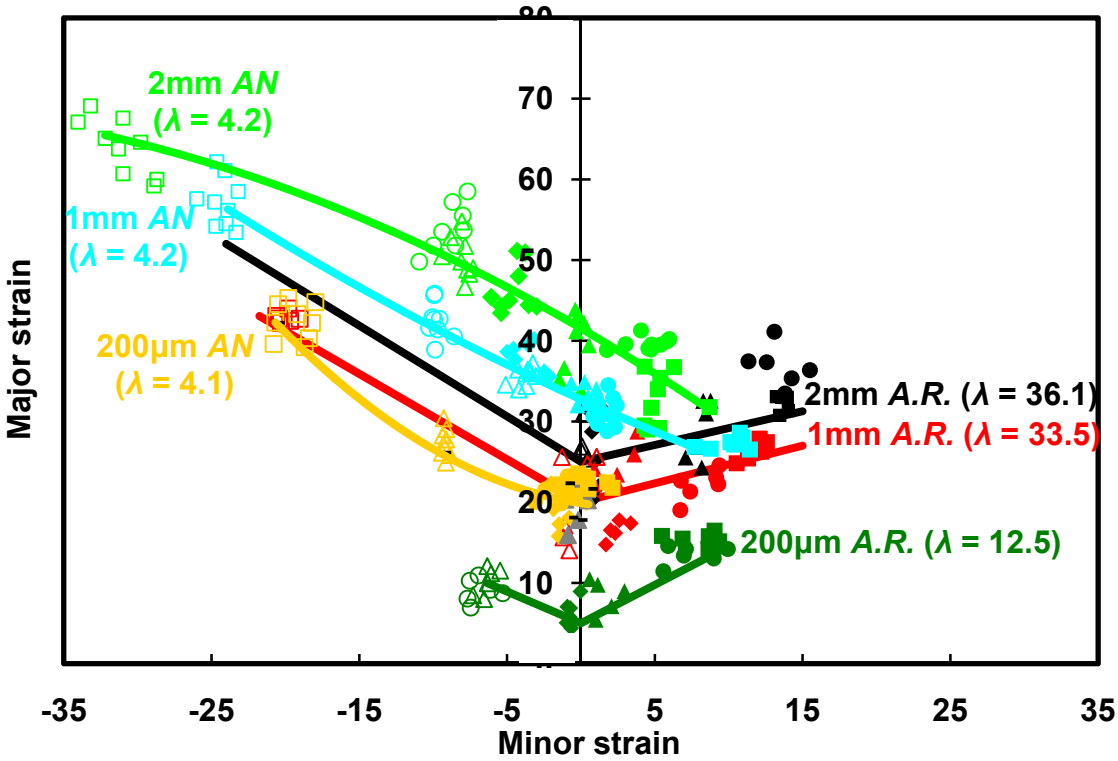

Figure 3- 9 FLDs for as-received as well as annealed states

The total number of surface, inner, and total deformed grains were calculated for the deformed volume of the biaxial, plane-strain, and uniaxial strain samples. *Figure 3-10* shows an illustration of how surface and inner grains were selected. *Table 3-4 and 3-5* show the values of deformed grains for both cases.

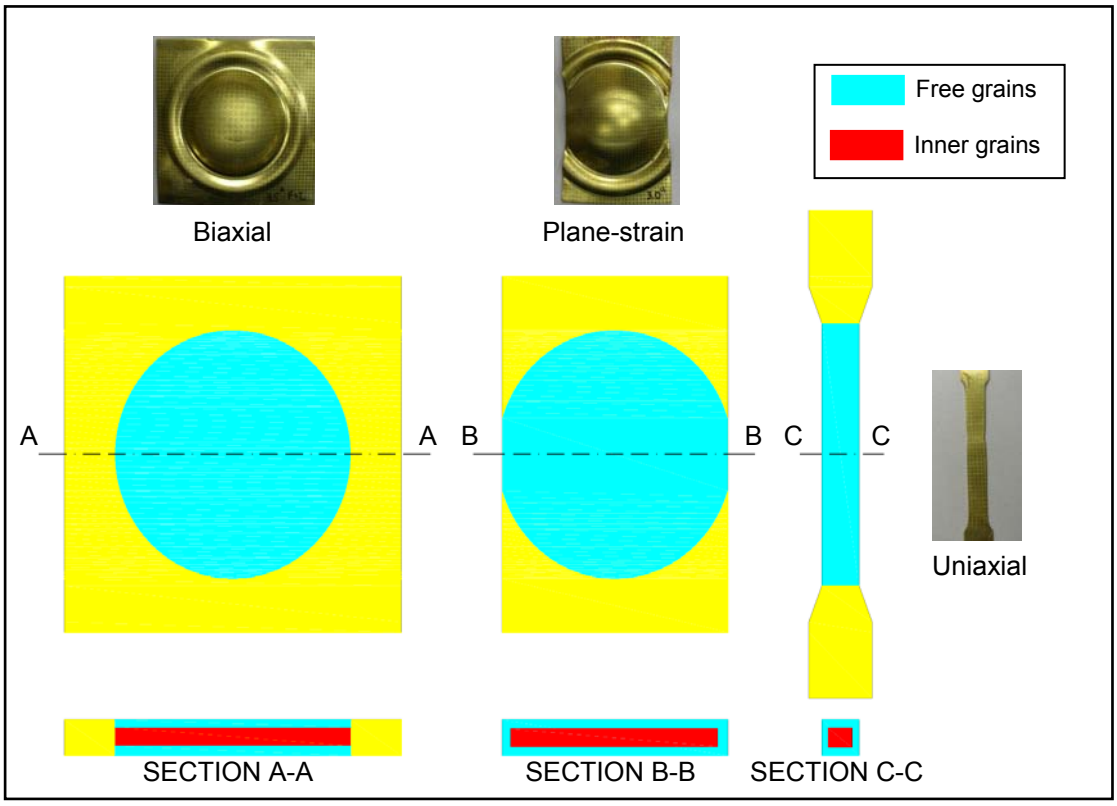

Figure 3- 10 Surface and inner grains in deformed volumes

Table 3-4 Calculated numbers of both surface and inner grains for as-received (AR) and annealed (AN) sheets

Thickness	N_s (x10^6)			N_i (x10^6)		
	Biaxial	**Plane-strain**	**Uniaxial**	**Biaxial**	**Plane-strain**	**Uniaxial**
2mm *AR*	1.730	1.647	0.047	91.786	86.206	23.271
1mm *AR*	5.961	5.637	1.516	293.075	275.290	74.397
200µm *AR*	20.816	19.581	5.286	369.491	347.091	93.798
2mm *AN*	0.023	0.022	0.006	0.125	0.117	0.031
1mm *AN*	0.094	0.089	0.024	0.498	0.468	0.126
200µm *AN*	2.238	2.104	0.568	11.519	10.819	2.924

Table 3-5 Total number of grains in deformed sheets

Thickness	N_t (x10^6)		
	Biaxial	Plane-strain	Uniaxial
2mm *AR*	93.517	87.853	23.740
1mm *AR*	299.036	280.927	75.913
200μm *AR*	390.308	366.672	99.083
2mm *AN*	0.148	0.139	0.038
1mm *AN*	0.592	0.556	0.150
200μm *AN*	13.756	12.923	3.492

Table 3-6 Ratios of surface grains to inner grains

Thickness	N_s/N_i (%)		
	Biaxial	Plane-strain	Uniaxial
2mm *AR*	1.88	1.91	2.02
1mm *AR*	2.03	2.05	2.04
200μm *AR*	5.63	5.64	5.63
2mm *AN*	18.87	19.10	20.23
1mm *AN*	18.87	18.99	19.20
200μm *AN*	19.43	19.45	19.44

3.5 Discussion and Data analysis

Formability analysis of the tested sheets was categorized into four cases of comparison depending on the sheet thickness, annealing condition, and average grain size. The first comparison was between as-received sheets, the second was between annealed sheets, the third was between as-received and annealed sheets of the same thickness, while the fourth comparison was between an extreme case of as-received and annealed sheets having different thicknesses. For each comparison, the analysis of sheet formability was regarded with respect to the thickness t, thickness to grain size ratio λ, grain size d, surface-to-inner grains ratio N_s/N_i, and the total number of deformed grains N_t.

3.5.1 As-Received Sheets with Varying Thickness

For the batch of as-received sheets (*Figure 3-7*), formability increased with increasing thickness, λ ratio, and grain size. Although the N_s/N_i ratio was higher in thinner sheets, which should result in a higher share of free grains, and therefore less restriction to deformation, formability decreased along with thickness. This decrease in formability can be regarded by the overall number of deformed grains N_t, which increased with decreasing thickness. According to dislocation theory, dislocations tend to pile up behind grain boundaries; which means that a higher grain boundary density will occupy a higher dislocation density. As a result, the fewer overall deformed grains for thicker sheets were less restricted to the deformation of the whole sheet and showed higher formability limits. Thus, the total number of deformed grains showed more influence on ranking formability than the share of surface grains. This observation validated what is known about the decreasing formability with decreasing thickness and thickness-to-grain-size ratio mentioned in [42-45].

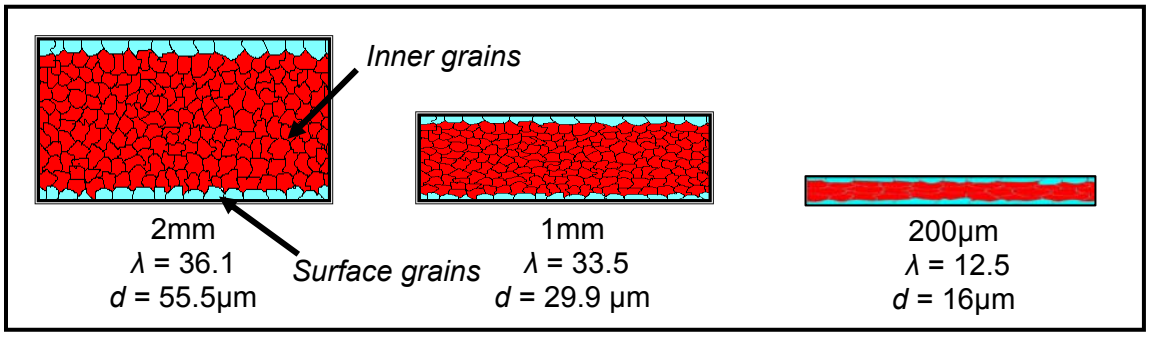

	2mm (*AR*)			1mm (*AR*)			200μm (*AR*)		
	Biaxial	Plane-strain	Uniaxial	Biaxial	Plane-strain	Uniaxial	Biaxial	Plane-strain	Uniaxial
N_s/N_i (%)	1.88	1.91	2.02	2.03	2.05	2.04	5.63	5.64	5.63
N_t (x10^6)	93.517	87.853	23.740	299.517	280.927	75.913	390.308	366.672	99.083

Figure 3- 11 Comparison of As-Received Sheets with Varying Thickness Values

3.5.2 Annealed Sheets with Varying Thickness

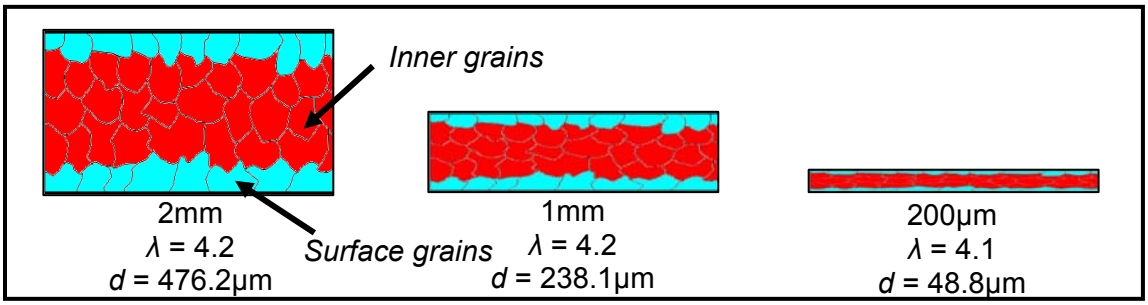

	2mm (*AN*)			1mm (*AN*)			200μm (*AN*)		
	Biaxial	Plane-strain	Uniaxial	Biaxial	Plane-strain	Uniaxial	Biaxial	Plane-strain	Uniaxial
N_s/N_i (%)	18.87	19.10	20.23	18.87	18.99	19.20	19.43	19.45	19.44
N_t (x10^6)	0.148	0.139	0.038	0.592	0.556	0.150	13.756	12.923	3.492

Figure 3- 12 Comparison of Annealed Sheets with Varying Thickness

For the batch of annealed sheets (*Figure 3-8*), while all sheets had the same λ and N_s/N_i ratios (to a close margin), formability increased with increasing grain size d and decreasing total number of deformed grains N_t. Again, the fewer number of deformed grains resulted in less restriction to deformation in thicker sheets, therefore more formability. This observation also validated the proportionality between formability, or ductility, and sheet thickness. Another observation on the tested annealed sheets was the form of the obtained FLCs which did not comply with the well known conventional form. Although the strain limits of the uniaxial strain path seemed to be in the expected range on the FLD, the strain limits of the biaxial strain path were lower than those of the plane-strain path for all FLCs, which is uncommon in what is known about sheet metal behavior. The decreasing ductility with increasing sample width is thought to be a result of the increased restriction of grains in biaxial samples to deformation, even though the number of surface grains in all strain conditions did not differ much (not more than 7%).

For further explanation, the designation of surface and inner grains in *Figure 3-10* was considered. From the illustration, it can be said that the grains at the perimeter of the deformed dome in the biaxial strain path are restricted by the surrounding ones, leading them to become inner grains at the perimeter of the deformed volume, which is not the case in plane-strain samples that had free unrestricted grains on the sides of the samples. Therefore, the deforming coarse grains of the biaxial specimens resulted in a restricted forming limit on the FLD due to the retardation of adjacent grains to rotate into its preferred orientation that enables them to deform plastically, which was not the case for the deformed grains of the plane-strain samples which had free grain around the deformed perimeter that will assist in the deformation of adjacent grains. This behavior resulted in lower strain limits of biaxial samples along the major axis than that of the plane-strain samples, which yield the unconventional trend of the FLC .The observed restriction demonstrated low values in minor strain for the spherically bulged sheets that decreased with decreasing thickness (*Figure 3-8*). In general, significantly large grains tend to affect the behavior of sheet formability.

3.5.3 As-received and Annealed Sheet of Same Thickness

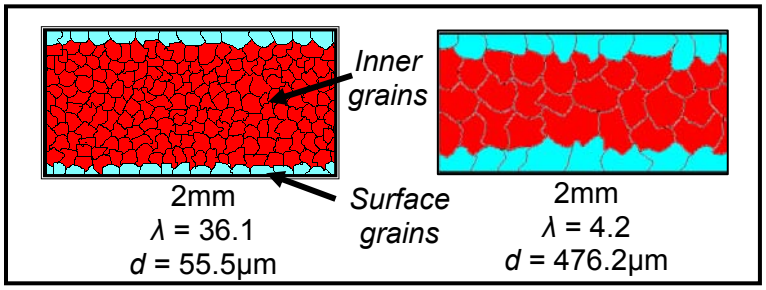

	2mm (*AR*)			2mm (*AN*)		
	Biaxial	Plane-strain	Uniaxial	Biaxial	Plane-strain	Uniaxial
N_s/N_i (%)	1.88	1.91	2.02	18.87	19.10	20.23
N_t (x10^6)	93.517	87.853	23.740	0.148	0.139	0.038

Figure 3- 13 Comparison of As-received and Annealed Sheet of Same Thickness

For sheets of the same thickness, formability increased with increasing grain size and N_s/N_i ratio, but decreasing λ ratio and total number of deformed grains. It can be said that the share of surface grains in the annealed sheet was greater than that of the as-received one which meant less restriction to deformation. Along with that, the number of grains through thickness, λ, as well as the total number of deformed grains were also fewer for the annealed sheet, which meant less restriction to the overall number of grains in the deformed sheets for all three strain paths; according to dislocation theory.

3.5.4 As-received and Annealed Sheet of Different Thickness

An unconventional case was chosen for comparing formability with respect to varying thickness and annealing condition, or grain size. The 1mm annealed sheet demonstrated a higher ductility than the 2mm as-received one, which contradicts the fact of increasing ductility with sheet thickness. The influencing factors for increased

formability, or ductility, are the increasing grain size and the N_s/N_i ratio along with the decreasing number of deformed grains and λ ratio. In this case the thicker sheet demonstrated less formability due to greater restriction to grains to deform because of increased grain- density when compared to the thinner sheet.

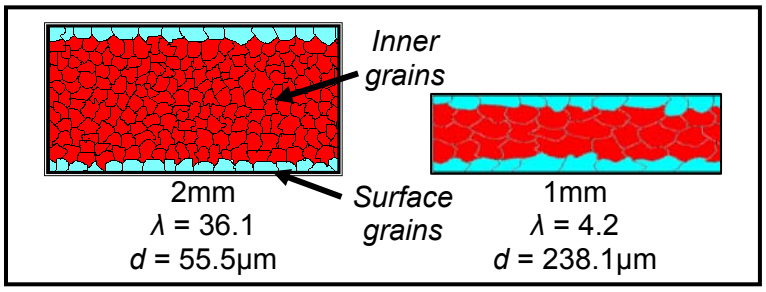

	2mm (*AR*)			1mm (*AN*)		
	Biaxial	Plane-strain	Uniaxial	Biaxial	Plane-strain	Uniaxial
N_s/N_i (%)	1.88	1.91	2.02	18.87	18.99	19.20
Nt (x10^6)	93.517	87.853	23.740	0.592	0.556	0.150

Figure 3- 14 Comparison of As-received and Annealed Sheet of Different Thickness

For all the mentioned cases of comparison, it can be said that thickness was the dominant factor for ranking the formability of sheet metal. However, grain size and the number of grains across thickness start to impose an effect into the mentioned ranking at a certain value of grain size in the microstructure of tested sheets as seen in the comparison between the 2mm as-received sheet and 1mm annealed one. Nevertheless, sheet thickness has a more dominant effect on sheet formability ranking in the case of a fine-grain structure, as can be seen conventionally [40-45]. By lowering the number of grains across thickness, and consequently the total number of deformed grains, the formability enhanced significantly, but the high surface roughness, which was clearly identified visually by the naked eye, is a limitation to such sheet metal processing if a smooth surface finish is a requirement. This might limit its use in industrial applications,

as mentioned by Yamaguchi and Mellor [42]. More detailed analysis should be performed to understand the form and nature of FLDs for sheets with a few grains across its thickness.

Overall, the ranking of sheet metal formability was regarded with respect to the grain size d and the total number of deformed grains N_t. The reason for the previous parameters being dominant factors in characterizing formability is the significant decrease in dislocation density due to the decrease in N_t. This corresponds with the dislocation theory which states that dislocations tend to pile up on their slip plains behind grain boundaries [47-48]. Knowing that in the case of the more ductile sheets, which held fewer grains than less ductile ones, the grain boundary density of the aforementioned sheets is significantly less than that of the later mentioned ones which have smaller grains. Therefore, applying equal punch forces will yield in higher formability for annealed sheets because they demonstrate less restricted grains that will have to rotate to obtain the proper orientation for material deformation meaning, fewer obstacles for grains to deform under loading forces [47]. The influence of the selected parameters on formability are shown in *Table 3-7*, where arrows pointing up represent increasing values while arrow pointing down represent decreasing values. All the corresponding measurement and analysis for the tested sheets with different cases are summarized in Appendix III.

Table 3-7 Characterization of sheet formability for selected scenarios

Case	Formability	t	λ	d	N_s/N_i	N_t	Grain boundary density
AR vs. *AR* (varying *t*)	↑	↑	↑	↑	↓	↓	↓
AN vs. *AN* (varying *t*)	↑	↑	-	↑	-	↓	↓
AN vs. *AR* (constant *t*)	↑	-	↓	↑	↑	↓	↓
AN vs. *AR* (varying *t*)	↑	↓	↓	↑	↑	↓	↓

3.6 Concluding Remarks

The effect of sheet microstructure on its formability was addressed by characterizing sheet formability with respect to its thickness, thickness-to-grain-size ratio, volume-to-grain-size ratio, surface-to-inner grains ratio, and total number of deformed grains. Formability seemed to decrease with decreasing thickness along with thickness-to-grain-size ratio and volume-to-grain-size ratio. FLDs of annealed sheets showed a different trend with higher strain limits than as-received ones of the same thickness. Overall, the increase in formability seemed to be a result of less number of deformed grains in all cases which was accompanied by a lower grain boundary density, meaning less restriction to grain deformation. The total number of deformed grains and grain size showed more influence on sheet formability than sheet thickness at a certain grain size. This study is regarded as a first step towards addressing size effects on thin sheet formability from surface strain-limits point of view. In Chapter 6, size effects will be identified through a comparison between the results in this chapter and the results of strain analysis at the microscale level. More analysis into the effect of grain size within a certain sheet thickness on the formability of sheet metal should be conducted for the benefit of sheet metal formability in related industries, such as the automotive industry.

CHAPTER FOUR

DEVELOPMENT OF MICROFORMING SETUP

4.1 Introduction

As mentioned before, the lack of knowledge in predictive models and testing methods that can help us understand metal forming and material flow at the microscale level calls for more extensive research in the area of characterizing formability for microforming processes. In this work, initial efforts to make use of existing testing setups such as the Tinius-Olsen® cup test setup and the Rheometrics Scientific Inc. ® RSAIII nano-indentation setup were undertaken. Although results were obtained from thin sheet bulging by those setups, a lot of limitations and undesired parameters could not be avoided regarding testing conditions. Some of the drawbacks of the aforementioned setups when incorporating microforming of thin sheets through bulging are:

1. Lack of accuracy in force measurement of minute amounts of loading when considering thin sheet bulging on conventional drawing tests machines.
2. High amount of clamping forces which tend to tear thin sheets along its deformation parameter instead of on the deformed area.
3. Lack of existing dies to accommodate forming of sheets in microscale or mesoscale levels.
4. Lack of high precision and tight tolerances which govern thin sheet formability at the microscale level.
5. Inability to ensure proper alignment between the punch and die, which were developed for its use in the RSA III nano-indentation setup, although loading and displacement readings were accurate enough.

In view of the above mentioned limitations, a major effort was put into identifying and capabilities of a testing setup which can accommodate the following requirements for characterizing thin sheet testing such as:

1. A microforming fixture that can demonstrate the required high precision and tight tolerances for measuring formability at the microscale level.
2. A proper thin sheet clamping mechanism to assure the required stretching while keeping the deformed sheets from drawing into the die hole.
3. A perfect alignment mechanism between the punch and die-hole, which will ultimately eliminate any worries about proper load sensing and reading.
4. A control system for controlling the forming process while having the ability to end testing at certain level of force drops, as exhibited by conventional large setups, which is a challenge when considering the minute applied forces.
5. A data acquisition system for recording force and displacement readings during testing.

In this chapter, a newly developed microforming setup, which demonstrates the above requirements, is introduced. This setup is considered to be the back bone of this work, as will be mentioned in the following chapters.

4.2 Microforming Setup

The purpose of developing a microforming setup was to ensure proper thin sheet stretching for characterizing formability at the microscale level. The microforming setup was scaled down from the actual layout of the Tinius Olsen dome test machine according to the ASTM bulging test standard E643-84 [51]. The scaling resulted in an actual

microbulge forming setup with a punch-die arrangement. The hemispherical punch tip is 1.5 mm in diameter. The punch is mechanically driven by a Haydon Switch & Instruments® stepper-motor-driven linear actuator. Two linear actuators which demonstrate a high precision factor are used; one for forming 25μm thickness sheets at 1.5 μm per step and another for forming 50μm thickness sheets. The accuracy of the stepper motors given by the manufacturer [52] is 6-7% per step; which translates to 0.1μm and 0.2μm per step for the smaller and bigger actuators respectively. The punch and linear actuator are connected by a miniature Cooper Instruments and Systems® load cell which is capable of reading minute force measurements through significantly low voltage pulses (0.2 mV). These low voltage pulses must be amplified by a voltage amplifier up to 5V. The resolution of the load cell is set around 450 milligram. The linearity and hysteresis provided by the manufacturer [53] is ±0.5% with a repeatability factor of ±0.1%. The accuracy of the voltage amplifier which delivers force readings to the data acquisition system is 0.02%.

A die fixture with a simple screw mounting mechanism was fabricated for holding thin sheet specimens. Although the die hole was just slightly larger than 1.5 mm (the punch diameter), the required specimen size was 9x9 mm for facilitating handling of samples and applying proper gripping. The die arrangement provided enough clamping forces to restrict material movement along the clamped region, which forbids thin sheet drawing into the die opening while forming. This conclusion was drawn upon testing thin sheet stretchability through measuring distances between identified points on the tested specimens before and after forming measured using an Olympus® BX41 optical microscope. Random points were designated across the bulging area as well as same

sides of bulging area. Repeated measurements of three specimens were taken for statistical purposes, as detailed in Appendix IV, and averaging the readings resulted in a $0.2\%^{+0.04}_{-0.07}$ material deformation under the clamped region with a 0.06 standard deviation and 0.3 coefficient of variation. From this result, we concluded that the presented microforming setup demonstrates total stretching capabilities for limiting-strain characterization.

In order to ensure proper alignment between the punch and the die hole, a kinematic coupling mechanism with a six-point contact layout was fixed between the bottom of the die and the fixture frame (*Figure 4-1*). An electronic processor was developed for controlling speeds and depths of the forming punch. A data acquisition system complemented the setup for providing in-situ force and displacement measurements during testing. Figure *4-2* shows the layout of the microforming setup. A unique feature which enables us to choose stopping the bulging process at a preferred level of force drop (0-100%) after achieving the maximum point was added to the control setup. Thin sheets were deformed into a hemisphere until the initiation of a crack on the surface, as can be seen in *Figure 4-3*. It can be said that this forming setup has microforming capabilities [1] since the cross section of the bulged thin sheets is always in the microscale level; which is the fundamental definition of microforming processes. The experimental procedure for thin sheet bulging can be seen in Appendix V. The outcome of the presented apparatus is a unique feature by which thin sheet formability at the microscale level can be characterized and results can be more accurate than using existing testing setups which do not represent the actual deformation mechanism in a proper way.

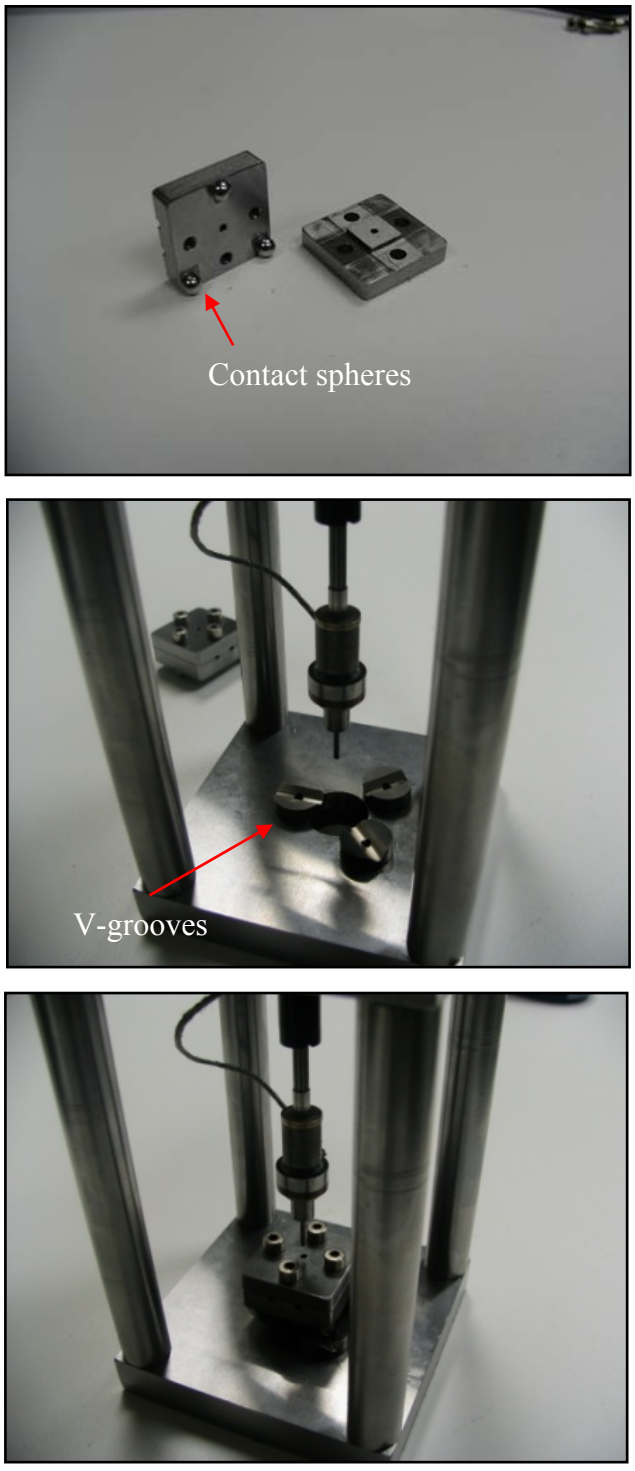

Figure 4- 1 Die-Frame arrangement complemented by a kinematic coupling mechanism

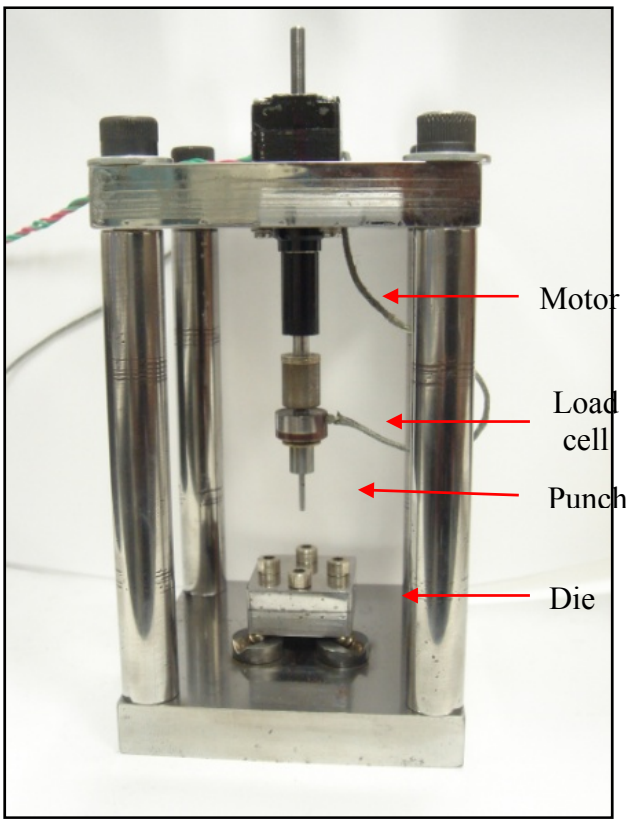

Figure 4- 2 Microforming apparatus

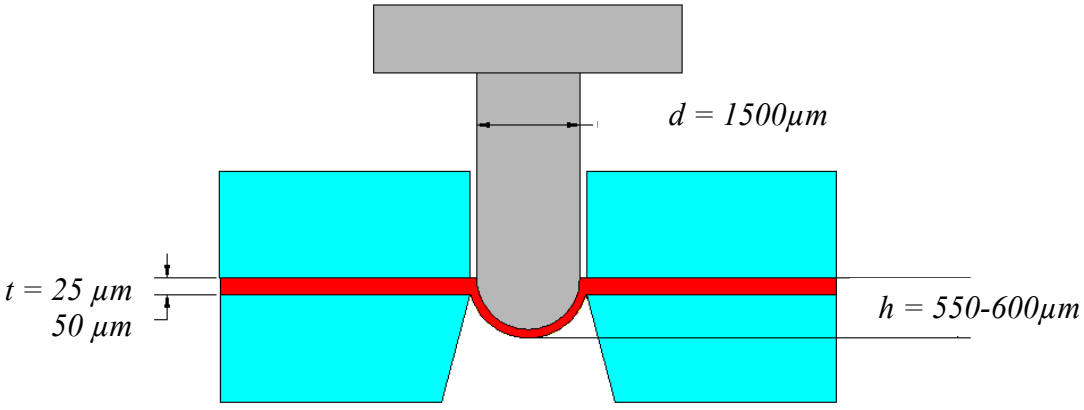

Figure 4- 3 Punch-die schematic of a 25µm microformed thin sheet

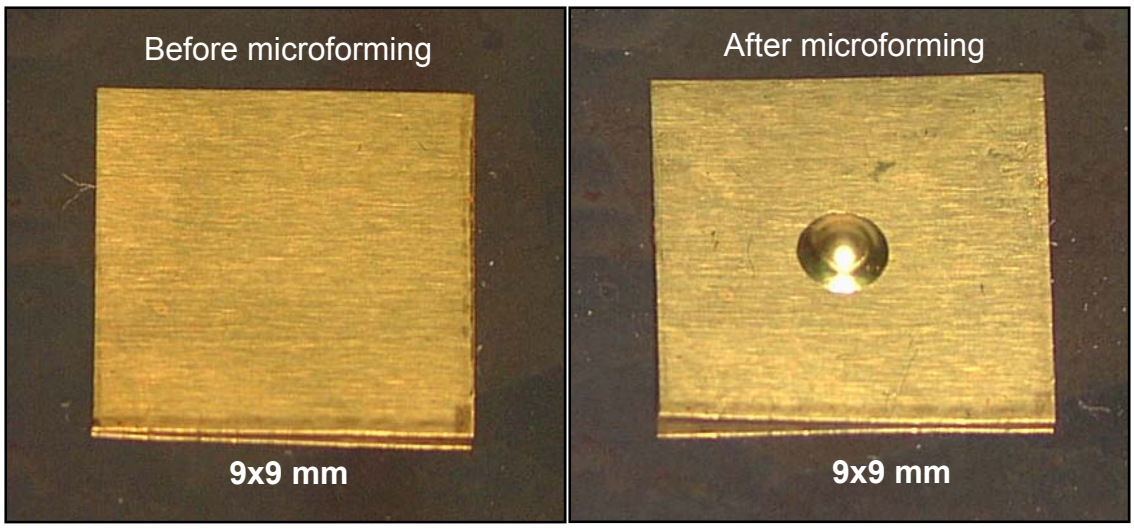

Figure 4- 4 A Test specimen (CuZn30) before and after bulging

4.3 Materials

The materials were chosen based on their significance in the micromanufacturing field. Cartridge brass (*CuZn30*) was chosen due to its favorable use in micro-electro-mechanical systems (MEMS) [1-9, 11, 13-17, 20, 25, 26, 54]. The significance of this particular alloy comes from its excellent mechanical and electrical properties which are essential aspects in electronic devices. Brass alloys have the advantage of demonstrating excellent ductile behavior when cold worked, high strength and corrosion resistance, and excellent formability characteristics for sheet metal operations. This alloy is used in MEMS components such as IC sockets, circuit boards, and electronic connectors. *Table 4-1* lists the nominal composition of *CuZn30* alloy.

Table 4-1 Composition of CuZn30 alloy (wt%) [55]

Material	*Cu*	*Zn*	*Pb*	*Fe*	*Mn*	*Al*	*Sn*
CuZn30	68.5-71.5	balance	0.05	0.1	0.05	0.02	0.05

Another alloy which holds similar significance with *CuZn30* is Al 1100. This high purity aluminum alloy demonstrates the same favorable mechanical and electrical properties for fabricating MEMS parts [1,3,4,5,10,11,18,19,31,32,56,57]. Since *Al1100* is currently implemented in MEMS micro-structures which are fabricated by photolithography and LIGA techniques [3,4,58,59], mastering microforming processes on such an alloy at the microscale will enable the mass production of microparts in significantly lower lead time. Another advantage of microforming aluminum alloys is the assurance of maintaining any desired intricate geometries without worrying about adding more costly techniques into the production process. The nominal composition of *Al1100* is listed in *Table 4-2*.

Table 4-2 Composition of Al1100 alloy (wt%) [55]

Material	*Al*	*Si+Fe*	*Cu*	*Mn*	*Zn*	Other
AA1100	99	0.95	0.05-0.2	0.05	0.1	0.05

Both *CuZn30* and *Al1100* are supplied in the form of thin sheets, with cartridge brass in half hardened condition (H02-tempered) [60] and Al110 in a fully annealed condition (O-tempered) [61]. In this work, thick sheets of *CuZn30* with 2mm, 1mm, and 0.2mm thicknesses were tested. Thin sheets of *CuZn30* and *Al1100* with 25.4μm and 50.8μm thicknesses were also tested.

CHAPTER FIVE

INVESTIGATIONS OF THE EFFECT OF PROCESS PARAMETERS ON THIN SHEET FORMABILITY

5.1 Introduction

The first step to a proper optimization approach for thin sheet microforming processes is to identify the major process parameters that influence the nature of material behavior at such a scale, which can ultimately lead to a better understanding of size effects on microforming processes. In this study, loading profiles along forming displacements were analyzed while varying specifically identified process parameters. The chosen parameters are forming speed, sheet thickness, microstructure, and lubrication. Identifying the existence of any influence by the aforementioned parameters on the loading profiles will benefit the micromanufacturing industry by establishing means of adjusting process parameters to facilitate in obtaining preferred results and functionalities. For all conducted tests in this study, tested specimens were categorized into four batches with two different alloys; *CuZn30* and *Al1100* thin sheets with 25μm and 50 μm thicknesses for each alloy. The aim of parameter testing in this study is to determine whether the identified parameters do have an influence on thin sheet formability for microforming applications and processes. The effect of each parameter was investigated separately and a cumulative comparison was made in order to establish the effect of all identified parameters.

5.2 Effect of Forming Speed on Thin Sheet Formability

5.2.1 Procedure and Experimental Data

To investigate the effect of forming speed on microscale formability, particularly microbulging, the previously introduced microforming setup was used (described in

Chapter Four). Microbulging tests for each batch of material and thickness were performed at four forming speeds; 1.5, 15, 150, and 1500 μm/s. In each test, thin sheets were clamped, as mentioned in Chapter Four, and bulged until failure which was detected automatically by the microprocessor through the DAQ system after sensing a 10% force drop from the peak force value. The recorded forces were then plotted along the punch stroke to form loading profile of the actual bulging process. For each batch of thin sheets, every test under a particular speed was repeated three times for assessing statistical scatter in the data. The loading profiles were then averaged from the repeated experiments. *Figure 5-1* shows the plotted loading profiles for *CuZn30* while *Figure 5-2* shows the loading profiles for *Al1100*.

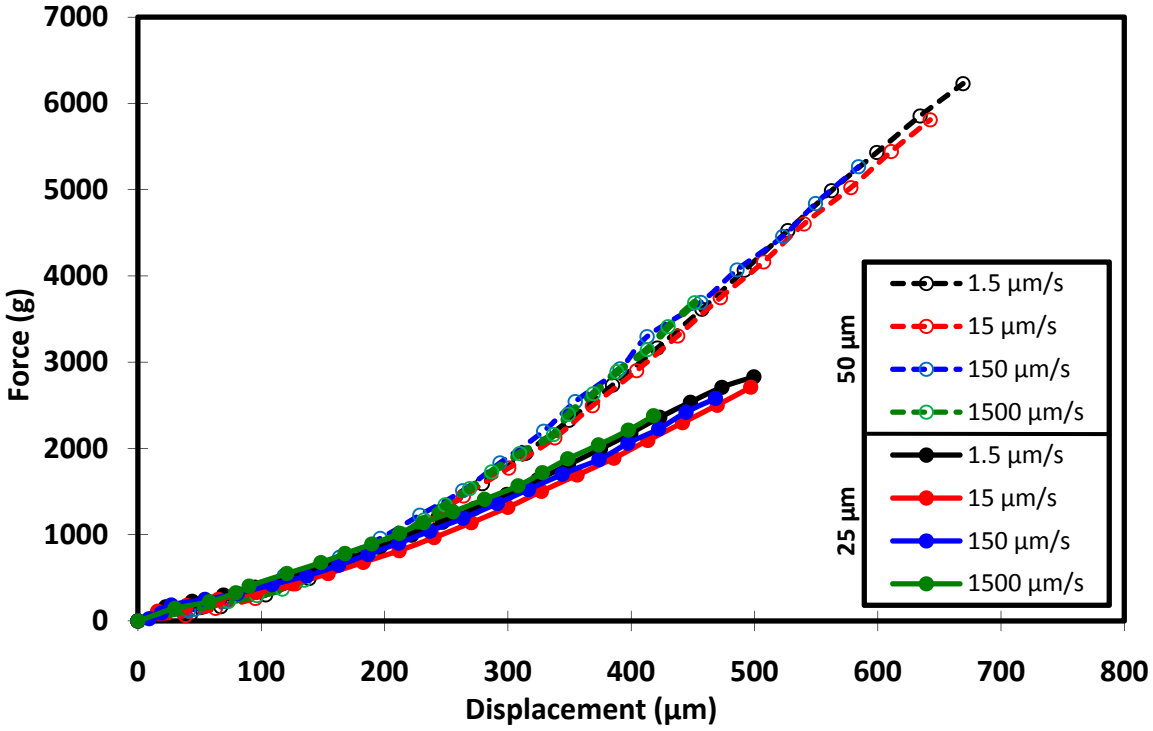

Figure 5- 1 Force profiles of CuZn30 with varying thickness

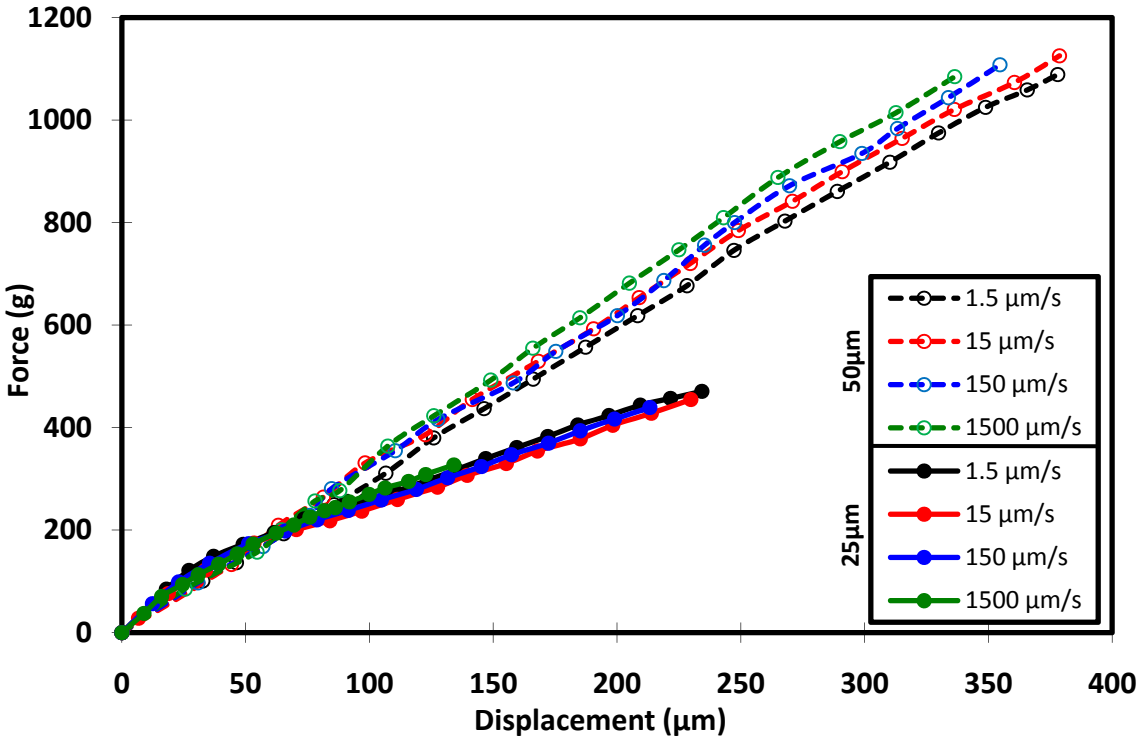

Figure 5- 2 Force profiles of Al1100 with varying thickness

5.2.2 Discussion

From the loading profiles presented above, it can be said that the form of loading profiles with respect to the forming depth of the punch for each of the four batches was nearly identical. This means that the loading path by which the material is deformed is not affected by the forming speed, even though there seemed to be some variation in the plotted curves due to measurement and acquisition errors which were quantified in Chapter Four. From this observation, it can be said that the loading profile for a certain material at the microscale is independent of the forming speed, at least between the indicated range of forming speeds. This observation goes together with the less-dependability of flow stress on forming strain rates at room temperature at the macroscale level [48, 62, 63].

Table 5-1 Numerical values of limiting dome-height and forces for CuZn30 tested sheets

Forming Speed (μm/s)	Limiting dome-height (μm)		Limiting force (gm)	
	25μm	50μm	25μm	50μm
1.5	501.50	705.58	2829.26	6355.31
15	500.56	680.36	2709.30	6107.37
150	468.41	584.47	2579.08	5265.38
1500	404.18	451.59	2378.22	3688.09

Table 5-2 Numerical values of limiting dome-height and forces for Al1100 tested sheets

Forming Speed (μm/s)	Limiting dome-height (μm)		Limiting force (gm)	
	25μm	50μm	25μm	50μm
1.5	234.29	390.43	470.78	1066.79
15	229.80	389.01	454.95	1158.25
150	213.26	381.11	439.25	1176.18
1500	134.10	315.88	327.18	1195.84

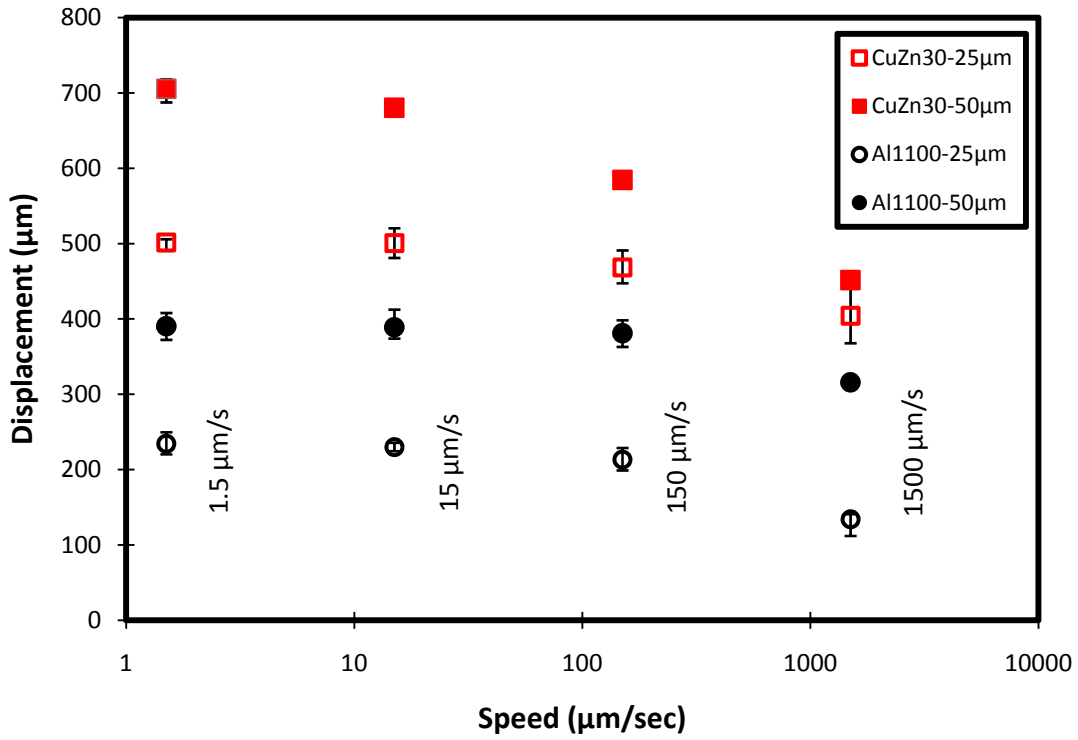

Figure 5- 3 Effect of varying speed on limiting height for microbulged thin sheets

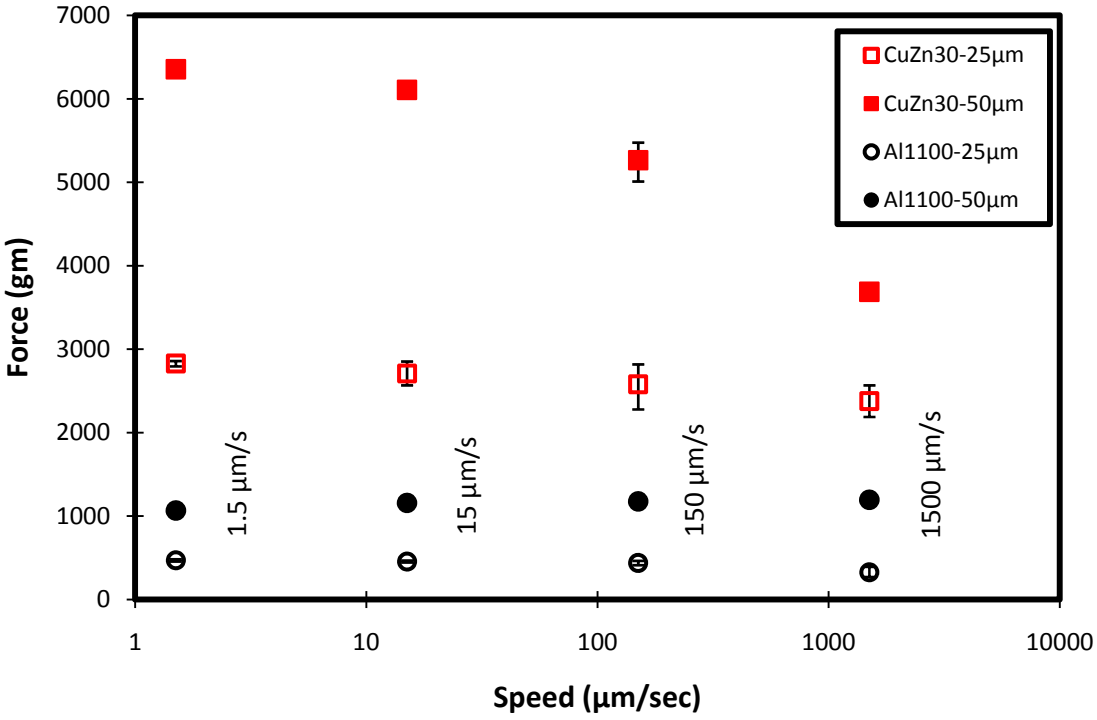

Figure 5- 4 Effect of varying speed on limiting force for microbulged thin sheets

Limiting values of dome heights and forces were extracted from loading plots of both tested alloys and quantified in *Tables 5-1 & 5-2*. Those values were plotted in *Figures 5-3 & 5-4* to illustrate the trend of limiting values. For *CuZn30*, values of limiting dome-heights for both 25µm and 50µm thin specimens seemed to decrease with increasing forming speed. The rate of drop in limiting dome-height was greater for thicker sheets; having a drop of 19% and 36% between slowest (1.5µm/s) and fastest (1500µm/s) forming speeds for 25µm and 50µm tested sheets respectively. The same trend was observed for limiting forces with varying speeds for both tested thicknesses. The drop in limiting force also increased for the thicker sheet, having a maximum drop of 42% for 50µm sheets versus 16% for 25µm thin sheets. In both cases, the rate of drop for the 50µm sheets demonstrated a steeper trend than that of the 25µm ones. For limiting values of *Al1100* tested sheets, limiting dome-heights for both tested thicknesses decreased with increasing forming speed. Again, thicker sheets showed more drop in forming height with increasing forming speed than thinner ones; with 50µm sheets having a maximum drop of 42% (at 1500µm/s forming speed) while 25µm thin sheets having only a 20% drop. However, resulting limiting forces did not follow the same trend, instead limiting forces increased with increasing forming speed with around 12% increase in 1500µm/s forming speed from 1.5µm/s.

In general, for *CuZn30* tested thin sheets, there seemed to be some dependence of limiting heights and forces on forming speed that can be related to work hardening effects. This observation is contrary to the increasing tensile elongation of *CuZn30* and several other metal alloys with increasing strain-rate at the macroscale [48, 62-65]. However, this dependency cannot be explained by linking limiting values to

corresponding materials only. The effect of other process parameters must be incorporated in the analysis of speed dependence, such as sheet thickness and average grain size, which have been proven to have a significant impact on formability comparison at the macroscale [42-45]. Therefore, the mentioned dependency will be addressed along with other parameters that will be investigated in the following sections.

5.3 Effect of Sheet Thickness on Thin Sheet Formability

5.3.1 Procedure and Experimental Data

Since the sheet thickness is the first parameter that is usually considered, especially when investigating the extent of sheet formability for achieving a certain formed shape or geometry, loading profiles of the two tested thicknesses, 25 and 50 μm, were compared for each tested material; *CuZn30* and *Al1100*.

5.3.2 Discussion

From *Figures 5-1 & 5-2*, the loading profiles for each tested thickness of both alloys can be clearly distinguished. For both *CuZn30* and *Al1100*, thicker sheets showed superior forming dome-heights to thinner ones. The forces needed to obtain higher dome-heights for thicker sheets were also higher than that needed for thinner ones. However, in the analysis of the limiting dome-heights and forces for each thickness and alloy separately, as shown in *Figures 5-3 and 5-4*, another trend was observed in the comparison of formability of varying thicknesses of the same alloy. For *CuZn30*, the reduction in limiting dome-heights and limiting forces between 50μm and 25μm tested sheets seemed to decrease with increasing forming speed; having a limiting height

reduction of 29% at 1.5μm/s forming speed, which decreased to a 10% reduction at 1500μm/s forming speed. Limiting forces also showed the same trend in reduction between the two tested thicknesses; having a 55% reduction at 1.5μm/s forming speed while holding a 35% reduction at 1500μm/s forming speed. These results can be characterized by a steeper drop in limiting values for 50μm when compared to 25μm ones, as mentioned in previous section. For *Al1100*, the recorded limiting dome-height and forces did not project the same trend as what was observed for the *CuZn30* alloy. The decrease in limiting height between 50μm sheets and 25μm ones seemed to be greater at lower speeds (being 40% and 56% at 1.5μm/s and 1500μm/s forming speeds respectively). The same result was found for limiting forces (having reductions of 58% and 73% at 1.5μm/s and 1500μm/s forming speeds, respectively). From the obtained results it can be seen that reducing sheet thicknesses for thin sheet microbulging reduces the required forming loads, but on the other hand reduces the limiting dome-height, which ultimately reduces the ductility of the formed thin sheets. This observation will be incorporated with grain size investigations that will be discussed in the next section.

5.4 Effect of Average Grain Size (Microstructure) on Thin Sheet Formability

5.4.1 Procedure and Experimental Data

Due to the continuous association of microforming with the average grain size *d* in most recent and current investigations [5-21], the average grain size for each alloy and thickness was determined after performing the proper microstructural analysis that included polishing and etching techniques. Since it is an extremely difficult task to mount

and polish thin sheets in the same conventional manner that was followed for thicker sheets described in Chapter Three, an electrolytic polishing and etching technique was applied to reveal the microstructure on thin sheet surfaces. This procedure is presented in Appendix VI. Two methods were undertaken for revealing the microstructure; conventional electrolytic etching for *CuZn30* and electrolytic anodizing for *Al1100*. The unique feature about anodizing is that grain boundaries are not attacked by a chemical agent as it is the case in chemical etching; rather, an oxide layer is created on top of the polished surface. This oxide layer gives a remarkably clear representation of grain on the surface of sample by means of a polarizer module which reflects grain colors according to their orientation in the microstructure. Grain-structure images of tested samples were taken by an Olympus® BX41 metallographic microscope that contains a polarizer module for anodized samples. The software used for capturing actual images is Image-Pro Plus®. For each batch, the measurement was repeated three times for assessing statistical scatter in the data. Statistical analysis, including standard deviations and coefficient of variations, are listed in Appendix VII.

Microstructural images of 25μm and 50μm *CuZn30* thin sheets are shown in *Figure 5-5*. Grain size measurement of the two alloy thicknesses are presented in *Table 5-3*. It can be said that the grains of both *CuZn30* thicknesses are considered equiaxed, thus the *CuZn30* thin sheets are considered as having a homogeneous microstructure that should represent an isotropic behavior. Microstructural images of 25μm and 50μm *Al1100* thin sheets are shown in *Figure 5-6*. Grains of *Al1100* thin sheets seemed to be elongated along the rolling direction. Thus, the microstructure of the tested *Al1100* alloy was said to be inhomogeneous and its behavior was regarded as anisotropic. Therefore,

grain size measurement of tested samples was irrelevant to address the size effects through a varying microstructure. Hence, correlation of bulging profiles and loading limits with *Al1100* grain sizes were not included in this investigation. Furthermore, any generalization of size effects on process parameters was restricted to the tested *CuZn30* alloy.

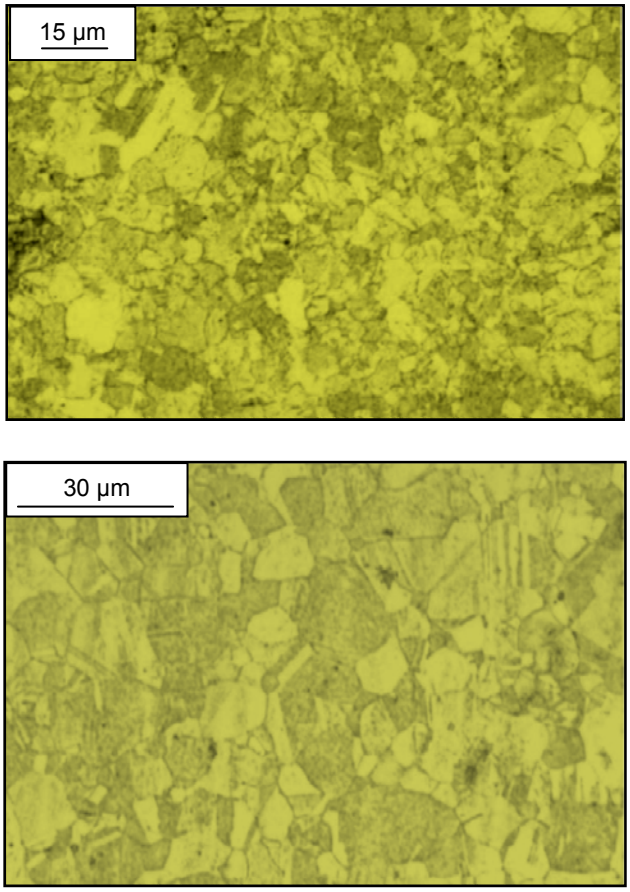

Figure 5- 5 Microstructural image of 25 µm (top) and 50 µm (bottom) CuZn30 thin sheets

Table 5-3 Grain size, d, measurement of the tested CuZn30 thin sheets

Thickness (μm)	d_1	d_2	d_3	d_{ave} (μm)	SD	V (Coeff. of variation)	λ
50	13.5	14.3	13.9	13.9	0.72	8.79	3.7
25	7.4	8.8	8.4	8.2	0.40	2.88	3.1

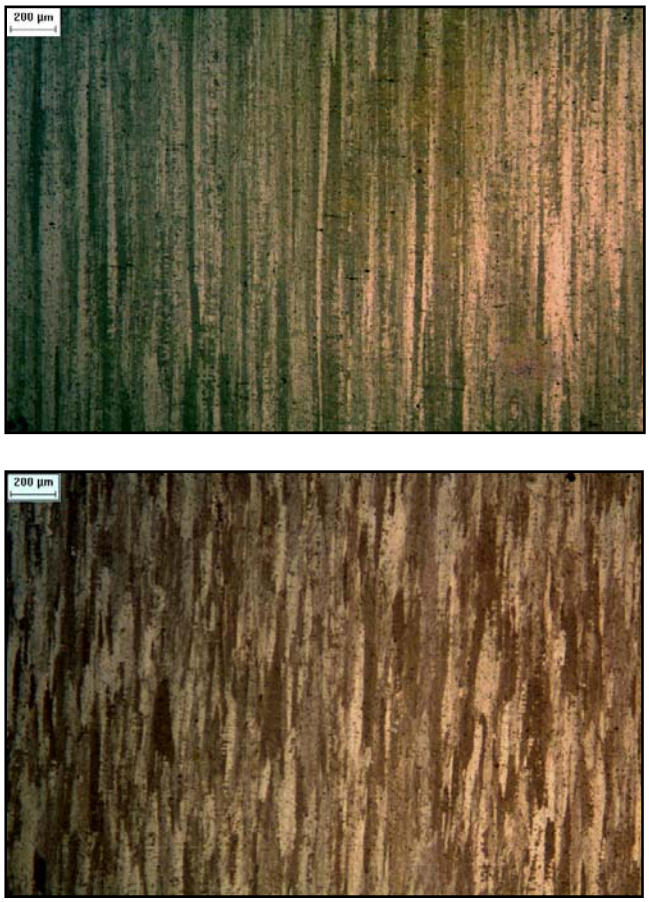

Figure 5- 6 Microstructural image of 25 µm (top) and 50 µm (bottom) Al1100 thin sheets

5.4.2 Discussion

It can be said that the 25µm and 50µm sheets, which have 8.2 µm and 13.9 µm grain sizes respectively, can be regarded as fine-grained due to the small numerical values when compared with grains of thicker sheets [66]. Nevertheless, by considering that only between three and four grains constitute the thickness of these thin sheets, it can

be assumed that these tested sheets of the aforementioned thicknesses are coarse-grained. By referring to the loading profiles of *CuZn30* in *Figure 5-1*, for both 25µm and 50µm tested sheets, thin sheets with smaller grain size had less formability, or ductility. However, the comparison cannot be based on grain size alone since the varying grain size is accompanied by thickness variation too. Therefore, a more accurate parameter should be chosen for investigating the effect of varying microstructure on thin sheet formability at the microscale. As introduced in Chapter Three, the thickness-to-grain-size ratio λ was applied for comparison in this study. Values of λ ratio are presented in *Table 5-3*. In order to have a reasonable correlation between the λ ratio and the obtained loading profiles for *CuZn30*, measured forces were compared for each thickness for the same certain punch depth. For example, by observing the projected force value at a 400µm dome height (*Figure 5-1*), it is clear to say that sheets with a higher λ ratio needed higher forces to obtain that particular dome-height. This result can be generalized for all loading profiles starting at 200µm dome heights and greater; since below that value the projected forces were identical for both λ ratios of each thickness. The reason behind the mentioned trend could be the restricted deformation caused by the presence of more grains across thickness, as was concluded in formability analysis of *CuZn30* sheets at the macroscale level (Chapter Three) and mentioned in [1,47,48]. To generalize the effect of grain size on thin sheet formability at the microscale, more grains through sheet thickness develop an increasing restriction for grains to rotate to its preferred orientation for the deformation of the continuum material.

5.5 Influence of Lubrication and Effect of Friction on Thin Sheet Formability

5.5.1 Procedure and Experimental Data

The effect of friction has been mentioned in Chapter Two. As established in previous literature [12-17], friction has a great effect on some process parameters in microforming processes. In this study, the effect of friction was investigated by analyzing the loading profiles of dry-bulged thin sheets as well as lubricant-bulged ones and then comparing their form and accompanying trends. In order to follow a reasonable approach for applying the term "size effects", which is the main concern in data analysis of microforming, a particular forming speed of 15μm/s was chosen in this comparison. The reason for choosing this forming speed comes from fact that it is the closest to the scaling of the common applied speed of 1.5 in./min by 50 times (resulting in 12.7μm/s forming speed). This scaling corresponds with the scaling of the previously introduced microforming setup presented in Chapter Four, as well as the characterization of thin sheet formability which will be presented in Chapter Six. The lubricants used were WD-40® and DuPont Teflon® commercial lubricants. The compositions of both lubricants are considered classified information; therefore their composition could not be acquired. However, Teflon® is considered as one of the major lubricants used in numerous applications including automotive, aerospace, agricultural, and construction applications [67-68]. Teflon® lubricant was particularly chosen for lubrication testing because it is commonly used in the construction of FLDs to expand the strain limits of balanced biaxial stretching conditions beyond its limits at dry forming [49, 69-72]. Loading profiles of the tested *CuZn30* with 25μm and 50μm thicknesses are presented in *Figures 5-7 & 5-8.*

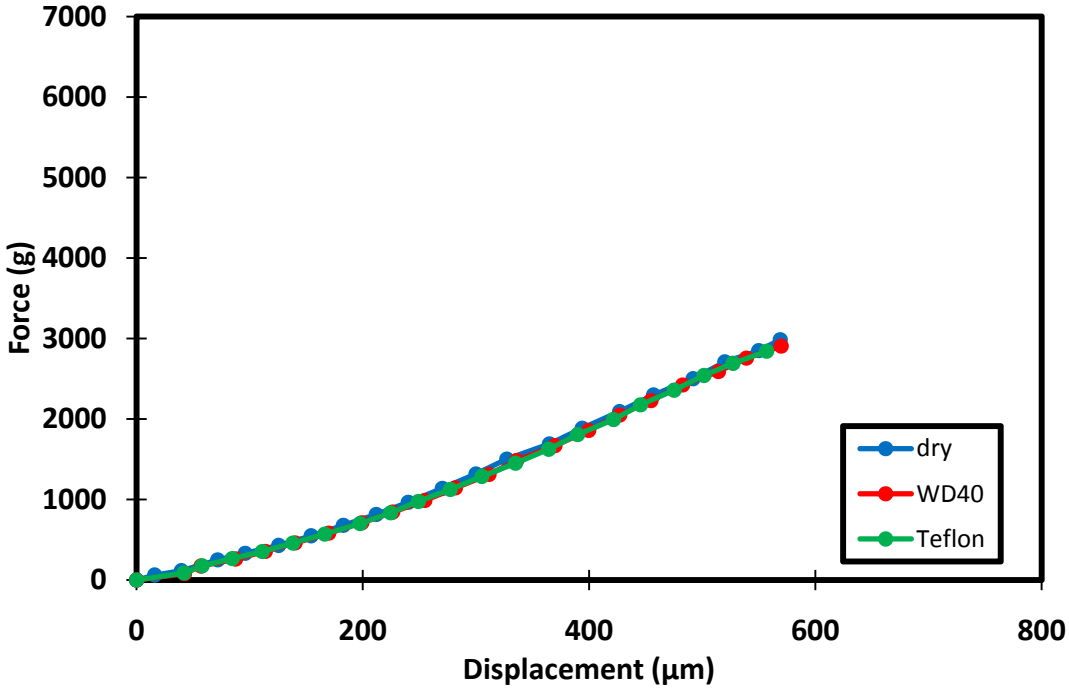

Figure 5- 7 Loading profiles for dry and lubricated 25µm CuZn30 thin sheets

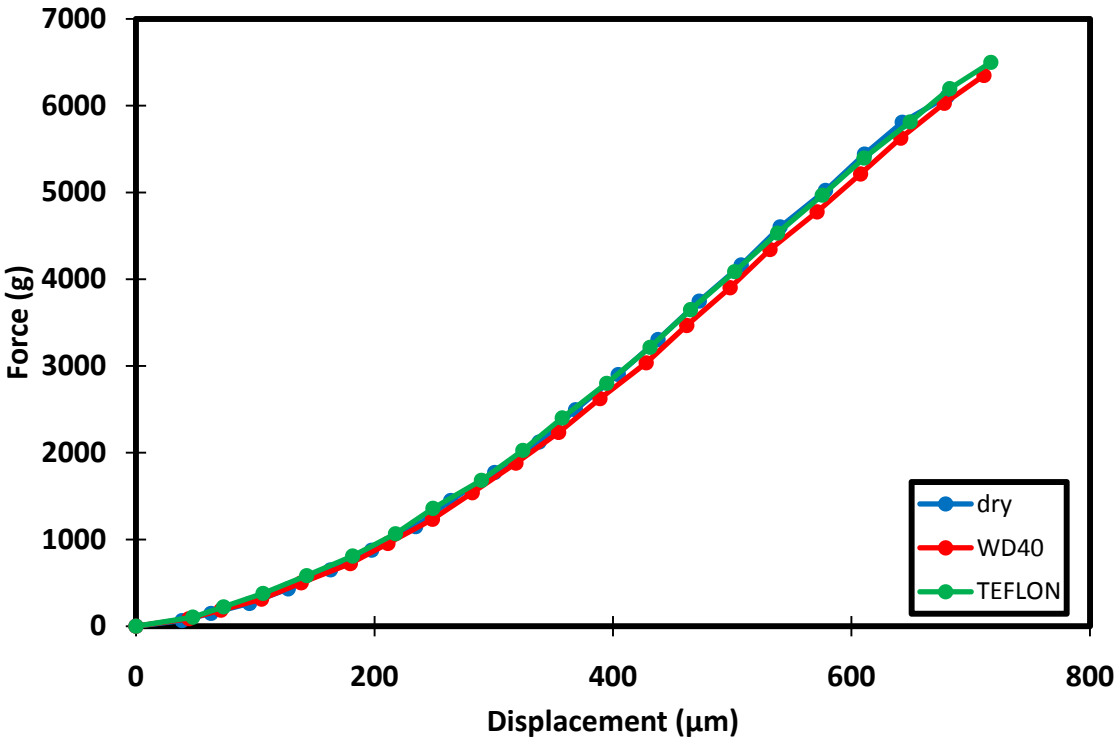

Figure 5- 8 Loading profiles for dry and lubricated 50µm CuZn30 thin sheets

5.5.2 Discussion

From the presented plots (*Figures 5-7 & 5-8*), it is clear that the lubrication did not affect the form of loading profiles for tested *CuZn30* thin sheets. However, a slight variation between limiting dome-heights and forces for dry and lubricated sheets was detected. *Figures 5-9 & 5-10* demonstrate those variations in terms of limiting values for both tested thicknesses respectively. A statistical analysis, in the form of data scatter of recorded measurements, was first considered. Although it seemed that the variation of upper limits and lower limits to averaged values were high for all tested sheets when observing the limiting diagrams in *Figures 5-9 & 5-10*, indicating a high data scatter, calculated percent variation for the mentioned values showed a variation of 0.1-4.5%. The range can be regarded as reasonable error bounds. In other words, a large data scatter was not observed in the results of measured limits.

The variation of limiting heights and forces of lubricated tested sheets, with both WD-40 and Teflon, are presented in *Table 5-4*. For both *CuZn30* thicknesses, limiting dome height increased with lubrication. However, the decrease in limiting forces, which is expected in macroscale testing, occurred only for 25µm lubricated sheets, while limiting forces increased for 50µm lubricated sheets. By referring to percent variations in limiting values in *Table 5-4*, variation in limiting heights was in the range of 1-3.5% for 25µm lubricated sheets and 4-5% for 50µm lubricated sheets when compared to limits of dry conditions, while the variation in limiting forces of lubricated sheets was in the range of 2.5-5% for 25µm thickness and 4-6.5% for 50µm thickness from limits of dry conditions. Considering the measured outputs of dome heights maximum forces, it can be said that the calculated percent variations for both parameters were insignificant to affect

the microforming process. In other words, obtained results indicate that applying lubrication to thin sheet microbulging does not affect the formability of thin sheets when forming depth and maximum loading are the case. Furthermore, a consistent result was obtained from the presented study. This result is a slight increase in forming heights of bulged thin sheets when applying a lubricant; which agrees with investigations on microextrusion testing of *CuZn15* [16,17,73,74], where the conclusion was derived from microextrusion of micropins after coating it with *CrN*, *TiN*, and *DLC-Si* (diamond like carbon) coatings to increase the extrusion length.

Table 5-4 Variation in limiting values of lubricated bugled sheets from values of dry ones

Lubricant	Variation in limiting dome-height (%)		Variation in limiting force (%)	
	25μm	50μm	25μm	50μm
WD-40	+3.5	+4.3	-2.7	+3.9
Teflon	+1.3	+5.1	-5.0	+6.4

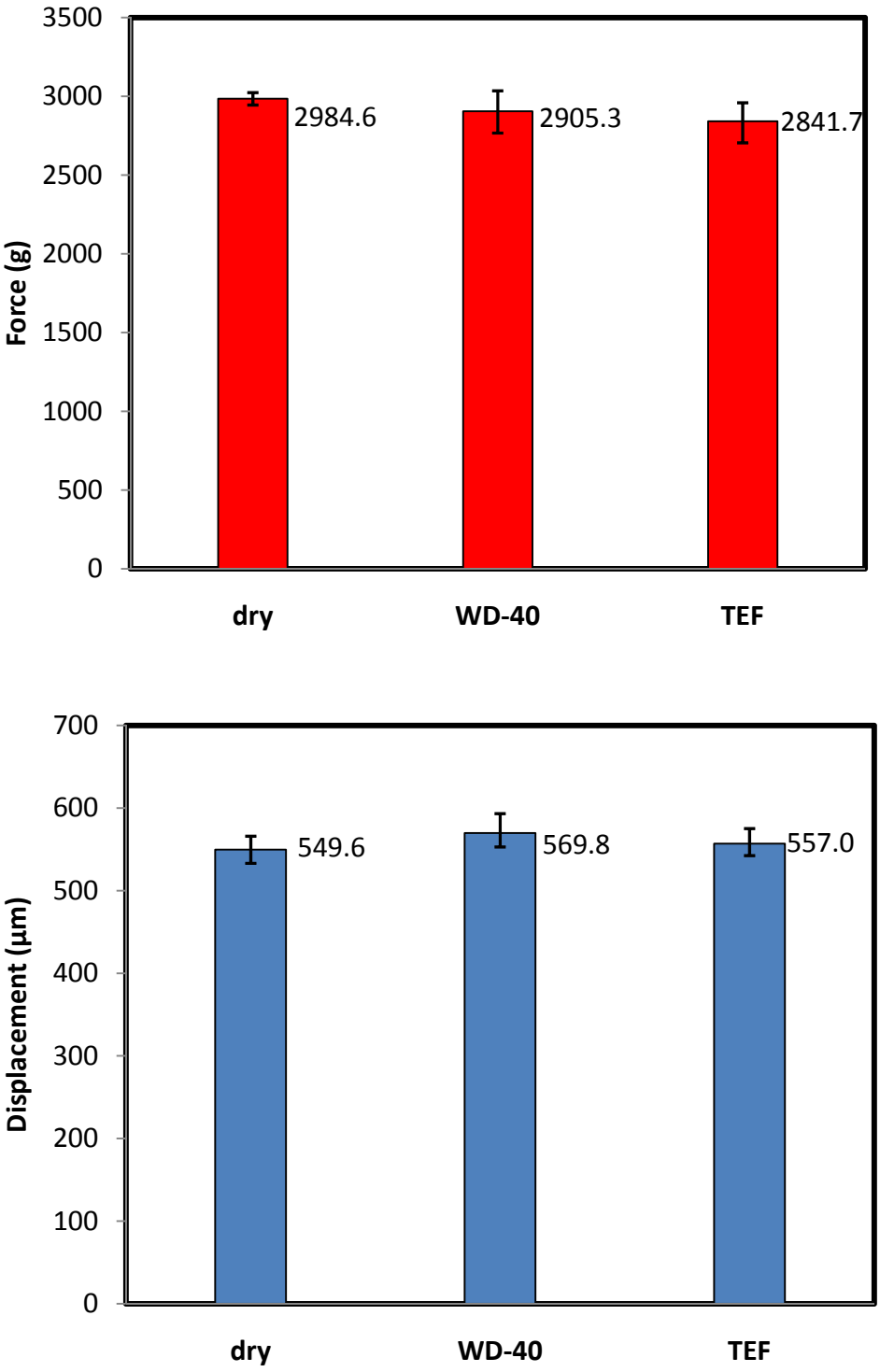

Figure 5- 9 Limiting forces (top) and dome heights (bottom) for dry and lubricated 25µm CuZn30 thin sheets at 15µm/s forming speed

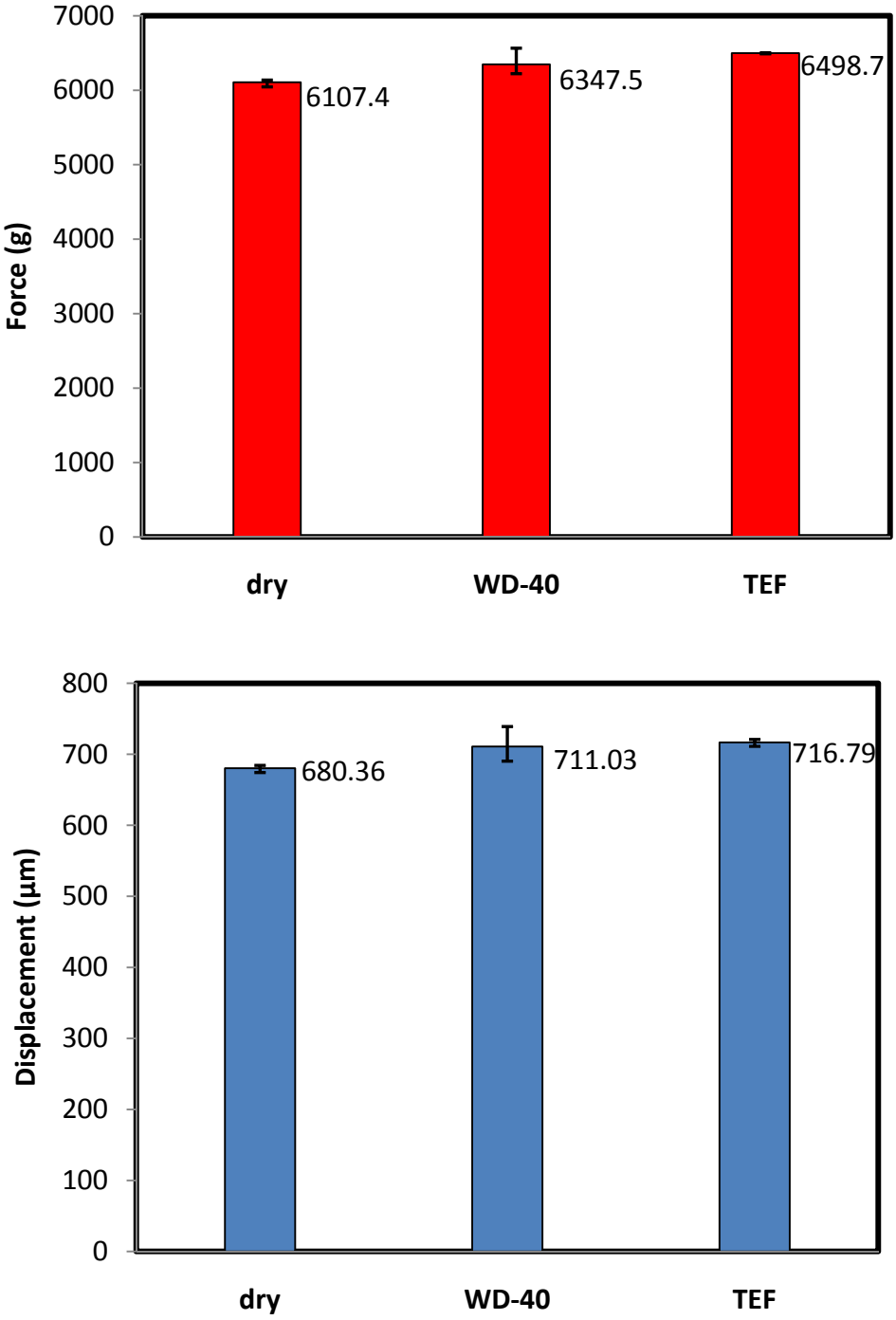

Figure 5- 10 Limiting forces (top) and dome heights (bottom) for dry and lubricated 50µm CuZn30 thin sheets at 15µm/s forming speed

5.6 Analysis of the Effect of Combined Process Parameters on Thin Sheet Formability

After investigating the effect of process parameters in a separate manner, a more thorough analysis of thin sheet formability by combining all investigated parameters was considered. The variation of limiting values for 25μm and 50μm *CuZn30* thin sheets with varying parameters was characterized by three cases of comparison that incorporated forming speed, sheet thickness, average grain size, and lubrication since all of them influence material behavior in general. The first case presented a comparison under constant thickness and average grain size while varying forming speed. In the second case, the comparison was made at a constant speed with varying thickness, average grain size d, and thickness-to-grain-size ratio λ. The third case directed the comparison under constant thicknesses and average grain size while varying friction effects.

5.6.1 Constant Thickness and Grain Size with Varying Forming Speed

In this case, forming heights and projected forces decreased with increasing forming speed. From this observation, size effects were said to be present, this result was not obtained for macroscale testing of *CuZn30*. The behavior can be explained by the mechanism of plastic deformation for polycrystalline materials. Since grains need to rotate into its most preferred orientation in order to deform by slipping or twins, and dislocations that pile up behind grain boundaries have to move to a certain slip system, increasing the forming speed will cause grains to rotate faster and dislocations to move faster too. The result is a faster development of slip systems within the microstructure and therefore failure is obtained at a lower forming height and force. When the

proportionality between strain-rate and forming speed was considered, as deduced form the definition of strain-rate, it can be said that increasing forming speed resulted in an increased strain-rate. As a result, higher strain-rate sensitivity resulted in restricted deformation, contrary to what is known about material behavior at the macroscale. It can be said that with increasing miniaturization, higher forming speeds tend to restrict deformation depth in thin sheet microforming.

Limiting values	Forming speed (µm/s)			
	1.5	15	150	1500
Dome height (µm)	501.50	500.56	468.41	404.18
Force (gm)	2829.26	2709.30	2578.08	2378.22

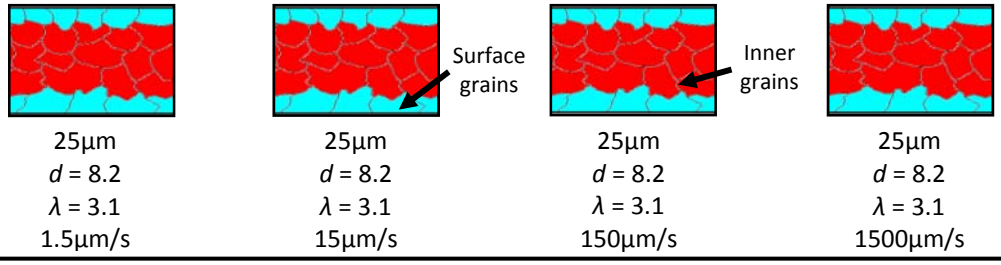

Figure 5- 11 Comparison of limiting values of 25µm microformed CuZn30 sheets

Limiting values	Forming speed (µm/s)			
	1.5	15	150	1500
Dome height (µm)	705.58	680.36	584.47	451.59
Force (gm)	6355.31	6107.37	5265.38	3688.09

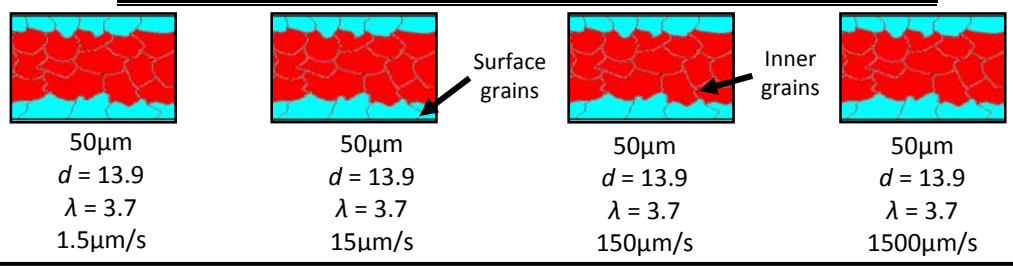

Figure 5- 12 Comparison of limiting values of 50µm microformed CuZn30 sheets

Since both tested thicknesses demonstrated the same behavior (*Figures 5-11 & 5-12*), the previous explanation is generalized for microformed *CuZn30* thin sheets. The drop in limiting heights and forces was stills greater for 50µm sheets than that of 25µm ones and a steeper rate of decrease was detected for the thicker sheets (50µm), as indicated earlier. The detected drop increase with increasing thickness can be explained by comparing the thickness-to-grain-size ratio λ for both tested thicknesses. From *Table 5-3*, the λ ratio for 50µm and 25µm were 3.7 and 3.1 respectively. In other words, 50µm thin sheets have more grains across its thickness than 25µm ones, therefore, more dislocation density will be present at grain boundaries, which will result in more hindering to grain deformation [47, 48].

5.6.2 Constant Forming Speed with Varying Thickness and Grain Size

Thickness (µm)	λ	d (µm)	Limiting height (µm)	Limiting force (gm)
25	3.1	8.2	500.56	2709.30
50	3.7	13.9	680.36	6107.37

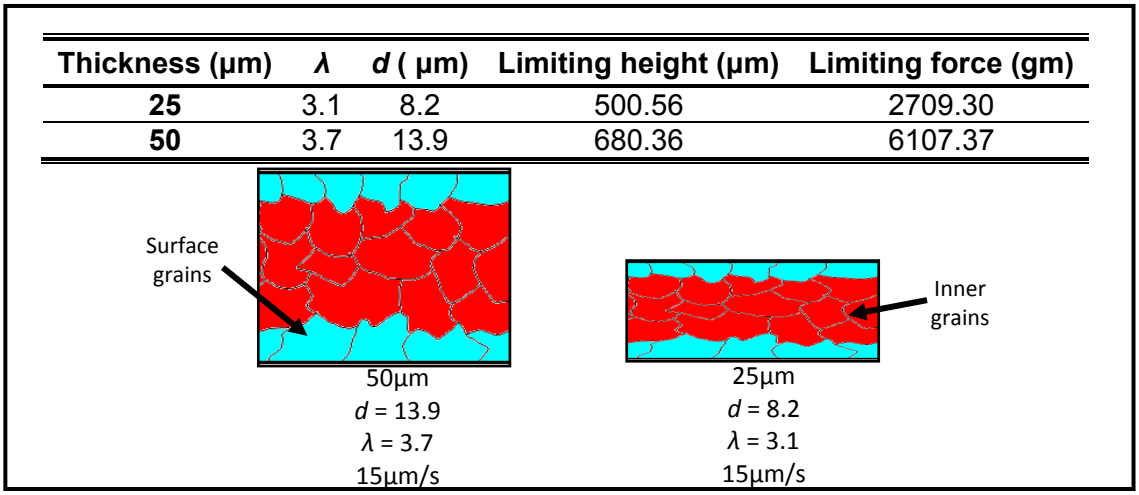

Figure 5- 13 Comparison of limiting values of microformed CuZn30 sheets at 15µm/s

In this case, limiting heights and forces of *CuZn30* tested sheets decreased with decreasing thickness along with decreasing grain size and λ ratio (*Figure 5-13*) for all tested speeds. As stated earlier, grain boundaries tend to act as obstacles to slip

dislocations, which are responsible for plastic deformation [47]. By considering the λ ratio for both thicknesses, there were slightly more grains through sheet thickness for 50µm thin sheets than that through 25µm ones. Knowing that the planar geometry of the bulged area is the same for both thicknesses and considering the grain size difference (around 70%); we can say that 50µm deformed specimens had fewer deformed grains than 25µm specimens, due to the clear variation in grain size and λ ratio. Hence, less grain boundary density will be present in the 50µm deformed specimens and fewer obstacles to slip dislocations will develop, which will lead to less needed forces for deformation. Therefore, for thin sheet testing, we can say that limiting values increase with increasing thickness and decreasing number of deformed grains.

5.6.3 Constant Thickness and Grain Size with Varying Friction Effects

Lubrication	Limiting height (µm)	Limiting force (gm)
Dry	549.6	2984.6
WD-40	569.8	2905.3
Teflon	557.0	2841.7

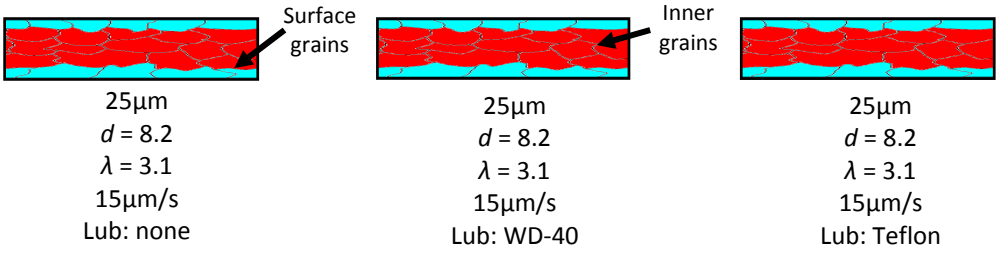

Figure 5- 14 Comparison of limiting values of lubricated 25µm microformed CuZn30

In the case of varying friction effects by means of applying lubrication to the bulge testing process, it can be seen in *Figures 5-14 & 5-15* that the limiting values of

dome height and accompanying loading were not affected to a large extent. As presented in *Table 5-4*, the percent variation in both parameters did not exceed 6.5% which can be considered as a negligible value when compared to present readings. The explanation to this material behavior, which is contrary to what is known about lubrication testing at the macroscale, can be explained by the model of open and closed lubricant pockets model proposed by Geiger et al. [1,75,78] as seen in *Figure 5-16*.

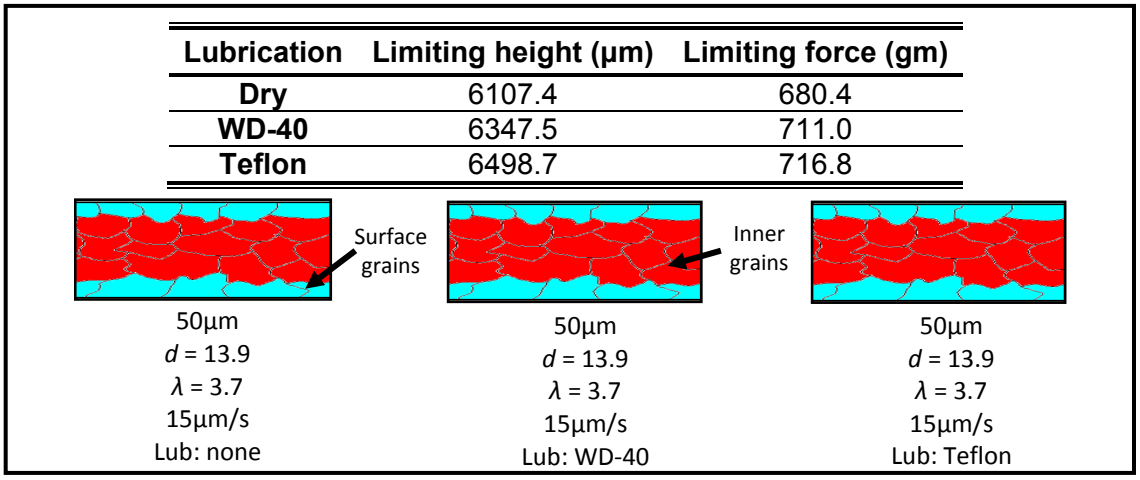

Figure 5- 15 Comparison of limiting values of lubricated 50µm microformed CuZn30

Since the tested as-received *CuZn30* thin sheets, which were rolled into the obtained thicknesses, did not demonstrate a completely flat surface, roughness peaks develop on surfaces. These roughness peaks are accompanied by roughness valleys. At the macroscale, applying lubrication to tested sheets will cover the roughness valleys with trapped lubricant, and will consequently redistribute forming loads that reduces the applied normal pressure. This behavior could not be achieved for the microformed thin sheets in this study. The reason for this is that the hemispherical geometry of the forming punch could not cover the roughness valleys and trap the lubricant. Instead, the lubricant

escaped from the asperities while the punch was applying deformation forces and only roughness peaks. The presence of open pockets in lubrication testing is said to occur where the deformation is applied on a free-surface workpiece, as seen in the microbulged *CuZn30* thin sheets.

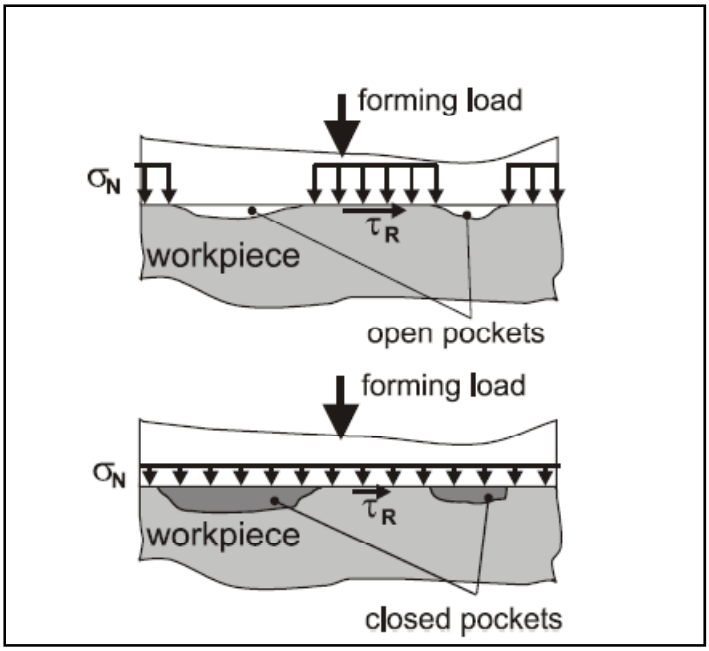

Figure 5- 16 Open and closed lubricant pockets [1]

Table 5-5 Characterization of parameters effect for selected scenarios

Constant parameters	Dome height	Max force	*t*	*d*	*λ*	speed
Thickness and grain size	↑	↑	-	-	-	↑
Forming speed	↑	↑	↑	↑	↑	-

5.7 Concluding Remarks

An investigation for identifying the influence of size effects on thin sheet formability by varying identified key process parameters in microbulging of *CuZn30* and

Al1100 was conducted. The identified parameters were forming-punch speed, sheet thickness, grain size, and lubrication. In all performed tests, limiting dome-heights and limiting forces of hemispherical-microbulged thin sheets were measured and presented for comparison. From the obtained results, it can be said that altering the process parameters in thin sheet formability at the microscale had an effect on the outputs of the process. Analysis of *Al1100* bulging profiles was not considered since it demonstrated an inhomogeneous microstructure with elongated grains along thin sheets' rolling direction; resulting in an independent sensitivity of limiting values to forming speed. For microbulging of *CuZn30*, limiting dome-heights and forces were dependent on the forming speed. Both height and force limits decreased with increasing speed, which indicated the size effects on miniaturization. The size effect was identified by the limited dome height or forming depth with increasing forming speeds as miniaturization in applied, which is opposite to the behavior of the same material at the macroscale. Although the recorded reduction was in the range of 15-40%, considering the scale at which the process is conducted gives a reason to regard these variations as partially significant for thin sheet formability at the microscale level. The discovered speed dependency was explained by the mechanism of plastic deformation. Sheet thickness showed a major influence on microforming of thin sheets, similar to the macroscale. Thickness effects were explained by the comparison of grain boundary density and accompanying dislocations that assist in material deformation. Thicker sheets displayed higher limiting dome-height but required higher forming loads than thinner ones. Therefore, if a thinner sheet is utilized for loading limitations at the microscale, designers and manufacturers should compensate for the reduction in formality, which might

sometime be within the allowable range as seen in the 10% reduction in limiting dome height between 50μm and 25μm microformed *CuZn30*. It was concluded that the limiting values increased with increasing thickness along with decreasing number of deformed grains. Thicker sheets had a steeper trend of dropping limiting values with increasing forming speed than thinner ones. This was explained by the increased limitation for grains to rotate and deform in thicker sheets, since they demonstrated a higher grain boundary density through thickness. The average grain size seemed to influence the formability of thin sheets at microscale too, especially when the thickness-to-grain-size ratio λ is considered. In order to obtain a certain dome height in *CuZn30* testing, sheets with a higher λ ratio needed higher forces for thin sheet deformation. This was due to the increasing number of grains across thickness which consequently increases restrictions on deforming grains too, as mentioned in Chapter Three. Lubrication did not impose a significant effect on limiting forming loads and heights. This conclusion is based on recorded variations of no more than 6.5% for both parameters between lubricant tested thin sheets and dry tested ones. Open and closed lubricant pockets were the model by which this behavior was explained. It was concluded that with increasing miniaturization, lubrication starts to take less effect on lowering forming loads in thin sheet formability.

From this study it can be seen that incorporating the investigated process parameters for characterizing formability at the microscale can be sufficient for uniaxial testing, but is not enough to address the characterization of thins sheet formability with formability regarded as biaxial since we are dealing with microscale thicknesses. Therefore, investigations on surface strain limits will be conducted on microbulged thin sheets in Chapter Six in order to expand the study on size effects. Again, the presented

information can be of extremely vital for “design for manufacturing” (DFM) techniques for currently applied microforming processes; which mostly utilizes such statistical and experimental information.

CHAPTER SIX

CHARACTERIZATION OF THIN SHEET FORMABILITY AT THE MICROSCALE LEVEL

6.1 Introduction

The need to overcome the drawbacks of using conventional macroscale testing equipment to measure and characterize formability at the microscale was discussed in Chapter Four. As a result, a microforming setup which demonstrates high precision and tight tolerances was introduced to accommodate the requirements of microscale testing and analysis. Since the 1950s, significant efforts were put into optimizing sheet metal forming processes, which drew a substantial interest from researchers as well as related industries [38-45]. Eventually, several methods and apparatus were introduced for characterizing sheet formability. In Chapter Three, one of these methods was used for analysis. Yet again, applying any of the conventional methods cannot accommodate the highly regarded requirements of accurate thin sheet formability at the microscale level, as mentioned in Chapter Four. Also since there is an increasing interest in utilizing microforming processes for the micromanufacturing industry, a more suitable method for characterizing sheet formability at the microscale is needed. In this study, an innovative approach towards characterizing formability of thin sheets for microforming applications is introduced. This approach is manifested by a microforming setup which was designed and built for conducting micro-bulge forming tests on thin sheets (Chapter Four). The testing procedure is complemented by a photolithography process, an electron microscopy technique, as well as a state of the art method for measuring surface strain limits at the microsclae level using an automated-strain-measurement commercial software package along with a designed and fabricated micro-target element which is responsible for identifying curved surfaces for accurate measurement of strain limits. The

proposed method, which was based on scaling down the strain measurement technique according to the ISO: 12004 standard for determining forming limit diagrams [76], is ultimately meant for constructing FLDs at the microscale level, which can be applied as a predictive tool that will eliminate the empirical techniques that are currently administered, and is expected to eventually lower the overall manufacturing cost. In this study, a new method for characterization of thin sheet formability is introduced. Investigation of size effects on limiting surface strains in thin sheet formability by considering the sheet thickness, average grain size, and lubrication was addressed as a major part of the overall objective for optimizing thin sheet formability at the microscale level.

6.2 Experimental Procedure

The proposed procedure is similar to the conventional method of sheet formability testing of metal alloys in automotive applications by determining FLDs with the exception of the varying geometrical sale. Existing microscale techniques as well as newly developed ones were incorporated for characterizing formability at the microscale. The procedure is divided into four major stages: Photolithography for thin sheet marking, microforming for thin sheet deformation testing, SEM imaging for failure capturing, and formability analysis for calculating surface strain limits. Tested material was *CuZn30* with 25μm and 50μm thicknesses. Detailed description on the procedure is presented in the subsequent sections.

6.2.1 Photolithography and Thin Sheet Marking

The photolithography technique was applied for marking a grid pattern on the surface of thin sheets, similar to the technique of marking at the macroscale obtained by electro-chemical etching. A micro-laser-etched photomask was developed for this purpose (*Figure 6-1*) with an 8x8 array of single grid arrangements for mass production of test specimens. Each single arrangement consists of a rectangular grid of circles 50 μm in diameter and is scaled from the conventional technique proposed by Keeler [38]. The applied photoresist is a Micropost *S1813* photoresist which was supplied by Shipley Co. This photoresist was spin-coated on the thin sheets at 4000 rpm for 30 seconds to form a 1.5μm uniform film thickness. Coated specimens were then baked at 110˚C for one minute to ensure sufficient bonding between the photoresist and thin sheet.

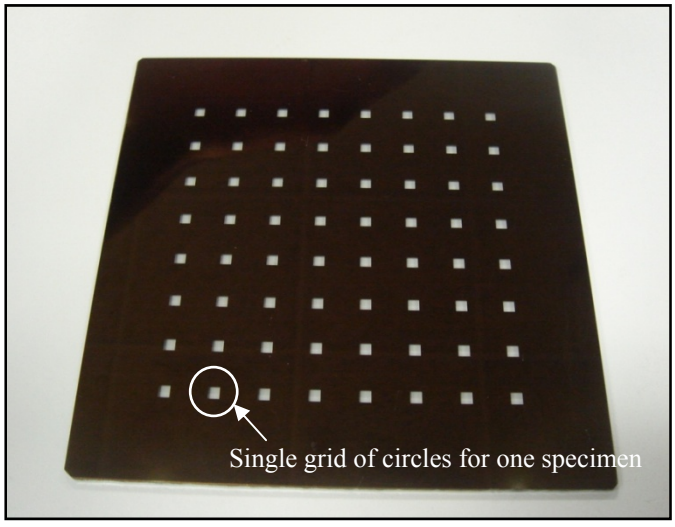

Figure 6- 1 4"x4" Micromachined Photomask with 64 separate arrangements

The coated specimens were then exposed to ultra-violet rays through the photomask and were baked at 110˚C for one minute. This caused the exposed part of the photoresist to nucleate. The final stage of thin sheet marking was specimen developing, where exposed coated specimens were immersed into an AZ400 positive developer provided by DATAK Corporation for one minute. This resulted in a well bonded and defined pattern of circles as seen in *Figure 6-2*. *Figure 6-3* details the steps for achieving well defined markings on the specimens. A detailed procedure for thin sheet marking is described in Appendix VIII. This marking technique resembled the spray painting technique for capturing in-situ deformation using the ARAMIS® [77] optical deformation and strain measurement system where a random pattern with well defined contrast has to be applied on the surface for characterizing formability.

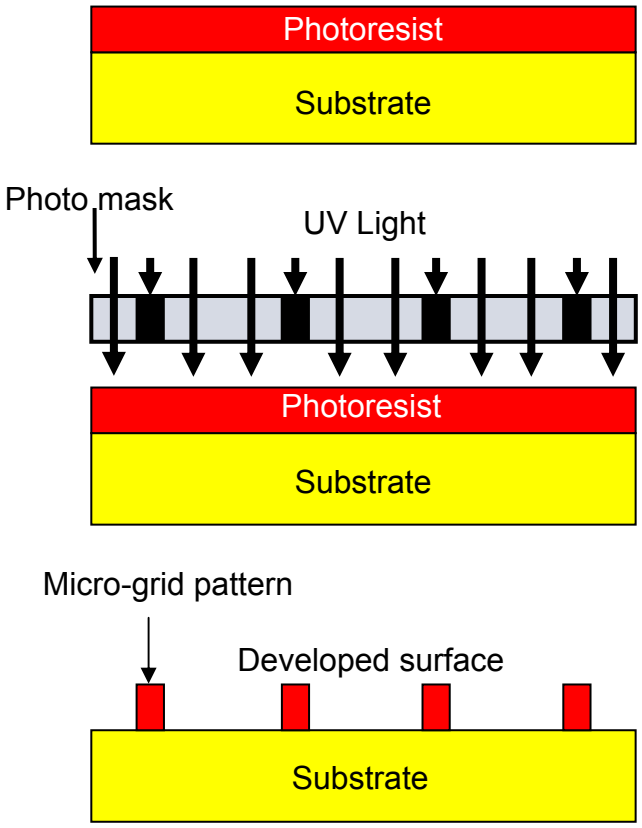

(a)

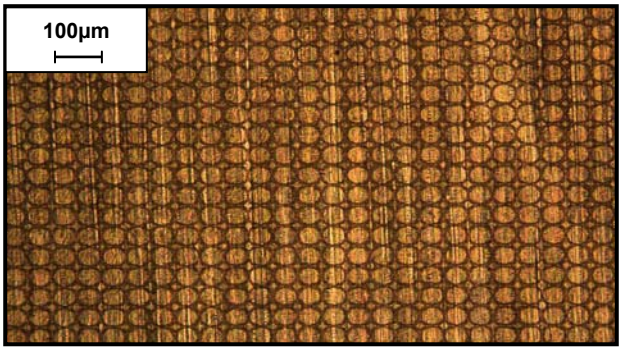

(b)

Figure 6- 2(a) Photolithography process and (b) Micro-grid pattern on a developed thin sheet surface

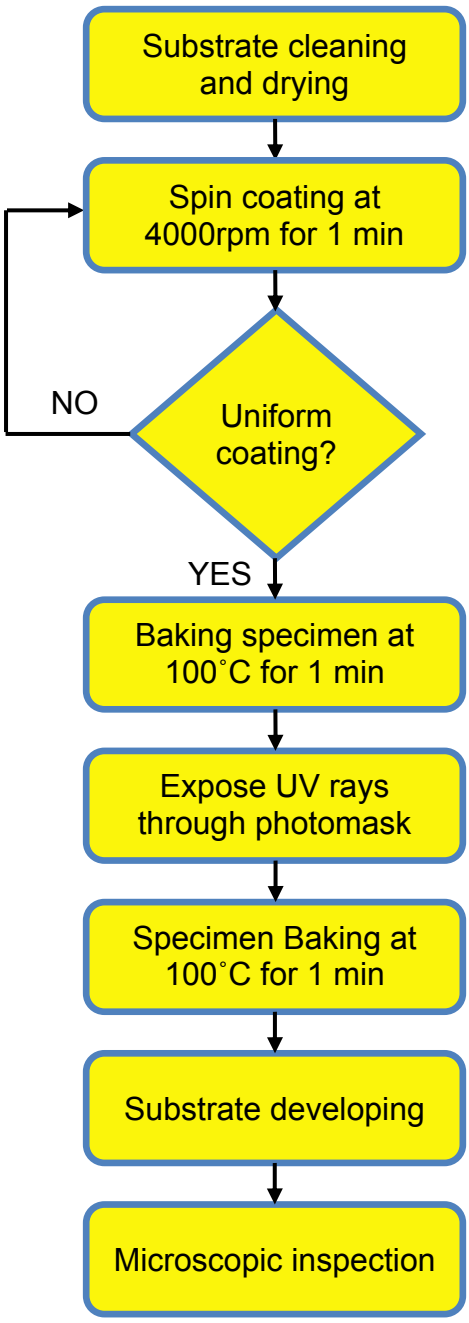

Figure 6- 3 Procedure for achieving grid markings on the tested thin sheets

6.2.2 Microforming of Test Specimen

For the microforming process, as described in details in Chapter Four, marked specimens were prepared by cutting them into 9x9mm size and clamping them between the two die halves before applying the bulging process that is controlled electronically and is stopped at a certain level of force drop; usually between 10 and 15%. Extra care was taken while cutting, mounting, and transferring specimens in order to preserve the micro grid-markings before and after testing. Specimens were then stored in containers in order to be examined in the following stage. *Figure 6-4* shows how the specimen is mounted onto the die before placing the latter onto the kinematic coupling grooves and performing the microbulge test.

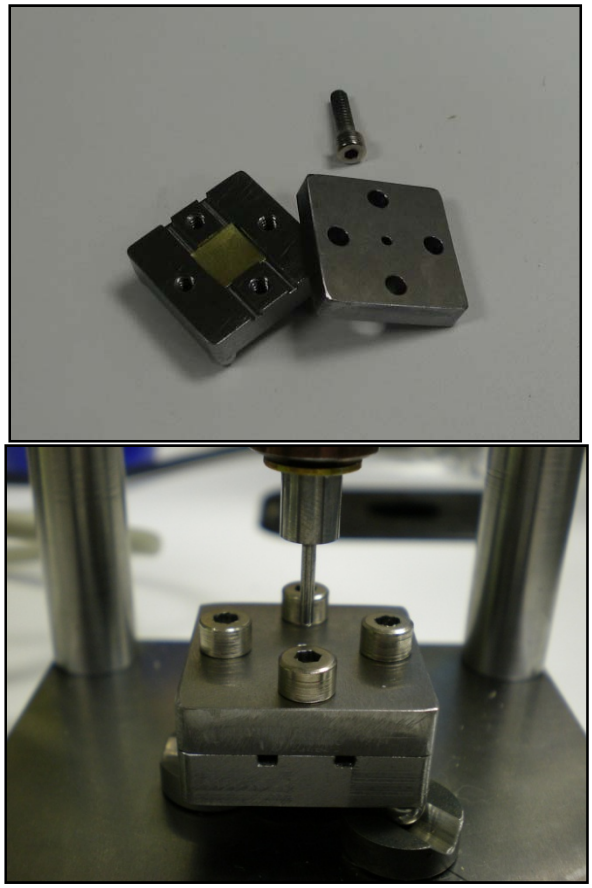

Figure 6- 4 Specimen mounting and die placement before microforming

6.2.3 Failure Capture by SEM Imaging

Scanning electron microscopy was used to assist in capturing the failure area on tested thin sheets. Images of the deformed specimen at the vicinity of the formed crack were captured using a HITACHI S3200 SEM machine (*Figure 6-5*). *Figure 6-6* shows an SEM image of a deformed sheet around the area of diffuse necking. By identifying random cracking of some deformed circles, it can be said that the layer of markings was sufficiently bonded onto the thin sheets, and according to the photoresist's physical properties, the marking layer should deform with the thin sheets in a continuum manner. Experimental verification to the bonding issue will be presented in the next section. *Figure 6-6* shows some parts of a bulged specimen which had the markings chipped off while preparing the specimen for testing as well as SEM imaging.

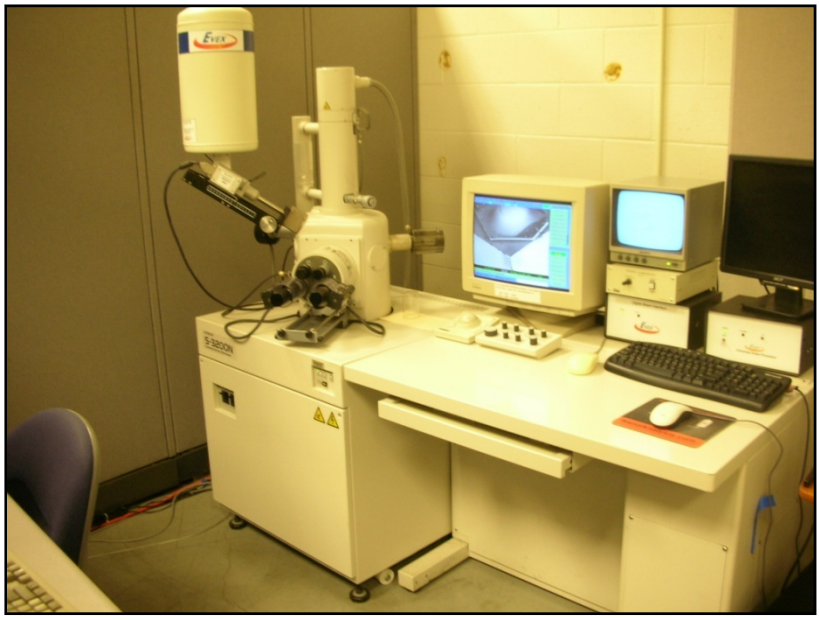

Figure 6- 5 HITACH S3200 SEM

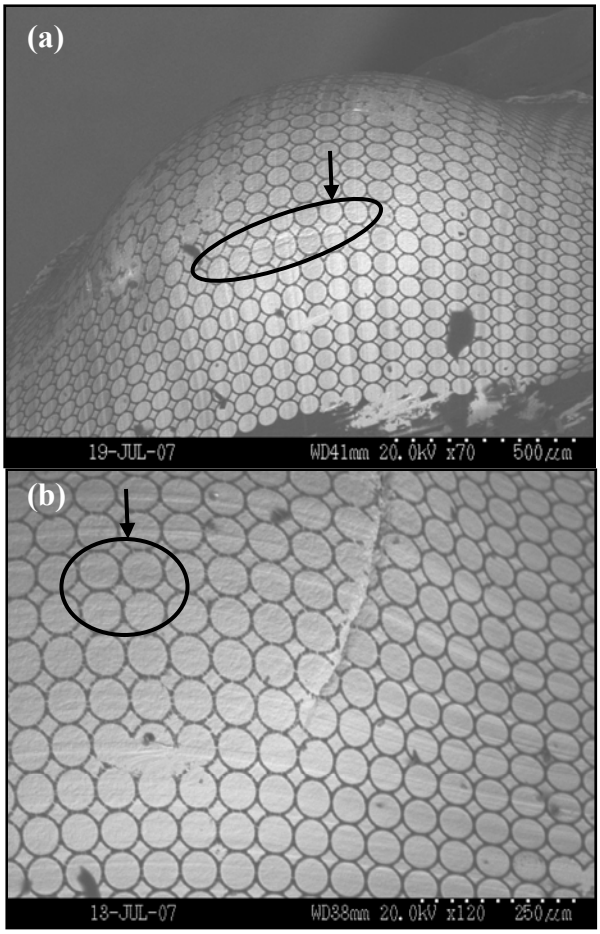

Figure 6- 6 SEM images of (a) micro-bulged thin sheet at failure, and (b) chipped off markings

6.2.4 Analysis of Deformed Thin Sheets

Preliminary analysis of the deformed grids were conducted by manual measurement of deformed circles around the formed crack from SEM images which yields limiting surface strains, assuming flat surfaces around the crack region. The results and analysis of this method of strain measurement will be presented in the following section. To accommodate for three-dimensional measurement in calculating surface strains of the deformed grids, which is an essential requirement for assuring proper and correct results, the ASAME (Automated Strain Analysis and Measurement Environment)

software was used, as described previously in Chapter Three for determining strain limits of bulged sheets at the macroscale. In order for the software to measure strains accurately, a target element that enables the software to recognize accurate strain measurement in three-dimensional space is required. The target element has a size of 25mm side and contains an identified grid as seen in *Figure 6-7*. The deformed grids of microformed specimens could not be captured by a conventional digital camera, therefore SEM imaging was used to identify the deformed grids around the crack area instead, and a cubic target which can be viewed around the vicinity of the micro crack was needed. For this purpose, a microscale target element was designed with a 50 times scaling factor from the actual macroscale target resulting in a 500μm micromachined target element. This microtarget element was scaled down accordingly with the scaling of the circular grid pattern so that the transferred images would hold the same proportions to macroscale dimensions. Only three faces of the micro-target were micromachined on a corner of a ¼" steel cube. This provides the ASAME software with the required three faces for target recognition as well as the ease of target handling due to its critical size. *Figure 6-7* also shows an SEM image of the developed micro target element along with commercial one for size comparison. *Figure 6-8* demonstrates an actual bulged specimen along with the microtarget in an SEM image. *Figure 6-9* shows the output of automatically determined surface strain limit measurements using the ASAME software.

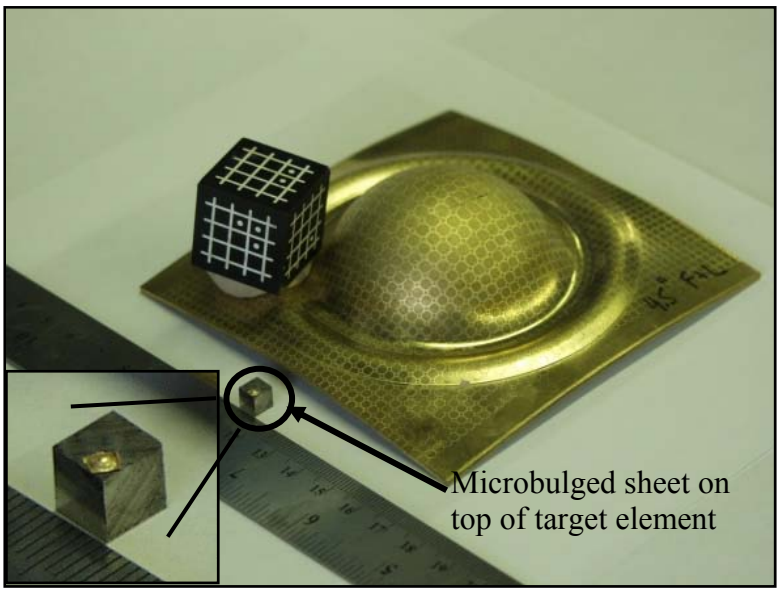

(a)

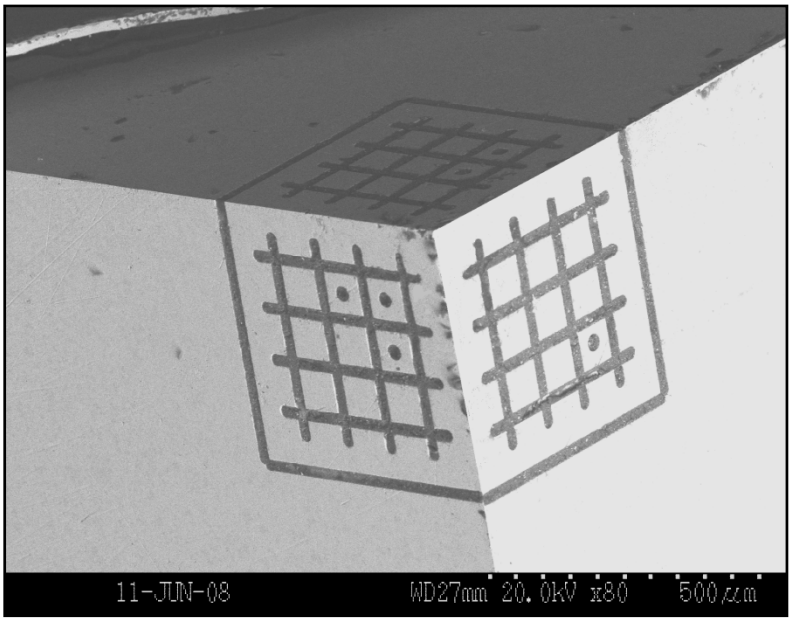

(b)

Figure 6- 7(a) Comparison between conventional target and micro-target element, and (b) SEM image of the micro-target element

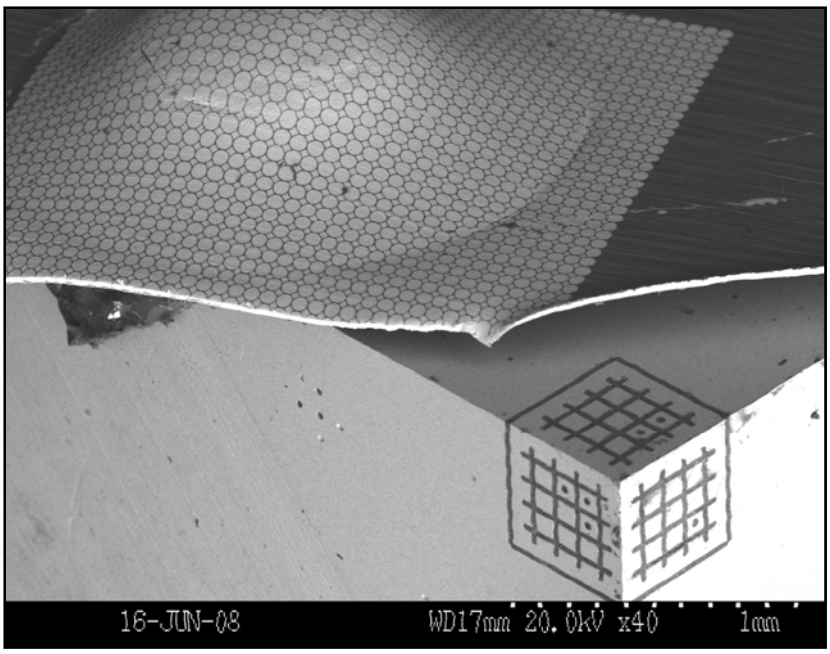

Figure 6- 8 SEM image of microbulged thin sheet along with microtarget

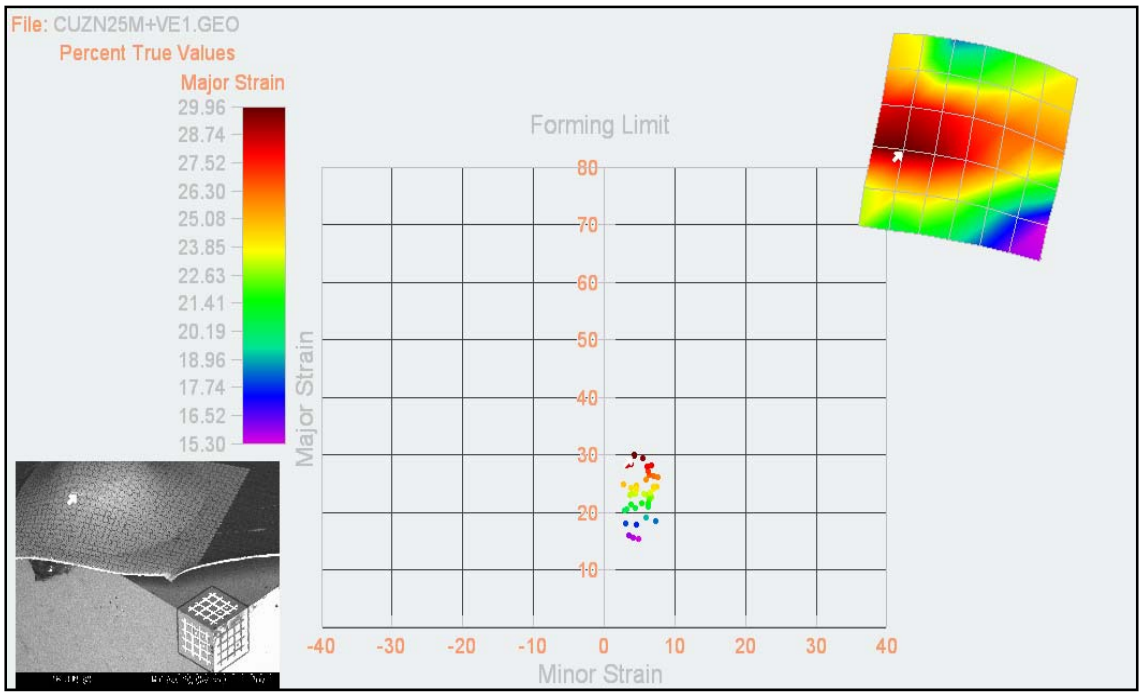

Figure 6- 9 Automatically determined strain limits using ASAME software

6.3 Characterization of Strain limits of Microformed Thin Sheets

Following the proposed method for determining surface strain limits of microformed thin sheets, actual testing was initiated on thin sheets of *CuZn30* which is, as previously stated, of major significance in electronic and MEMS applications. The investigation was initiated by establishing a proper justification for incorporating the automatic strain measurement concept over manual calculation as a feasible method for determining strain limits at the microscale. Following the procedure described above, thin sheet formability testing was conducted on 25μm and 50μm thicknesses under varying selected parameters: thickness, grain size, and lubrication.

6.3.1 Testing of automatic strain measurement and marking techniques

Surface strain measurements with manually calculated strain limits for the deformed *CuZn30* thin sheets are presented on the FLD shown in *Figure 6-10*. A horizontal scatter in the forming limit values was identified for that range of values in the FLD. The observed large scatter could be due to calculation errors arising from the assumption of flat surfaces around apparent cracks. It also could be due to the size effects on scatter in microforming processes, as described by Geiger et al. [1]. These authors discovered an increasing data scatter with increasing miniaturization while determining mechanical properties. Since the manual method of calculation is subjective and depends on how the three dimensional measurement of strain limits for the deformed grids is identified, the ASAME software was utilized to assure correct measurements. *Figure 6-10* shows two sets of automatically determined strain limits under the same process conditions of the manually determined strain limits. The automatically calculated strain

limits clustered around a line with a slope which represents a biaxial strain ratio ($\varepsilon_1/\varepsilon_2$=1). As a result, a justification for obtaining a more accurate method for determining thin sheet formability at the microscale was made viable; especially when confirmed with results of repeated tests.

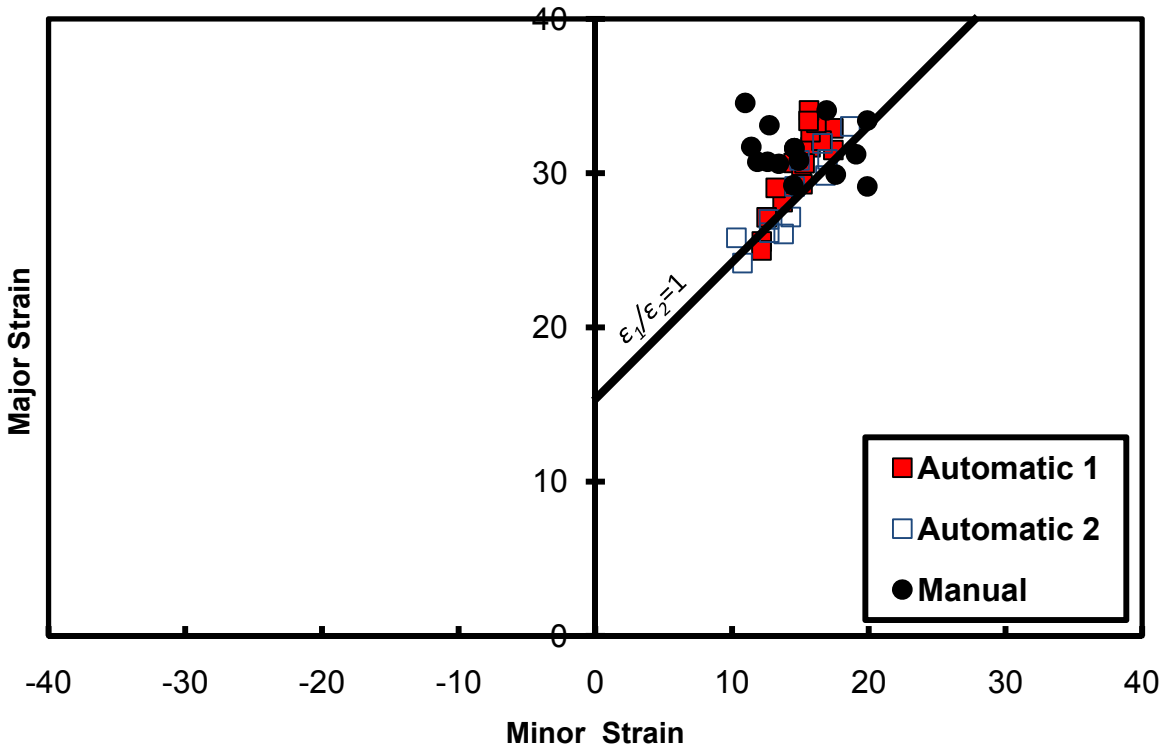

Figure 6- 10 Strain limits of microbulged sheets determined by manual and automatic calculations

The next step in testing the new automatic method was to verify adequate bonding between the photoresist markings and thin sheet specimens to prevent any shearing effect between them and to ensure proper representation of thin sheet formability by grid deformation. This was accomplished using test specimens marked by two different types of commercial photoresists. The first one was a Micropost *S1813*® positive photoresist

provided by Shipley Co. while the second was an *AZ5214*® positive/negative photoresist provided by DATAK Corporation. The photolithography process described in Section 6.1.1 and Appendix IX was used to mark the specimens. The marked specimens for each photoresist were then microbulged up to failure points. Consequently, automatic strain measurements were then performed on the tested specimens to determine their surface strain limits. *Figure 6-11* shows a plot of strain limits for a microformed 25µm *CuZn30* thin sheet with *S1813* and *AZ5214* positive photoresists. The lower bounds of strain limits are represented by surface strains calculated at 100µm away from the diffuse necking point, or tip of the crack. It can be concluded that the strain limits for the two types of photoresist markings were somewhat identical because they occupied the same region on the presented FLD (*Figure 6-11*), although they had different chemical compositions. From this observation, it can be concluded that the bonding of *S1813* photoresist is sufficient enough to be regarded as part of the deformed thin sheets during the microforming process, and that the geometrical representation of surface strains by the photoresist marking is considered feasible under the given experimental conditions.

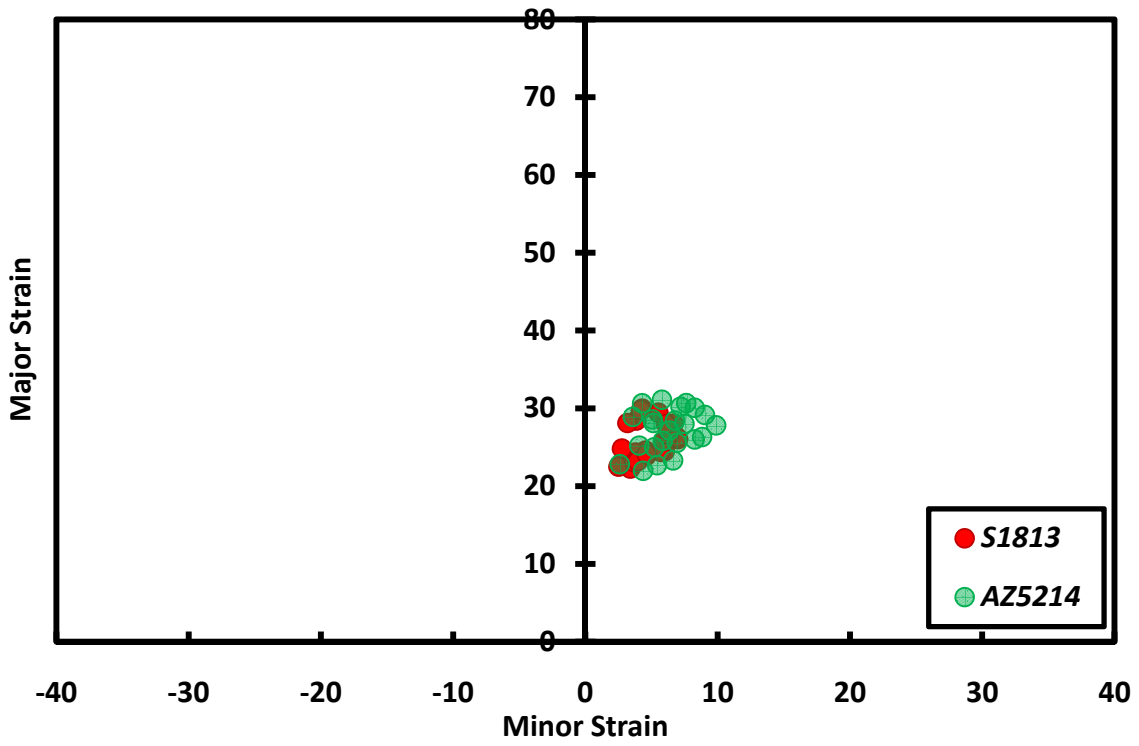

Figure 6- 11 Comparison of strain limits for S1813 and AZ5214 photoresist markings on 25µm CuZn30 thin sheets

6.3.2 Results and data collection

Formability testing using the proposed microbulging method was conducted on *CuZn30 at* 25µm and 50µm thicknesses. Allowable strain limits, or lower bound limits, were designated as surface strains of deformed circles located at 100µm away from the developed crack. *Figure 6-12* shows strain limits of 25µm and 50µm *CuZn30* tested sheets. The allowable strain ratios for hemi-spherically bulged samples are bounded by the lines of critical strain limits, which define the critical strain ratios for biaxial deformation, and consequently the marked safe regions were mapped on the FLD.

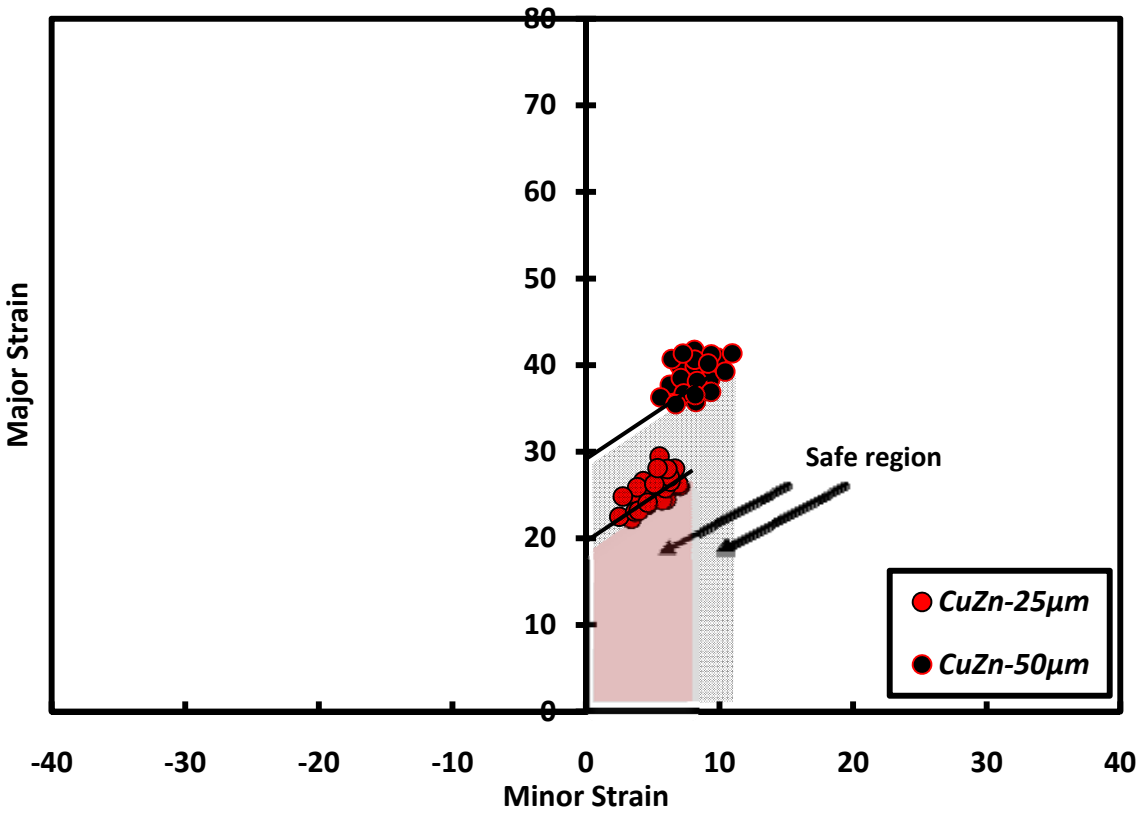

Figure 6- 12 Strain limits of microbulged CuZn30 thin sheets

In order to incorporate both size effects and friction on surface strain limits with this investigation, an additional set of experiments with lubrication testing of the same thicknesses was added. Du Pont Teflon® lubricant was particularly chosen for testing the effect of lubrication because it is commonly used in the construction of FLDs to expand strain limits of balanced biaxial stretching conditions beyond its dry forming limits [49, 69-72]. For each test, a marked specimen was clamped inside the die and placed on the kinematic coupling grooves on the microforming fixture, and then a drop of Teflon was added to punch-sheet interface side of the specimen. Due to the sufficient clamping of the specimen between the die halves, the rest of the specimen surface was sealed from any

lubricant contamination that can affect the gripping characteristics of the die. At the end of each test, the die had to be cleaned with alcohol to eliminate any presence of lubricants in the die cavity. For comparison and data analysis, strain limits of 25µm and 50µm lubricated specimens were plotted along with dry tested sheets, as seen in *Figure 6-13*. Again, for each case, the microbulging test was repeated three times for assessing statistical scatter. The limiting points that are presented on the FLD represent the extreme formability case, considering a biaxial state of deformation. Straight lines with a slope of unity were plotted for each case as an indicator to the deformation state. To analyze size effects on thin sheet formability from a surface strain limit point of view, strain limits of dry macroformed thick sheets, which were determined and presented in Chapter Three, were plotted along with the limits of the microbulged thin sheets in *Figure 6-14*.

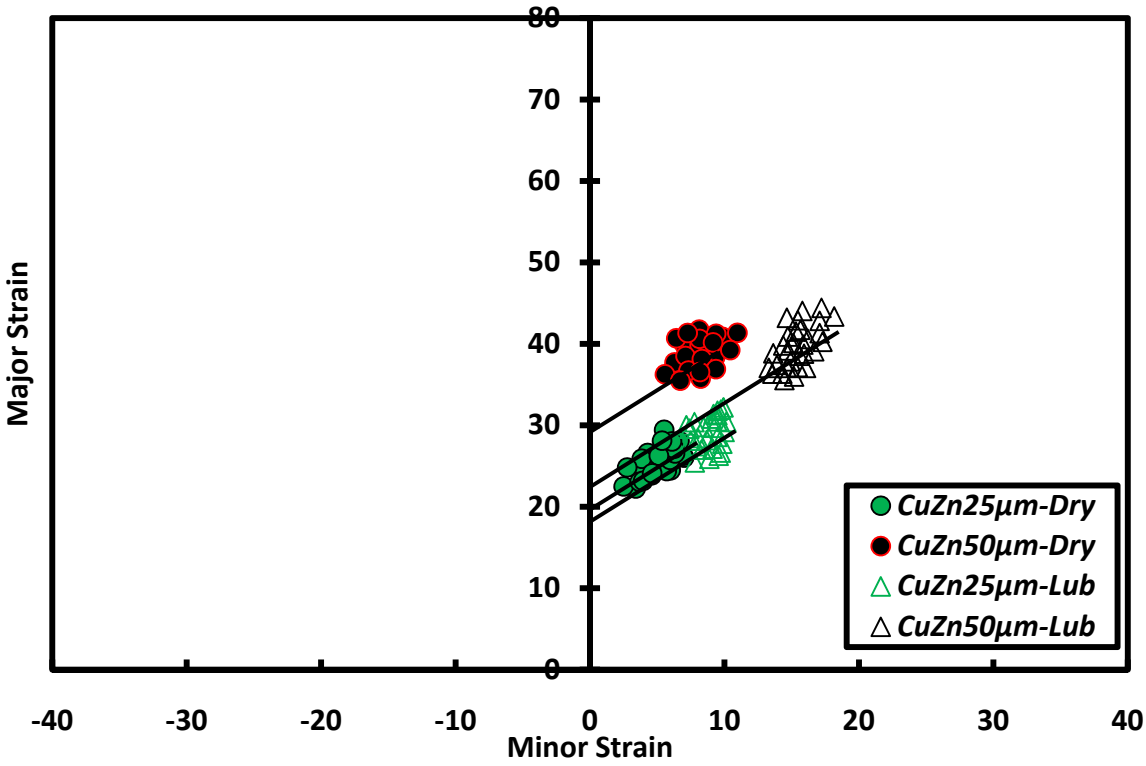

Figure 6- 13 Strain limits of 25µm and 50µm CuZn30 thin sheets in dry and lubricated (Lub) states

Furthermore, to investigate size effects on friction for sheet formability, another set of formability tests were conducted on 2mm, 1mm, and 200µm thick sheets on the Tinius-Olsen cup test by following the same steps that were discussed in Chapter Three. The added task in this set of experiments was applying a lubricant to the punch-sheet interface side of the specimen. The lubricant used was Du Pont Teflon®, which was sprayed onto the specimen surface. Strain limits of macroformed lubricated sheets were determined automatically using the conventional method presented in Chapter Three where the ASAME software was used. *Figure 6-15* shows a FLD with strain limits of all tested thicknesses of each scale at dry and lubricated conditions. The presented data were considered as the required results for addressing size effect on surface strain limits, or formability, at the microscale.

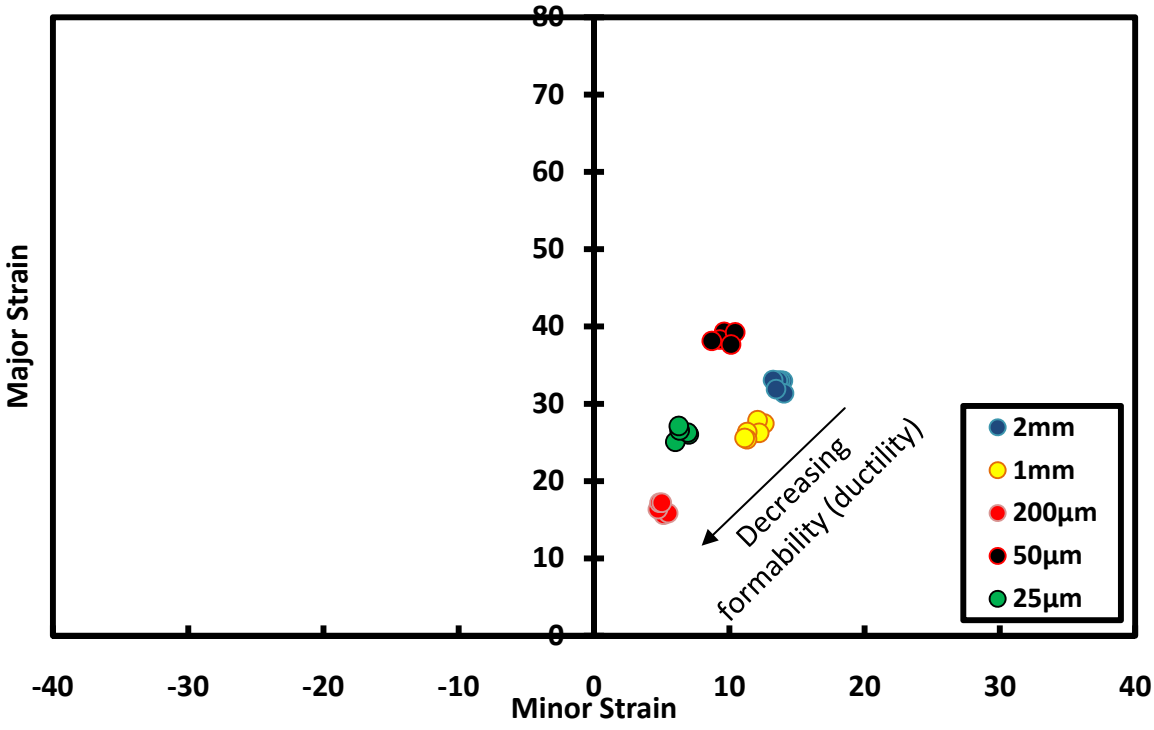

Figure 6- 14 Strain limits of microbulged CuZn30 thin sheets (25µm and 50µm thickness) and macrobulged CuZn30 sheets (2mm, 1mm, 200µm) under dry conditions

In order to relate size effects to the major influencing parameters in this study, grain structure analysis was also conducted for all types of sheets and their related values are presented in *Table 6-1*. Thickness, average grain size d, thickness-to-grain-size ratio λ, number of surface grains N_s and number of inner grains N_i and the ratio between them N_s/N_i, and the total number of deformed grains N_t were the parameters of comparison in this investigation.

Table 6-1 Calculated numbers of both surface and inner grains for Micro- and Macro-bulged CuZn30 sheets along with grain size d and thickness-to-grain-size ratio λ

Thickness (μm)	N_s (x10^6)	N_i (x10^6)	N_t (x10^6)	N_s/N_i (%)	d (μm)	λ	Scale
2000	1.730	91.786	93.517	1.88	55.5	36.1	Macro
1000	5.961	293.075	299.036	2.03	29.9	33.5	
200	20.816	369.491	390.308	5.63	16.0	12.5	
50	0.018	0.012	0.094	24.06	13.9	3.7	Micro
25	0.005	0.036	0.228	27.99	8.2	3.1	

6.4 Discussion and Data Analysis

The analysis of determined strain limits and related size effects were addressed by categorizing the obtained results into four cases of comparison. The first case between microbulged thin sheets, the second case between lubricated microbulged thin sheets and dry tested ones, the third case tackled size effects on strain limits between macrobulged and microbulged sheets, and the fourth case incorporated lubrication at both scales. The presented analysis was based on the microstructural parameters seen in *Table 6-1*.

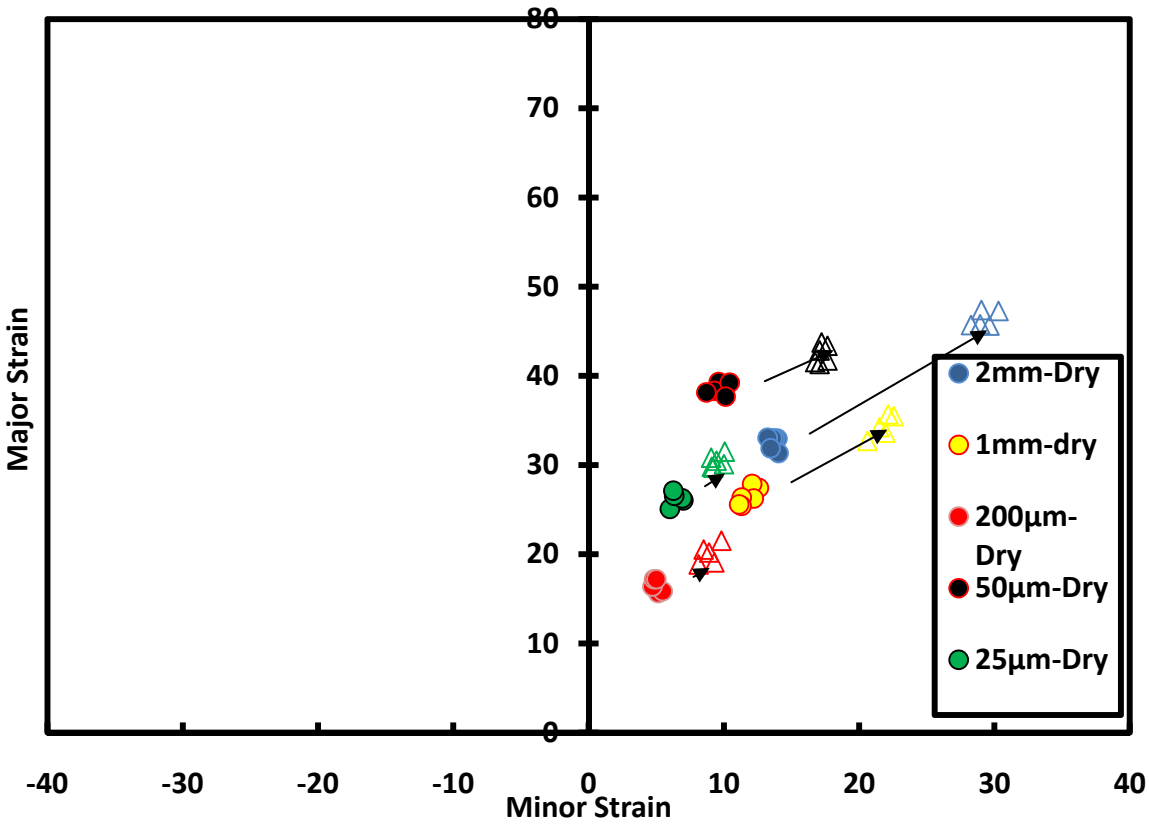

Figure 6- 15 Strain limits of microbulged CuZn30 thin sheets (25µm and 50µm thickness) and macrobulged CuZn30 sheets (2mm, 1mm, 200µm) for both dry and lubricated states

6.4.1 Microbulged thin sheets with varying thickness

Considering formability of *CuZn30* microbulged thin sheets at the microscale, formability decreased with decreasing sheet thickness as seen in *Figure 6-12*, similar to the behavior of sheet formability at the conventional macroscale level presented in Chapter Three [39-45]. A wider range of permissible strain ratios can be applied on 50µm thin sheets when compared to 25µm ones; by identifying the safe region below failure point which occupied a bigger area for 50µm tested specimens (*Figure 6-12*). Still, a correlation between the allowable strain ratios taken from FLD diagrams and limiting

force and depth analysis (Chapter Five), as well as sheet thickness, has to be established in order to optimize the microforming process, especially knowing that part size and weight are of significant interest when considering micro-components assembly. In terms of values of strain limits, around 100% increase in stretchability for both major and minor strains was achieved by doubling the thickness of a 25µm *CuZn30* thin sheet (*Figure 6-12*), which may provide more flexibility in the complexity of a microformed part. On the other hand, the mass of the processed part will also double, which may exceed the weight requirements for an assembled microscale structure.

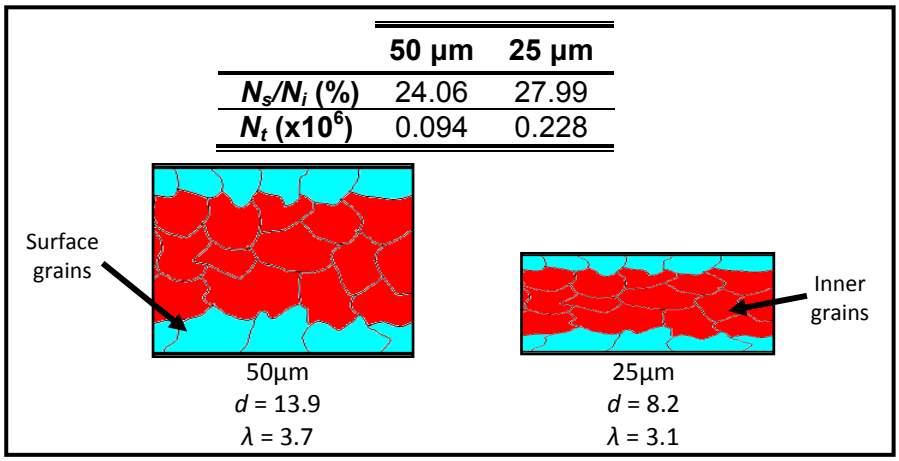

Figure 6- 16 Comparison between parameters of microbulged thin sheets

To explain the behavior of *CuZn30* in this case, microstructural parameters were considered (*Figure 6-16*). The higher formability of 50µm thin sheets in comparison with 25µm, was accompanied by a lower share of surface grains, which was the case in formability ranking of macroscale tested sheets of the same alloy, as was concluded in Chapter Three. The total number of deformed grains seemed to influence formability limits. Since the number of grains in the deformed volume of 50µm thin sheets was

almost half of that of 25μm, the accompanying lower grain boundary density, which affects the deformation of grains by locking dislocations, allowed for higher deformation strains and eventually better formability. From this observation, it can be said that at the microscale, not only thickness affects the formability of thin sheets, but also the total number of deformed grains has a significant effect on ranking the formability of microformed thin sheets. The share of surface grains did not affect the formability limits in this case. This effect is more dominant at the microscale than that at the macroscale level and seems to appear in coarse-grain microstructures, which agrees with macroformed coarse-grained *CuZn30* sheets presented in Chapter Three. In general limiting strains decreased with decreasing grains size and λ ratio.

Table 6-2 Effect of lubrication on strain limits of micro- and macrobulged CuZn30 sheets

Thickness (μm)	Increase in formability (%)		λ	N_t (x10^6)	Scale
	Major Strain	Minor Strain			
2000	43.8	107.1	36.1	93.517	Macro
1000	30.7	83.3	33.5	299.036	
200	25.0	80.0	12.5	390.308	
50	18.0	70.0	3.7	0.094	Micro
25	15.4	33.3	3.1	0.228	

6.4.2 Microbulged thin sheets in dry and lubricated conditions

It was possible to predict that lubricating *CuZn30* test specimens prior to its forming results in better formability (*Figure 6-13*) although the variations in limiting forces and dome heights were said to be negligible, as mentioned in Chapter Five. Although the limiting dome heights of the tested *CuZn30* showed a slight increase of 2% for 25μm specimens and 5% for 50μm specimens, surface strain limits showed an

increase of 15% in major strain and 33% in minor strain for 25µm specimens, and an 18% in major strain and 70% in minor strain for 50µm specimens (*Table 6-2*). Considering scale issues in microforming processes, it can be said that the increase in formability can be extremely utilized for material processing at the microscale level. By looking at the extension of strain limits by lubrication, strain limits of lubricated specimens increased more in the minor strain axis. This might mean that formability enhancement is also governed by the microstructure of the tested specimens; with only three or four grains across sheet thickness in this case. In other words, enhancing the formability of a coarse-grained thin sheet by lubrication will increase the formability in a certain strain direction more than in the transverse direction. The explanation to the effect of lubrication can be understood by incorporating the model of open and closed lubricant pockets [1, 75, 78]. Although it was mentioned in Chapter Five that the microforming of lubricated *CuZn30* thin sheets, that were considered as free-surfaces, could not contain the lubricant in roughness valleys to take advantage of the lubrication process, there seemed to be some surface pockets that did occupy the applied lubricant; causing them to be closed pockets. The result of such an assumption is a uniformly distributed load at the closed pockets which can be utilized in grain deformation instead of plastically flattening roughness peaks. Since the distributed load will act on a fewer number of deformed grains for the 50µm thin sheet when compared with 25µm thin sheets (*Figure 6-16*), the lower restriction on grain deformation will result in a higher increase in strain limits. In general, the increased effect of strain limits by lubrication seemed to decrease with decreasing thickness.

6.4.3 Microbulged thin sheets vs. Macrobulged sheets

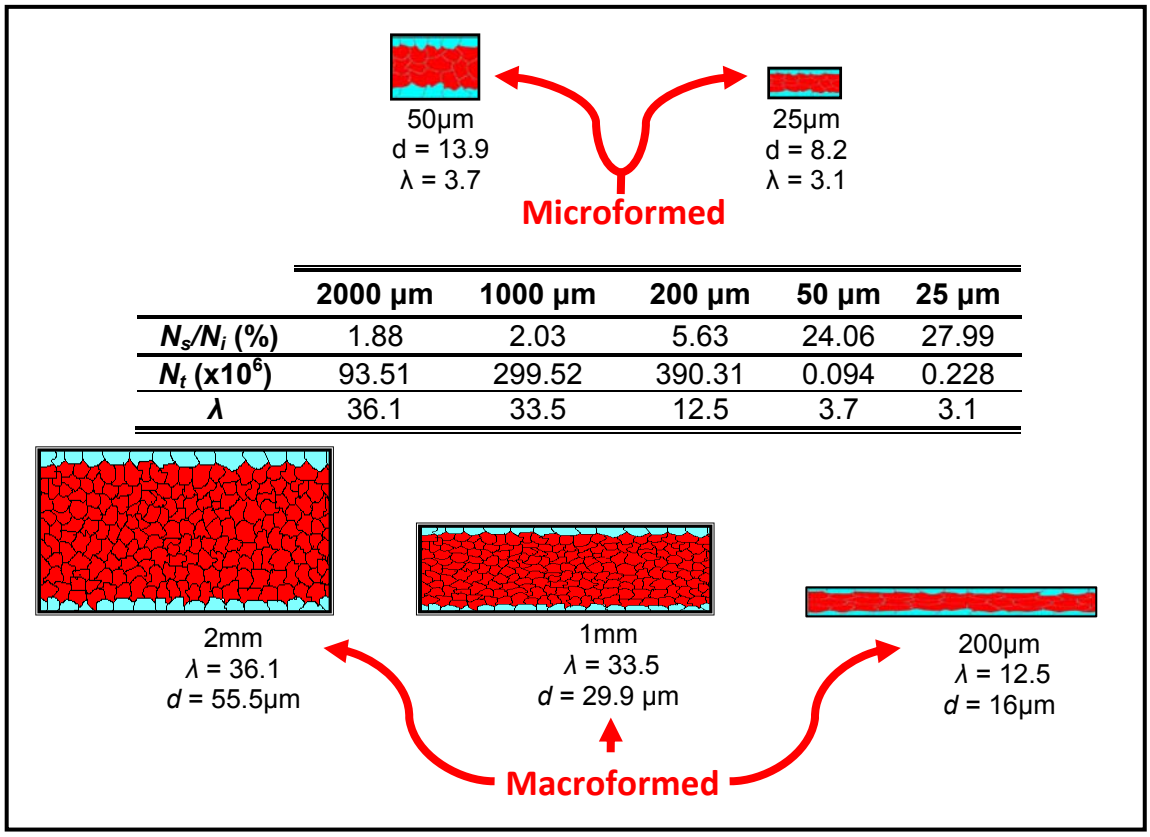

	2000 µm	1000 µm	200 µm	50 µm	25 µm
N_s/N_i (%)	1.88	2.03	5.63	24.06	27.99
N_t (x10^6)	93.51	299.52	390.31	0.094	0.228
λ	36.1	33.5	12.5	3.7	3.1

Figure 6- 17 Comparison between microformed and macroformed CuZn30 sheets

From the FLD in *Figure 6-14*, the trend of decreasing formability for spherically bulged sheets with decreasing thickness was clearly identified for both scales separately. Interestingly, strain limits of the microformed thin sheets were superior to that of macroformed ones, and did not follow the ranking of decreasing strain limits with decreasing thickness for macroformed sheets. The main reason for this behavior is the size effect in terms of a 50 fold geometrical scaling between the two scales. This is why the ranking of formability for the tested sheets at both scales could not be compared according to their thickness-to-grain-size ratios λ as seen in *Figure 6-17*. The reason for

the superior strain limits of the microformed thin sheets could be due to the significantly lower density of grain boundaries, resulting from having a lower number of deformed grains in its deformed volume, especially knowing that dislocations moving through grains tend to pile up at grain boundaries and retard the initiation of slip for plastic deformation [1, 18, 19, 37]. In this study, the surface layer model [1, 18, 19, 78] could not be validated for microformed thin sheets. The increase in surface-to-inner grain ratio N_s/N_i did not affect strain limits at the microscale (*Figure 6-17*). However, although 50μm and 25μm microformed sheets showed a high strain limit in the major strain direction, the strain limits were more restricted in the minor strain direction. This restriction might be due to the coarseness of the microstructure in microformed thin sheets, where grains occupy a bigger volume in the deformed samples and can result in an anisotropic behavior according to how grains will rotate to deform at its preferred orientation.

6.4.4 Microbulged thin sheets vs. macrobulged sheets in dry and lubricated conditions

The amount of increase in strain limits varied with thickness as well as geometrical scale. From *Table 6-2*, the increase in strain limits for all tested cases seemed to increase with increasing thickness and λ ratio. This relationship cannot be taken into perspective, since the geometrical scale eliminates the basis of comparison. Instead, by comparing the increase in strain limits of macroformed sheets to microformed thin sheets, it can be said that the increase in formability was greater for macroformed sheets (1mm, 2mm, and 200μm). The reason for this observation is due to better utilization of the

applied lubricant in macroformed sheets as seen in the model of open and closed lubricant pockets. For macroscale testing, the applied lubricant seemed to cover more roughness valleys than that in the case of microscale testing because the depths and widths of these valleys are almost negligible when compared surface area of the forming punch (60mm). Therefore, the applied film of lubricant will assist more in distributing the forming load, and consequently, increasing forming limits. On the other hand, applying the lubricant film in microscale geometries will not assist in distributing the load as efficient as in the case of macroscale geometries, hence, the increase in formability limits will be limited. This observation validates what is known about the decreasing ductility with increasing miniaturization in the form of increased brittleness. This brittleness can affect formability limits, but is still dependent on the type of material. Independent of the incorporating thickness and λ ratio in this comparison, a trend of decreasing ductility with increasing miniaturization was observed in thin sheet formability testing at the microscale. This result coincides with what is known about size effects on bulk microforming [1, 7, 9, 12, 13, 14, 18, 19]. In all cases, strain limits of microformed thin sheets were lower than that of macroformed sheets.

6.5 Concluding Remarks

A newly developed method for characterizing thin sheet formability at the microscale was introduced in this chapter. This method overcomes the obstacles and disadvantages that usually surface when considering micro-formability testing on conventional macroscale machines and apparatus. The method consists of four separate techniques. The first technique is a photolithography process for thin sheet marking with

a rectangular array of 50μm circles. The second technique is a microforming process of thin sheets by bulging until the initiation of a crack on its surface. The third technique is an imaging process using a SEM for failure capturing of deformed circles around the vicinity of the identified crack. The fourth technique is an automatic strain measurement process using ASAME commercial software and a developed microtarget to account for curved surfaces and 3D measurements. Strain limits of *CuZn30* with 25μm and 50μm thicknesses were achieved for dry formed specimens and lubricated specimens. Size effects were addressed from various aspects of affecting process parameters. Considering the thickness, thicker sheets showed better formability limits than the thinner sheets. This was due to the decreasing grain boundary density of thicker sheets resulting from the decreasing number of deformed grains in the deformed volume, similar to the behavior of macroformed *CuZn30* sheets. Correlation of allowable strain ratios and materials' size and weight can be made for especially in microscale assembly, and with imposed weight limitation. Lubrication seemed to enhance the formability of the microformed thin sheets. From the model of open and closed lubricant pockets, it was concluded that some surface pockets did occupy the applied lubricant, although the process was an open die forming process that cannot trap the lubricant between the die and tool, and more loading was distributed on the surface to act on the deformation of grains instead of plastically deforming roughness peaks. The increase in strain limits that was obtained with lubrication dropped with decreasing thickness due to the increasing restriction of the grains for 25μm thin sheets which are larger in number than that of the 50μm ones. Strain limits of the microformed thin sheets were superior to that of macroformed ones, and did not follow the trend of decreasing formability with decreasing thickness due to the

geometrical size effects. Size effects on strain limits between microformed and macroformed *CuZn30* could not be deduced from comparison according to thickness, grain size d, and thickness-to-grain-size ratio λ. However, size effects on thin sheet formability at the microscale were identified by considering open and closed pockets model. Lubrication had less effect with increasing miniaturization, where percent-increase in strain limits by using lubrication decreased with decreasing geometrical scale due to the less utilization of applied lubricants by roughness valleys at the microscale. The identified size effects in this study should be considered when ranking the formability of different sheet metals in favoring material selection for particular microforming process. Determining strain limits for other strain ratios should enable constructing FLDs which would demonstrate all allowable strain ratios for a certain material. And this will ultimately eliminate the costly trial and error process of determining those allowable stresses.

CHAPTER SEVEN

HIGH TEMPERATURE MICROFORMING AND ANALYSIS OF MATERIAL BEHAVIOR AT ELEVATED TEMPERATURES

7.1 Introduction

Early studies that focused on utilizing the advantages of achieving superior ductility and lowering forming loads by conducting high temperature testing at the microscale level have been reported in investigations by [27-37, 83-87]. Although their studies covered utilizing the Newtonian viscous flow of amorphous alloys at the microscale, applying bulk microforming techniques at higher temperatures, laser forming, and flow stress characterization through compression tests at elevated temperatures, there was a very minor emphasis on high temperature microforming of thin sheets. By utilizing the advantages of high temperature forming of thin sheets at the microscale, better optimization of material processing for microparts can be achieved, especially for structures that require highly intricate geometries and configurations. In this study, a new initiative to study size effects on high temperature microforming of thin sheets will be presented. The overall objective of this initiative is to develop a suitable testing method for characterizing thin sheet formability at high temperatures for microsclae applications. The ultimate achievement behind this objective is to be able to produce forming maps that could predict limits of superplasitcally formed thin sheets for more effective and efficient microscale manufacturing of components and parts. In this study, a testing method for performing high temperature microscale-testing of thin sheets and characterizing formability through surface strain limits was introduced. Thin sheets of *CuZn30* were tested at 25μm and 50μm thicknesses at 100˚C and 150˚C which are regarded as warm forming temperatures for such an alloy, since forming temperatures did not go as high as it is for superplastic forming range, which is 0.5-0.7 of its melting

temperature [89]. The focus of this investigation was the analysis of size effects on thin sheet formability through measured loading profiles and surface strain limits. The identified key parameters in this study were forming speed, forming temperature, sheet thickness, and microstructural parameters.

7.2 Experimental Apparatus and Procedure

In order to accomplish the goal of this study a high temperature testing module was added to the existing microforming setup that was introduced in Chapter Four. This module is based on heating the test specimens, or thin sheets, through heating the die where the specimens are clamped within. Heat is conducted into the inside of the die by a SunRod® cartridge electric heater provided by Sun Electric Heater Co. The cartridge heater has a diameter of 1/8" and is press fit into the side of the die. Heating temperature is controlled by a developed electronic control circuit. The control circuit induces the required voltage and electric current for the cartridge heater to heat the die depending on a feedback system in the form of a temperature sensor (known as a thermistor) which is placed inside the die. Upon achieving the required temperature, the temperature sensor gives a signal to the circuit to cut off the voltage; or turn the voltage on in case the temperature drops below the required value. For each test, the required temperature was set manually by setting an equivalent resistance on the potentiometer of the electronic control unit. The setup was calibrated and monitored using an external digital temperature-reader which is connected to a thermocouple that had contact with the base of the test specimen through the die hole. The calculated uncertainty for acquiring a desired heating temperature was in the range of ±3% error of the applied temperature.

Figure 7-1 shows how the cartridge heater and temperature sensor are connected to the forming die. The arrangement of a typical high temperature test is presented in *Figure 7-2*, showing the high temperature module integrated into the existing microforming setup.

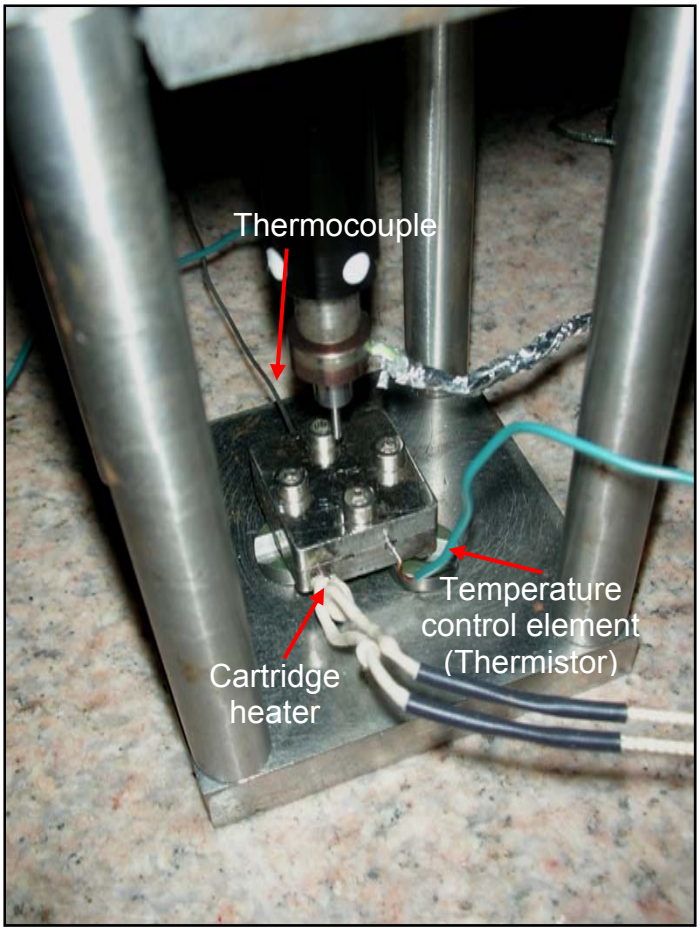

Figure 7- 1 Microforming setup with high temperatures testing apparatus

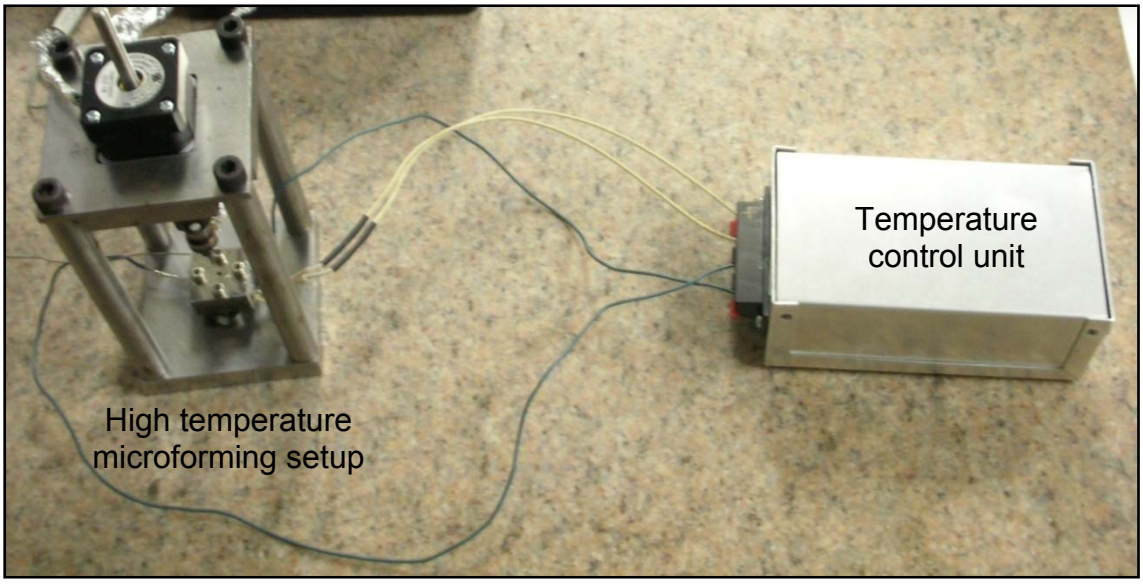

Figure 7- 2 High temperature testing module along with the developed microforming setup

For each microforming test, test specimens were kept inside the heated die for 10 minutes prior to initiating the test in order to establish a stable forming temperature. Due to the limitation of the heating capacity of the cartridge heater to 160˚C, testing of *CuZn30* with both 25µm and 50µm thicknesses was conducted at 100˚C and 150˚C, which are regarded as warm forming temperature for such an alloy. Testing at these temperatures may provide combined advantages of both cold and hot forming.

7.3 Study of Effects of Warm Temperature on Parameters of Microformed Thin Sheets

In this study, two cases were regarded for identifying the effect of warm temperature testing on thin sheet formability at the microscale, depending on the

variability of the following parameters; forming speed, forming temperature, and sheet thickness.

7.3.1 Effect of Warm Temperature with Varying Forming Speeds

Loading profiles for tested *CuZn30* thin sheets at 100˚C and 150˚C are shown in *Figures 7-3 & 7-4* for 25µm thicknesses and *Figures 7-5 & 7-6* for 50µm thicknesses. Numerical values of extracted limiting dome-heights and forces are presented in *Tables 7-1 & 7-2* for 25µm and 50µm thicknesses respectively. From the presented plots, it is obvious to say that for all tested sheets; higher temperature microforming affected the form of bulging profiles with varying forming speed. Force-displacement curves were ranked according to the applied forming speed. The result was higher forming loads corresponding to same displacement with increasing forming speed and in some cases, higher limiting dome height.

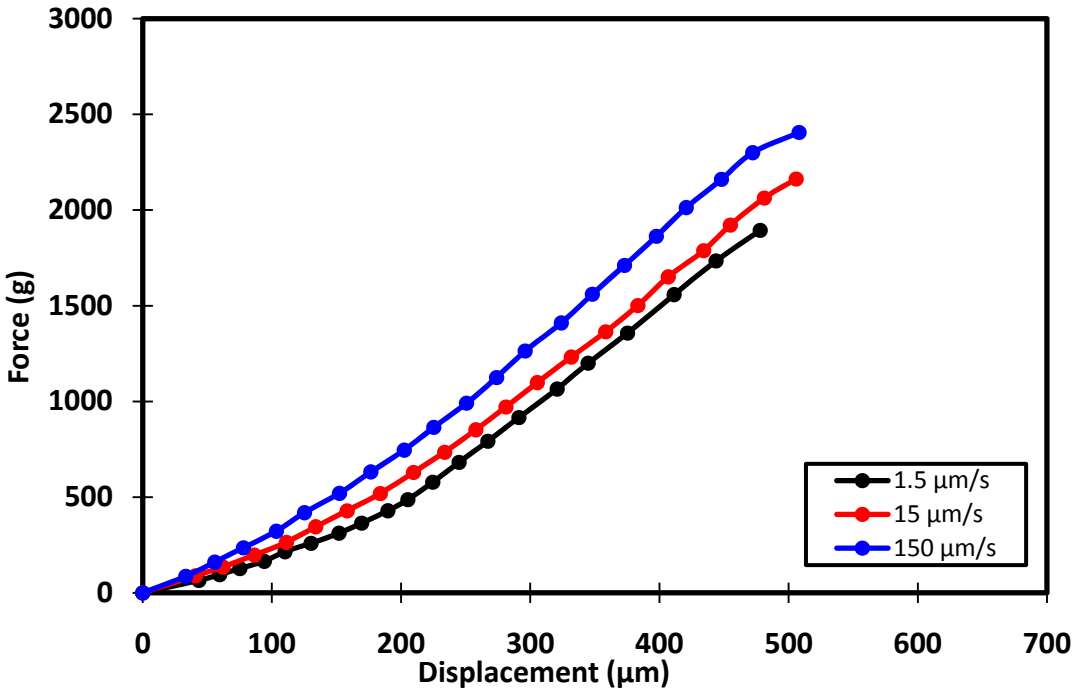

Figure 7- 3 Loading profiles for 25µm CuZn30 thin sheets at 100˚C

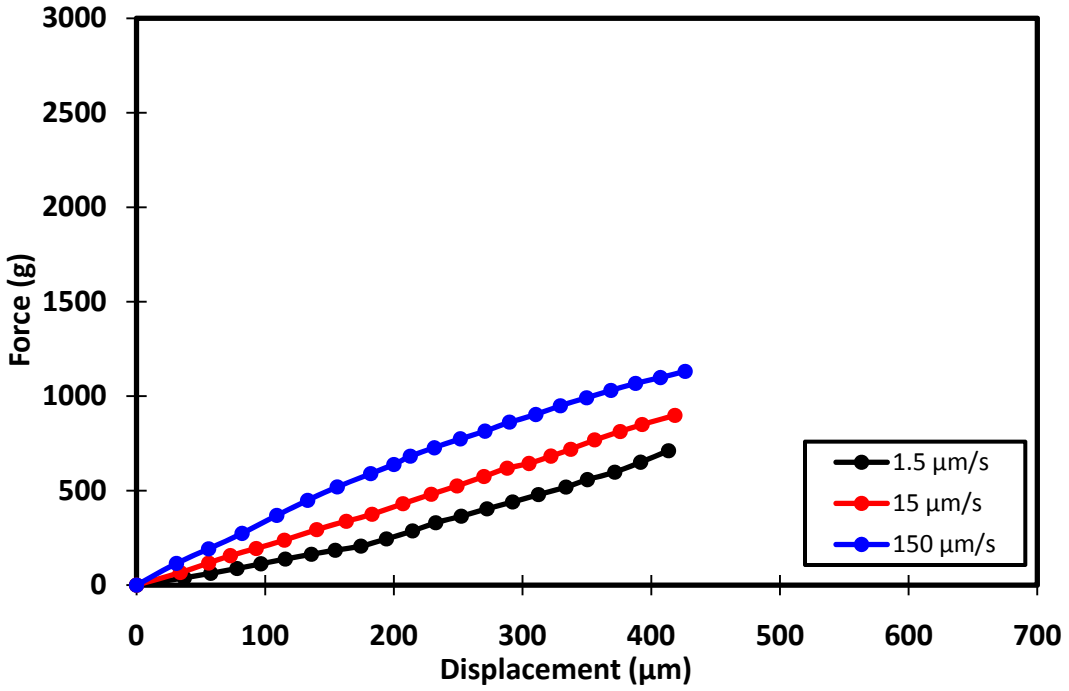

Figure 7- 4 Loading profiles for 25µm CuZn30 thin sheets at 150˚C

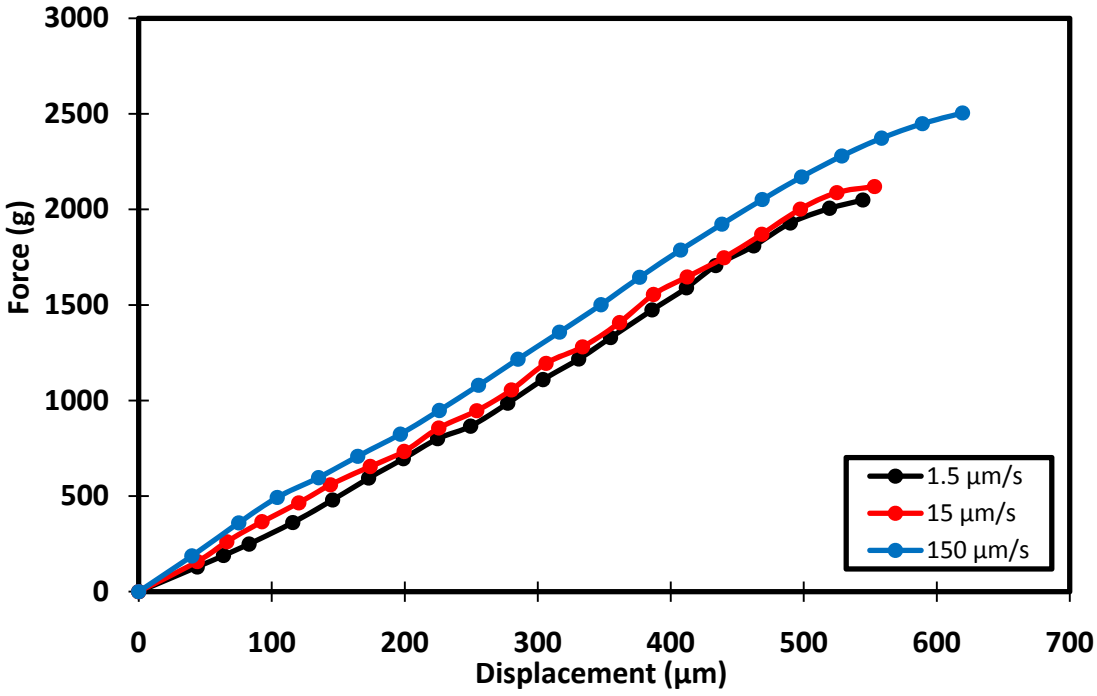

Figure 7- 5 Loading profiles for 50µm CuZn30 thin sheets at 100˚C

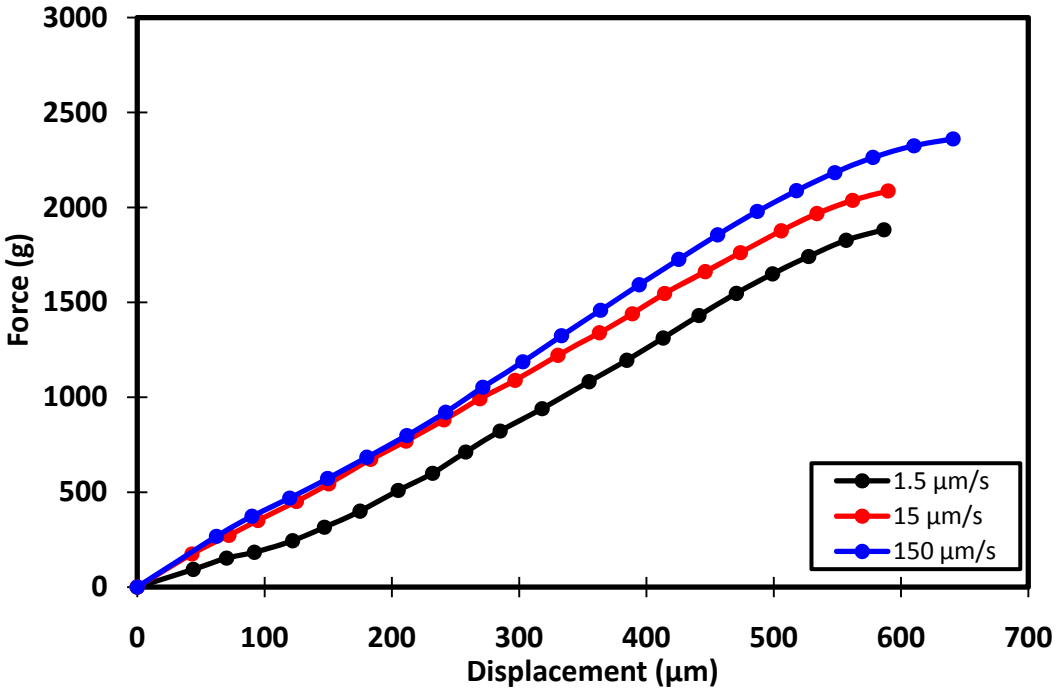

Figure 7- 6 Loading profiles for 25µm CuZn30 thin sheets at 150˚C

This observation is contrary to what was obtained from testing at room temperature (Chapter Five). The reason for the variation of bulging profiles with varying forming speed is due to the presence of additional thermally activated slip systems, which vary with varying heating temperature [37, 47, 48]. The resulting trend is a higher ranked profile with increased forming speed. As forming speed is increased, the added dislocations developed by the thermally activated slip systems will move faster behind grain boundaries of the faster rotating grains. These dislocations will pile up and act in opposing the applied deformation forces, resulting in higher forces for plastically deforming those grains. This trend was not obtained for 50µm microbulged sheets at 100˚C, as seen in *Figure 7-5*. For the aforementioned batch, the defying behavior of closely packed profiles at 1.5µm/s and 15µm/s forming speed could have been due to

statistical and/or measurement errors, or it might have been due to the lack of enough activated slip systems to induce plasticity forces on such a thicker sheet when compared to 25µm ones.

Table 7-1Numerical values of limiting dome heights for CuZn30 tested sheets at elevated temperatures

Forming speed (µm/s)	Limiting dome height (µm)					
	25˚C		100˚C		150˚C	
	25µm	50µm	25µm	50µm	25µm	50µm
1.5	499.50	669.19	478.00	544.46	413.40	556.79
15	497.00	680.36	505.78	553.16	418.36	561.91
150	468.41	584.47	495.44	619.42	426.39	610.11

Table 7-2 Numerical values of limiting forces for CuZn30 tested sheets at elevated temperatures

Forming speed (µm/s)	Limiting force (gm)					
	25˚C		100˚C		150˚C	
	25µm	50µm	25µm	50µm	25µm	50µm
1.5	2829.26	6228.44	1893.36	2049.00	711.00	1882.41
15	2709.30	6107.37	2161.94	2119.48	898.30	2087.26
150	2579.08	5265.38	2405.47	2504.68	1131.42	2360.57

The aforementioned trend was considered in an alternative approach by comparing limiting dome heights and forces of tested *CuZn30* thin sheets for each thickness at both high temperatures with room temperature. Percent variations between higher forming speeds (15µm/s and 150µm/s) to the lowest forming speed (1.5µm/s) were calculated from loading plots and are presented in *Tables 7-3 & 7-4* for 25µm and 50µm thicknesses respectively. *Figures 7-7, 7-8, 7-9 & 7-10* show a plot representation to the percent variations in limiting values. Limiting dome heights and forces increased

with increasing forming speeds at higher temperatures, which was opposite to results of testing at room temperature.

Table 7-3 Percent variation in limiting values from 1.5µm/s forming speed for 25µm CuZn30 at elevated temperatures

Forming speed (µm/s)	Variation in limiting dome height (%)			Variation in limiting force (%)		
	25˚C	100˚C	150˚C	25˚C	100˚C	150˚C
15	-0.2	+5	+1	-4	+14	+26
150	-7	+4	+3	-9	+27	+59

Table 7-4 Percent variation in limiting values from 1.5µm/s forming speed for 50µm CuZn30 at elevated temperatures

Forming speeds (µm/s)	Variation in limiting dome height (%)			Variation in limiting force (%)		
	25˚C	100˚C	150˚C	25˚C	100˚C	150˚C
15	-4	+2	+0.9	-4	+0.8	+11
150	-17	+14	+10	-17	+19	+25

In Chapter Five, it was said that for room temperature testing, higher forming speeds did not allow for further deformation due to work hardening of tested thin sheets, which resulted in decreased limiting values with higher speeds. At higher temperatures, work hardening tends to impose less effect on the deformation mechanism [37]. Therefore, increasing forming speeds at higher temperatures will not impede the deformation process. For higher temperature testing, it seemed that the thermally activated slip systems that developed while applying heat energy took effect into the plastic deformation mechanism by increasing the dislocation density in grain boundaries, which resulted in higher forming forces and displacements for higher forming speeds at both applied temperatures.

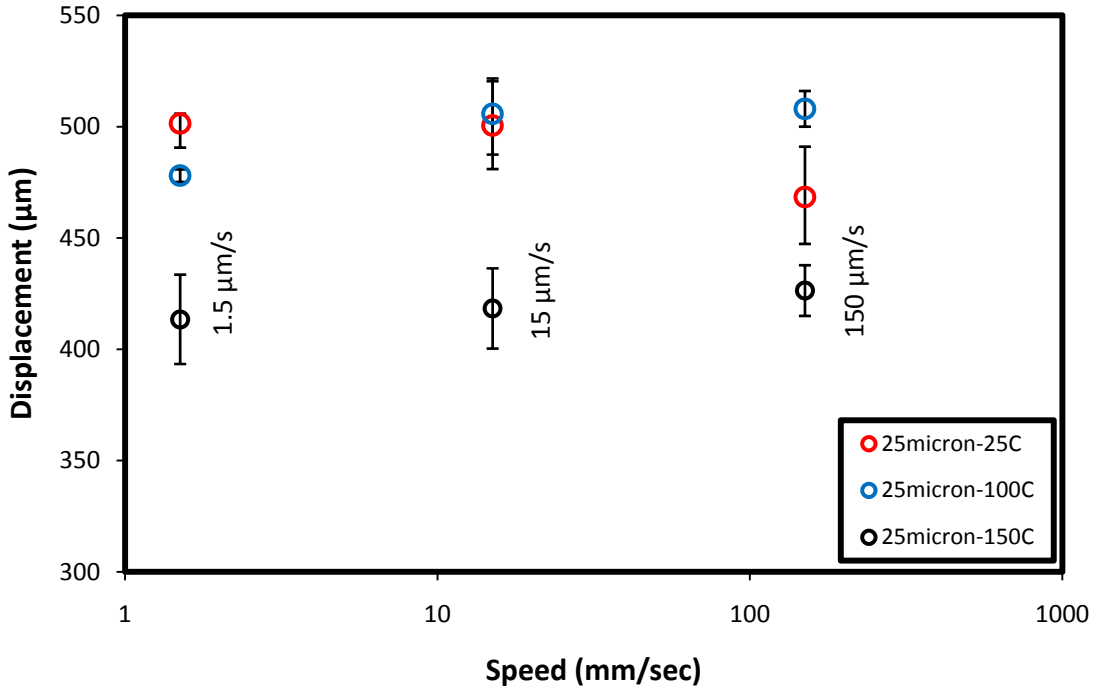

Figure 7- 7 Effect of varying speed on limiting dome height for 25µm microbulged thin sheets at elevated temperatures

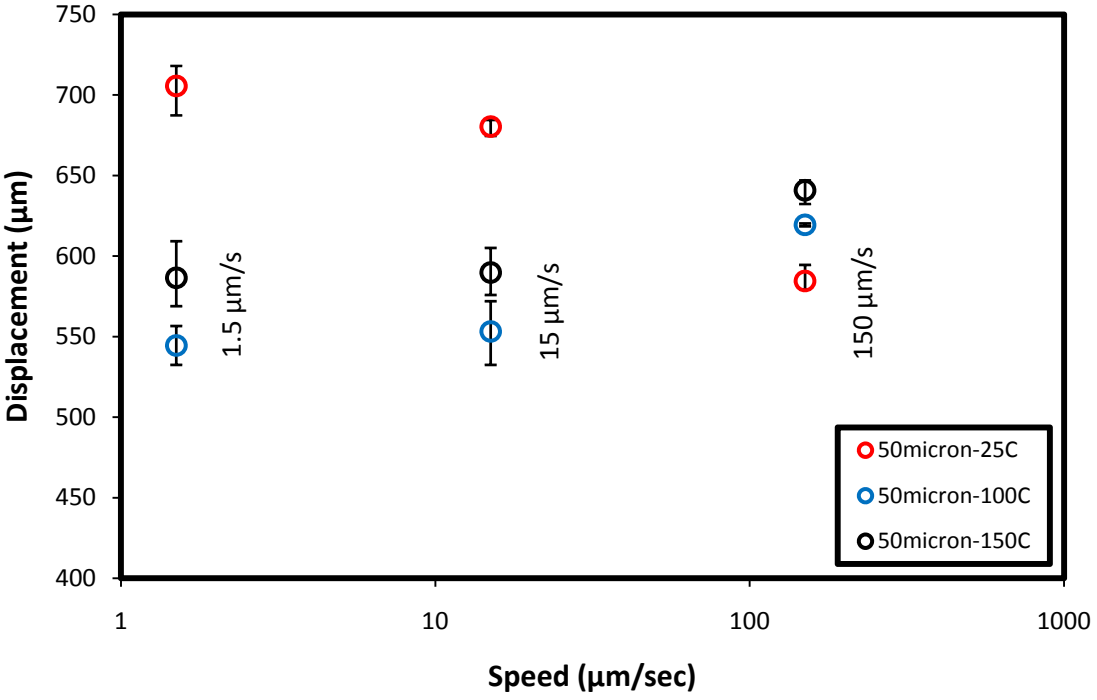

Figure 7- 8 Effect of varying speed on limiting dome height for 50µm microbulged thin sheets at elevated temperatures

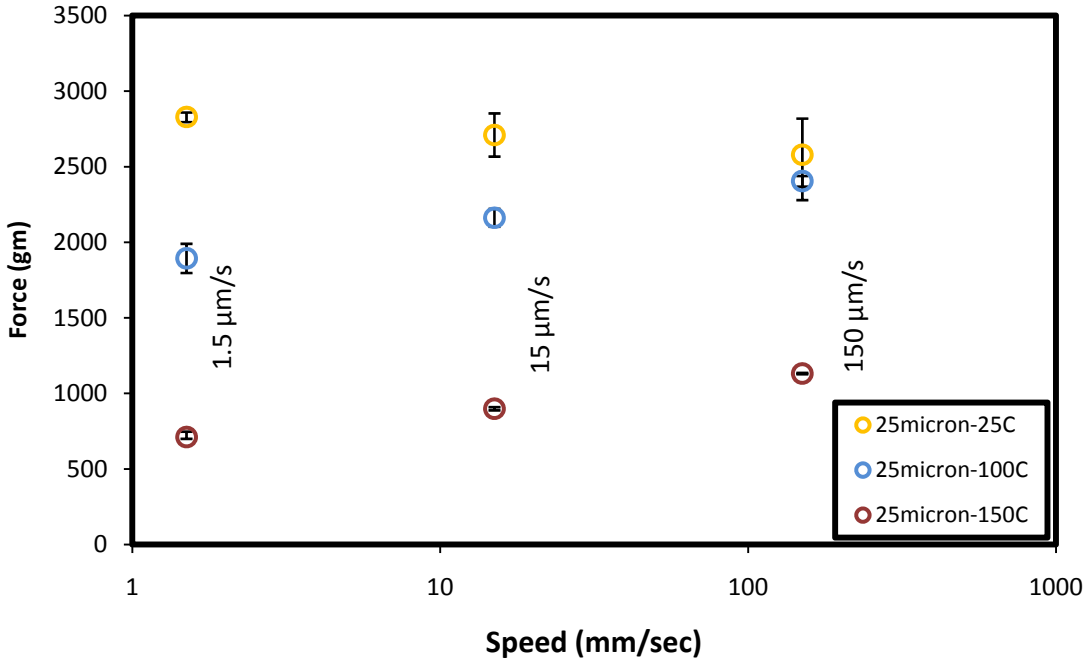

Figure 7- 9 Effect of varying speed on limiting forces for 25µm microbulged thin sheets at elevated temperatures

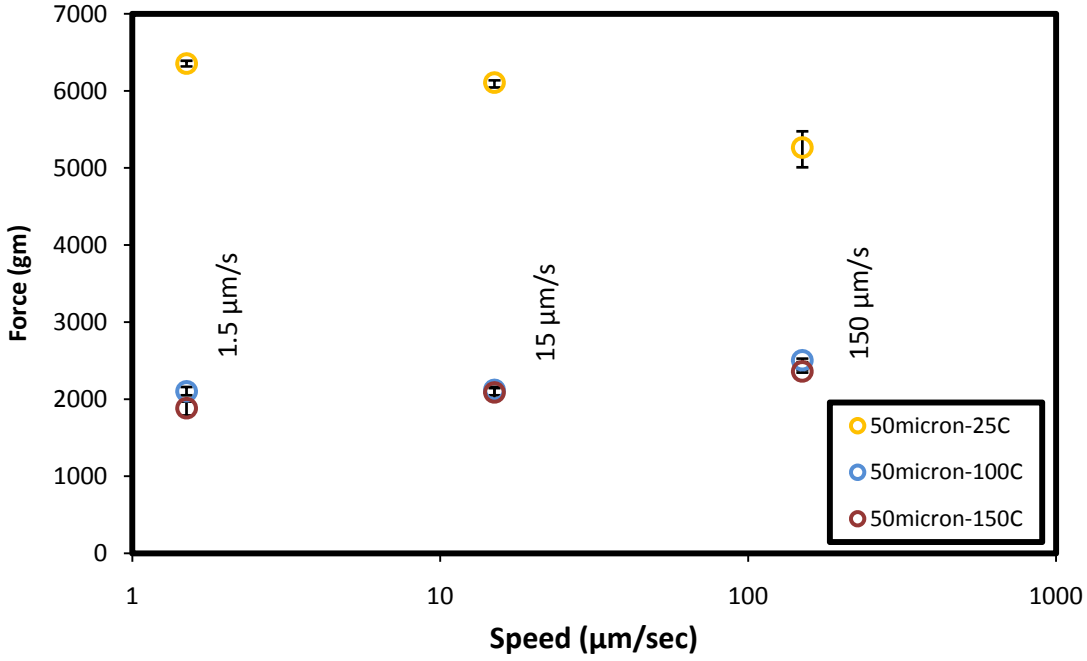

Figure 7- 10 Effect of varying speed on limiting forces for 50µm microbulged thin sheets at elevated temperatures

However, for both tested thicknesses, the increase in limiting dome heights with increasing forming speed at 100˚C was slightly higher than that at 150˚C while holding a lower increase in limiting forces (*Tables 7-3 & 7-4*). The reason for such an observation could be the releasing of more undesired slip systems at 150˚C, which may ultimately impede the deformation of grains by the presence of more dislocations that will oppose the applied forming loads on grains that must rotate to its proffered orientation. Considering that testing at those temperatures was conducted on the same thickness and microstructure, this result might indicate the consideration of optimum conditions for attaining better thin sheet formability [88,89]; meaning that microforming of *CuZn30* thin sheets improved more at 100˚C and should be considered if forming temperature is limited and component weight is a major factor too. Still, formability increased with increasing forming speed at higher temperature testing.

7.3.2 Effect of Warm Temperature with Varying Temperature

By looking at bulging profiles of 25μm and 50μm thin sheets with respect to forming speeds at different forming temperatures (*Figures 7-11*), significant drop in punch force was observed in most of the higher temperature forming tests, along with variations in maximum dome heights. Numerical values of percent variation in both limiting dome heights and forces between high temperature and room temperature testing of *CuZn30* are presented in *Tables 7-5 & 7-6*.

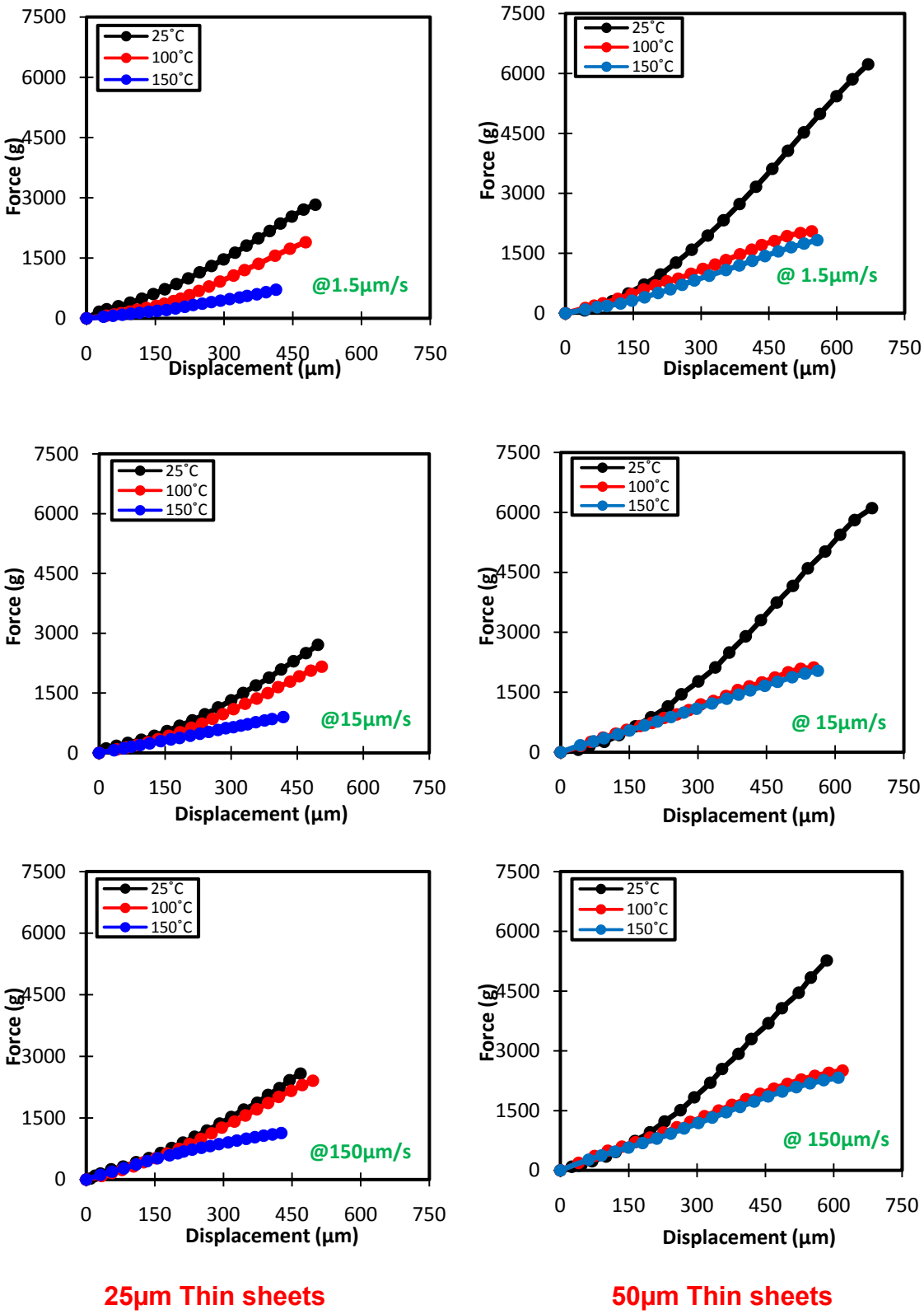

Figure 7- 11 Bulging profiles of 25µm (left) and 50µm (right) microbulged CuZn30 at indicated forming speeds

Table 7-5 Percent variation in limiting values of microbulged thin sheets between elevated temperatures (100˚C & 150˚C) and room temperature (25˚C) for 25µm CuZn30

Forming speed (µm/s)	Variation in limiting dome height (%)		Variation in limiting force (%)	
	100˚C	150˚C	100˚C	150˚C
1.5	-4	-17	-33	-75
15	+2	-16	-20	-67
150	+6	-9	-7	-56

Table 7-6 Percent variation in limiting values of microbulged thin sheets between elevated temperatures (100˚C & 150˚C) and room temperature (25˚C) for 50µm CuZn30

Forming speed (µm/s)	Variation in limiting dome height (%)		Variation in limiting force (%)	
	100˚C	150˚C	100˚C	150˚C
1.5	-19	-17	-67	-70
15	-19	-17	-65	-66
150	+6	+4	-52	-55

The identified decrease in dome height and limiting forces with increasing forming temperature for both tested thicknesses was in agreement to the behavior of similar face-centered cubic (FCC) metals that were tensile tested at the macroscale level [47]. The scientific explanation for this behavior is the strong dependency of work hardening in such alloys on forming temperature, demonstrated by a decreasing work hardening with increasing forming temperature. Therefore, forming at lower temperatures will have an increased work hardening effect and consequently would increase limiting forces and projected dome heights. This effect was not clearly distinguished in this study, since the applied forming temperatures were in the warm forming region and did not vary significantly. Nevertheless, the observation of decreasing dome height with increasing forming temperature, which is contrary to the behavior of stretched sheets at the

macroscale, can be considered as a size effect on high temperature testing of microformed thin sheets, especially considering the coarsening effects of the deformed microstructure on formability. For bulging profiles of the 25µm tested sheets at 100˚C, they seemed to be closer to the bulging profiles of at 25˚C for all forming speeds. This might mean that that the applied forming temperature for that particular sheet thickness did not eliminate the effect of work hardening on the deformation process, and therefore, with higher forming speeds, work hardening still demonstrated an effect on the resulting limiting values. This was not the case for 50µm tested thin sheets where the initiation of more thermally activated slip systems might have eliminated more of the work hardening effect.

7.4 Study of Effects of Warm Temperature on Surface Strain Limits of Microformed Thin Sheets

In order to characterize the formability of microformed thin sheets at higher temperatures, the same approach that was introduced and followed in Chapter Six was implemented here. For each test, specimens were marked by a photolithography process then clamped, heated, and formed, prior to image capturing of the failed region by electron microscopy and automatic surface strain measurement around the vicinity of the developed crack. Again, tested specimens were deformed at a speed of 15µm/s to follow scaling of the forming setup (Chapter Six).The obtained strain limits for 25µm and 50µm *CuZn30* thicknesses at 100˚C and 150˚C are presented in *Figures 7-12 & 7-13*.

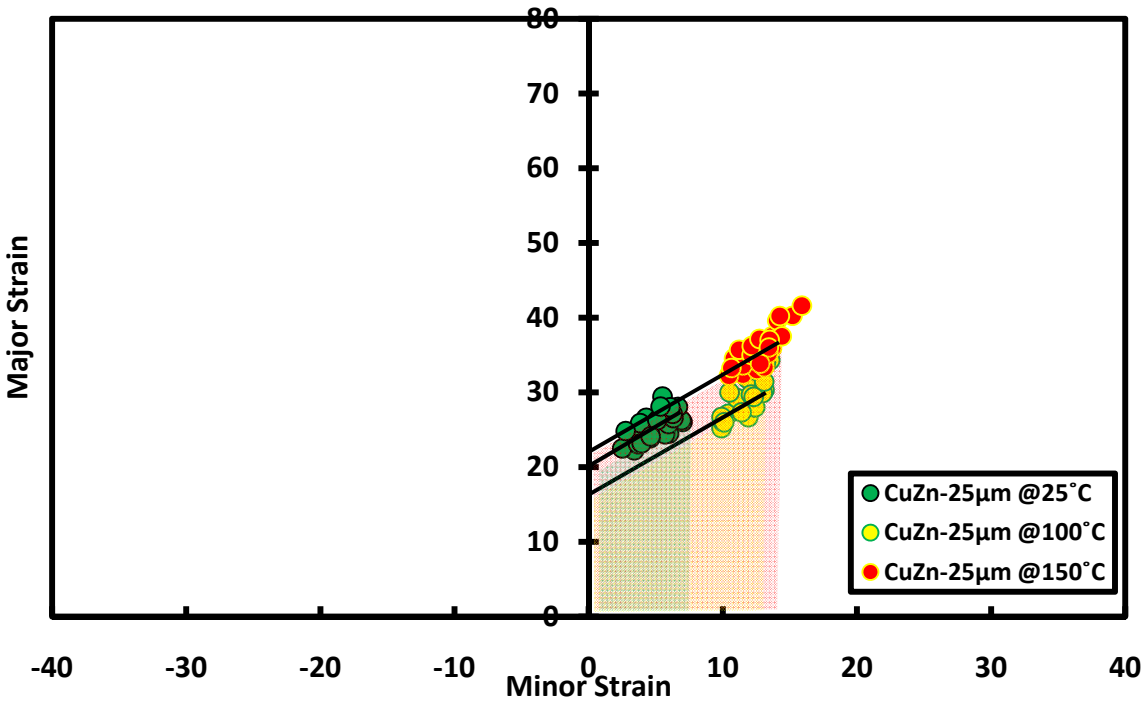

Figure 7- 12 Strain limits of microbulged 25µm CuZn30 thin sheets at various temperatures

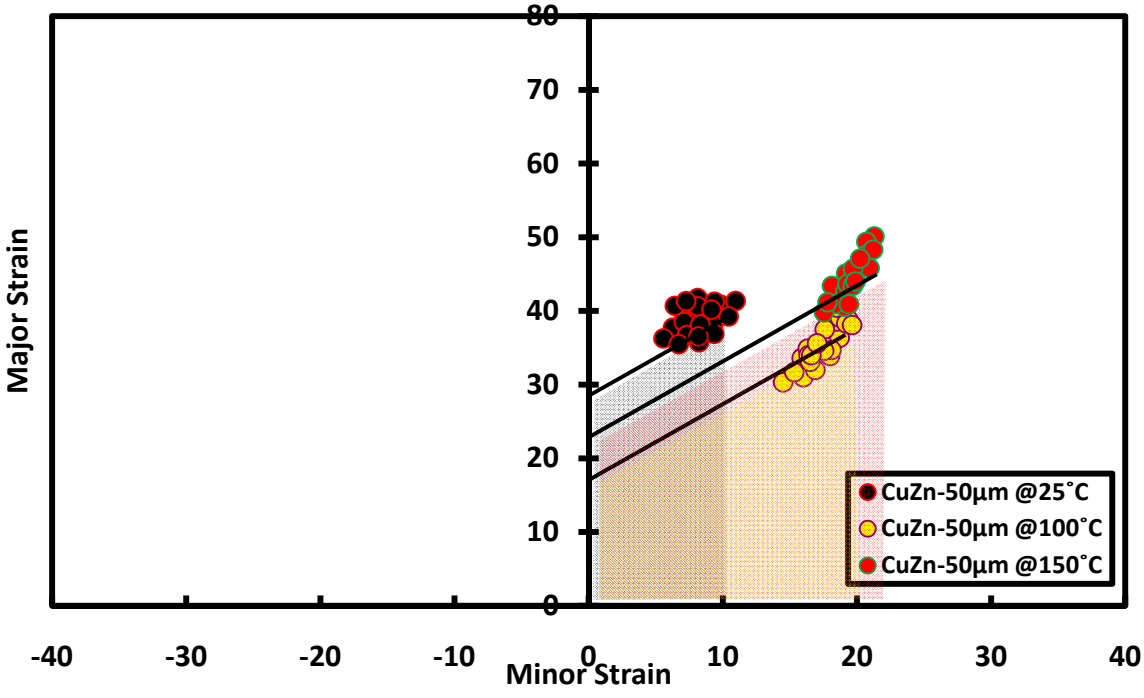

Figure 7- 13 Strain limits of microbulged 50µm CuZn30 thin sheets at various temperatures

Increasing surface strain limits by applying high temperatures was clearly identified in FLD plots for both tested thicknesses. This increase was also calculated in terms of percent variation and is presented in *Table 7-7*. The increase in strain limits with increasing temperature is a combined result of less work hardening and additional thermally activated slip systems within grains as a result of inducing heat energy [37, 47, 48]. More slip systems resulting from the presence of dislocations will allow for further deformation of grains, since slip systems are the governing mechanism for plastic deformation, and accordingly failure is prevented by the presence of high dislocation density. This increase in strain limits allows for applying a wider range of strain ratios which ultimately allows for achieving more intricate details in a deformed thin sheet of the same thickness with lower forces, as seen in the previous section. The increase in surface strain might be the reason for decreasing dome heights with increasing forming temperature as previously mentioned. Therefore, the limitation for achieving higher depth for microformed thin sheets must be considered along with the increasing stretchability when designing for such a microforming process.

Table 7-7 Measurement of the increase in strain limits of microformed CuZn30 thin sheets between room temperatures and higher temperatures along with microstructural parameters

Thickness (μm)	Temperature (˚C)	Increase in formability (%)		λ	N_t (x10^6)	N_s/N_i (%)
		Major Strain	Minor Strain			
25	100	14.8	85.7	3.1	0.228	13.9
	150	38.9	107.1			
50	100	2.6	85.7	3.7	0.094	150.0
	150	15.4	90.5			

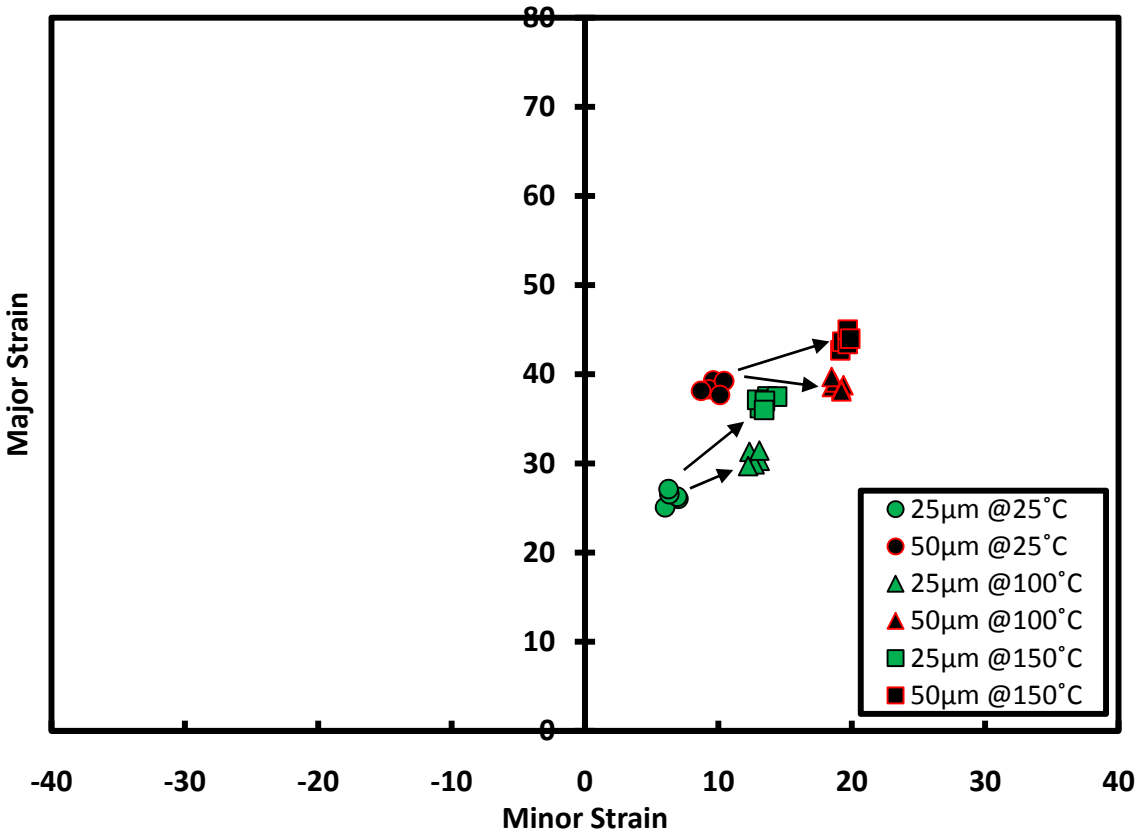

Figure 7- 14 Strain limits of microbulged CuZn30 thin sheets (25µm and 50µm thicknesses) at room temperature (25˚C) and higher temperatures (100˚C and 150˚C)

The above increase in surface strain limits seemed to dominate more in the minor strain direction and was minor in the major strain direction (*Figure 7-14*). This observation might be due to the coarse microstructure of the tested thin sheets. Deforming grains seemed to elongate along the major strain direction, resulting in an increased grain boundary density along the transverse direction (the curve of the major strain axis of the formed ellipse). Therefore, in the transverse direction, or minor strain direction, more grain boundary density will be available for dislocation to pile and take advantage of the developed slip systems that should increase the formability along this direction. When comparing between the percent increase in strain limits for 25µm and 50µm tested thicknesses (*Table 7-6*), 25µm thin sheets demonstrated higher formability

improvement in strain limits than 50μm thin sheets even with 50μm thin sheets having more share of surface grains than 25μm ones, which meant more unrestricted grains to deformation. The reason for the higher improvement could be the total number of deformed grains for 50μm which are less than that of 25μm ones (*Table 7-6*). The fewer number of deformed grains at higher temperature might reduce the number of thermally activated slip systems which affect the favorability of grain to deform plastically even without fully rotating to its preferred orientation of deformation.

7.5 Concluding Remarks

A newly developed method for characterizing thin sheet formability at high temperatures for microsclae applications was introduced. The method utilizes the previously developed microforming setup with all of the required features for achieving accurate microscale testing. A high temperature module was added to the existing microforming setup in the form of a cartridge heater that snap-fits to the forming die and heats the workpiece by heating the die that holds it. Heating temperature was controlled by an electronic control system which relies on varying applied voltage and current to achieve temperatures up to 160˚C. Formability was characterized by considering measured bulging profiles and calculated surface strain limits of tested *CuZn30* thin sheets. Ranking of bulging profiles of tested sheets at high temperatures varied with varying forming speed; contrary to what is observed in room temperature testing where all bulging profiles were identical in form and only differed in limiting values. The ranking of these profiles was a result of additional developed slip systems that were formed by heating and showed dependency on forming speed. Limiting dome heights and

forces increased with increasing forming speed due to the softening effect that heating induced on the workpiece, where the increased number of slip systems resulted in higher deformation forces and displacements. Nevertheless, limiting values at higher temperatures were lower than that at room temperature. Warm forming showed a decreased work hardening effect when compared to cold forming and resulted in limited stretchability. Therefore, it can be said that in high temperature forming of thin sheets, forming depth decreases with increasing miniaturization. Calculated surface strain limits of high temperature microforming were superior to strain limits obtained at room temperature and allowed for a wider range of permissible strain ratios for obtaining more complex forming geometries with the same thin sheet thickness. The indicated increase resulted from the additional thermally activated slip systems which facilitates the deformation of grains under lower applied loads. However, the limitation in limiting dome height accompanied the increasing formability, thus it should be accounted for in the design of the microforming process; especially when the advantage of achieving intricate details and configuration with the same thickness is implemented. In general, this study proved that high temperature forming can be utilized in thin sheet microforming processes although there seemed some limitations in acquiring sufficient forming depths, which is governed by size effects. The obtained results were also governed by the coarseness of the specimens' microstructure. More studies at higher applied forming temperatures and a wider range of thicknesses and grain size range are needed to incorporate the effect of grain size on thin sheet formability at high temperature.

CHAPTER EIGHT

SUMMARY AND FUTURE RECOMMENDATIONS

8.1 Conclusions

A novel and comprehensive approach was developed and adapted in this research work to obtain a better understanding of the material behavior at the microscale level, particularly on the formability of thin sheet-metal. *CuZn30* brass alloy alloys, which are of important and wide use in microforming industries, were tested in order to obtain optimum process parameters for improved utilization and processing of these alloys.

A special microforming setup was designed and built for conducting formability tests on thin sheets in the form of mechanical bulging. Photolithography and chemical etching techniques were developed for formability measurement of thin sheets at the microscale level. The characterization of formability was done by determining forming limits of deformed sheets through SEM imaging and dedicated software Automated Strain Measurement and Analysis Environment (ASAME). Size effects on limiting bulge heights, loading, and strains were identified for a group of well-defined process parameters. The coarseness of tested thin sheets showed a significant influence on the microformed thin sheets. The increasing share of surface grains increased the formability when formed sheets were compared at the micro- and macroscale levels. Sheet formability enhancement by applying lubrication seemed to diminish with increasing miniaturization. The developed integrated technique was shown to assist in determining and ranking thin sheet formability while exploring the effect of changing parameters for this particular process.

A high-temperature microforming setup was developed to investigate size effects on microforming processes and its parameters at elevated temperatures. Again, size effects were identified in the scope of the identified parameters. The development of

thermally activated slip systems resulted in a detected sensitivity of measured force profiles to forming speed. There seemed to be some limitations to thin sheet formability at elevated temperatures concerning limiting displacement, however, surface strain measurements indicated an enhancement of stretchability at the tested temperatures. This part of the work will make an important contribution to industrial applications of microforming.

The overall benefit of conducting this integrated approach is to be able to construct forming limits diagrams (FLDs) of microformed thin sheets which will in turn, provide us with a predictive tool for selecting materials and process parameters without worrying about the costly trial and error techniques that are currently administered in related microscale manufacturing industries. By optimizing microforming processes, the advantage of demonstrating mass production and optimum material utilization will push microforming towards replacing existing micromachining processes and ultimately lowering the overall development and production costs.

8.2 Unique Features and Contributions

- Characterization of formability of sheets by constructing FLDs under extreme grain size emphasis: Most of the available work tackles formability issues under a fine grain structure and excludes the appearance of coarse grains in strain limit analysis for determining FLDs. In this work more emphasis was put on deforming grains with respect to its restriction to deformation within the deforming volume.

- Development of a microforming setup for thin sheet formability testing: Existing formability testing setups demonstrated significant drawbacks and limitations to testing methods of thin sheets at the microscale level. The developed setup allowed for the accurate measurements and tight tolerances that are essential at such a geometrical scale.

- Identification of size effects on loading history in thin sheet bulging while considering affecting process parameters: Existing work focuses primarily on size effects through uniaxial testing and a few deep drawing and upsetting tests.

- Development of a testing method for measuring strain limits of deformed thin sheets: There is no current standard that identifies a procedure for measuring strain limits of microformed thin sheets. This method will enable the determination of FLDs for forming thin sheets at the microscale level. The outcome is a predictive tool for thin sheet formability a the microscale level that will provide related industries with a wide choice for selecting materials and process parameters, hence eliminating the know-how technique of mastering existing microforming technologies.

- Development of a testing setup for high temperature microforming of thin sheets through load recognition and strain limit determination: There is no current standard apparatus or method for characterizing high temperature thin sheet formability. This study is essential and can optimize, or replace, some of the

existing microforming processes. The approach of high temperature microforming arises from the well known brittleness of materials at the microscale level.

8.3 Recommendations for Future Work

- Incorporating thin sheet testing on a wider variety of commonly used alloys in the microforming industry (such as brass, aluminum, and plastic materials).
- Determining stain limits of thin sheets to accommodate all strain ratios in order to construct FLDs for microformed thin sheets and ultimately develop formability predictive data for targeted alloys.
- Upgrading the capabilities of the high temperature setup to incorporate higher temperature that can accommodate temperatures exhibiting superplastic conditions at the microscale level and ultimately providing a superplastic microforming setup for thin sheets.
- Eliminating undesired friction effects by developing a pneumatic bulge forming technique which is expected to overcome the unfavorable brittleness that is always detected in microscale testing due to the presence of friction.

APPENDICES

APPENDIX I: PROCEDURE FOR ELECRO-CHEMICAL MARKING OF *CuZu30*

Electrochemical etching was performed on a Universal Marking Systems ME3000T Marking Unit. The procedure was as follows:

1. Sheets were cut into required dimensions and cleaned using acetone, and then samples were air blown to dry.
2. The required electrolyte (ME5 for brass) was distributed on top of the sheet and then the required stencil was placed on top of the sheet. A felt pad was then soaked by electrolyte and placed on top of the stencil.
3. The cathode was connected to the sheet by clamping it to a custom grounding where the sheet lies.
4. Test parameters were chosen from the preset program list for adjusting voltage and time.
5. A metal roller, which is the anode, was used to transmit the applied current through the arranged parts by rolling it along the sheet area and circular markings were achieved on test samples.
6. After the marking process, samples were washed with water and air blown to dry.

APPENDIX II: MOUNTING, GRINDING, AND POLISHING OF SAMPLES FOR MICROSTRUCTURAL ANALYSIS

Procedure for Sample Mounting:

1. Sheet samples were cut to the required size in order to fit them into the mounting molds.
2. Commercial Epofix resin (EPOES by Struers Co.) was mixed with hardener (EPOAR) at a 25-3 wt% and then poured into the mounting molds with sheet samples at the bottom.
3. The epoxy was allowed to dry and cure and for 24 hours, then the mounted samples were removed from the molds.

Procedure for Grinding and Polishing Using the Struers RotoPol-22 and RotoForce-3 Machine:

1. Samples were mounted onto the mounting disk which will be placed onto the rotating shaft of the grinding machine and the automatic programming (Multidoser by Struers Co.) was set to the Al settings.

2. The grinding process was started by grinding samples with a *320 SiC* grit-size emery paper to ensure the flatness and required leveling of all samples. Then 500, 1200, 2400 and 4000 grit-size emery paper, was used orderly in consecutive stages until a smooth surface finish was obtained.
3. Polishing clothes (MD-Dac commercial cloth provided by Struers Co.) with corresponding diamond-particulate solution (Dac) was used to polish the samples and achieve a smooth surface (around 3μm roughness).
4. Step 3 was repeated if the apparent scratches were considerably large.
5. The final polishing stage was applied using the MD-Chem polishing cloth and the OP-U suspension solution until all visible scratches were eliminated and a smooth and shiny surface was obtained. The obtained samples can be used in microstructural analysis as well as brazing experiments.
6. If scratches were still visible, step 3-5 were repeated until a shiny and clean finish was obtained.

APPENDIX III: MATERIAL PARAMETERS CHART FOR *CuZn30* TESTED SHEETS OF ALL THICKNESSES AND ANNEALING STATES

Table III-1 Calculated parameters for CuZn30 Bulged Sheets

Geometry	Thickness	State	d (µm)	λ	π	N_s (x10^6)	N_i (x10^6)	N_t (x10^6)	N_s/N_i (%)	V (mm^3)
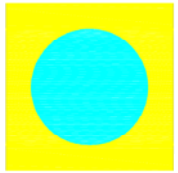	2mm	AR	55.5	36.1	150,824.9	1.730	91.786	93.516	1.88	8370.78
		AN	476.2	4.2	17,513.8	0.023	0.125	0.148	18.87	
	1mm	AR	29.1	33.5	139,979.6	5.961	293.075	299.036	2.03	4185.39
		AN	238.1	4.2	17,578.3	0.094	0.498	0.592	18.87	
	200µm	AR	16.0	12.5	52,317.4	20.816	369.491	390.307	5.63	837.08
		AN	48.8	4.1	17,153.2	2.238	11.519	13.757	19.43	
	2mm	AR	55.5	36.1	141691.2	1.647	86.206	87.853	1.91	7863.86
		AN	476.2	4.2	16,513.8	0.022	0.117	0.139	19.10	
	1mm	AR	29.1	33.5	131,502.7	5.637	275.29	280.927	2.05	3931.93
		AN	238.1	4.2	16,513.8	0.089	0.468	0.557	18.99	
	200µm	AR	16.0	12.5	49,149.1	19.581	347.091	366.672	5.64	786.39
		AN	48.8	4.1	16,114.5	2.104	10.819	12.923	19.45	
	2mm	AR	55.5	36.1	27,027.0	0.047	23.271	23.318	2.02	2125.00
		AN	476.2	4.2	4,462.4	0.006	0.031	0.037	20.23	
	1mm	AR	29.1	33.5	35,535.1	1.516	74.397	75.913	2.04	1062.50
		AN	238.1	4.2	4,462.4	0.024	0.126	0.150	19.20	
	200µm	AR	16.0	12.5	13,281.25	5.286	93.798	99.084	5.63	212.50
		AN	48.8	4.1	4,354.5	0.568	2.924	3.492	19.44	

Table III-2 Statistical values of grain size measurement for as-received CuZn30 Bulged Sheets

Thickness	d_1	d_2	d_3	d_{ave} (µm)	*SD*	*V* (Coeff. of variation)
2mm	58.0	53.6	54.9	55.5	2.24	4.03
1mm	31.0	28.8	29.9	29.9	1.07	3.58
200µm	17.1	15.0	15.9	16.0	1.03	6.47

Table III-3 Statistical values of grain size measurement for annealed CuZn30 Bulged Sheets

Thickness	d_1	d_2	d_3	d_{ave} (µm)	*SD*	*V* (Coeff. of variation)
2mm	4.3	4.0	4.4	4.2	0.21	4.92
1mm	4.1	4.5	4.0	4.2	0.26	6.18
200µm	4.0	4.1	4.1	4.1	0.06	1.49

Table III-4 Symbol abbreviations

Symbol	*Description*
d	Average grain size
λ	Thickness-to-grain-size ratio
π	Deformed volume-to-grain size ratio
N_i	Number of inner grains in deformed volume
N_s	Number of surface grains in deformed volume
N_t	Number of total grains in deformed volume

APPENDIX IV: DATA FOR SPECIMEN SLIPPAGE TEST

- L_o : Initial length
- L_f : Final length
- *SD* : Standard deviation
- *V* : Coefficient of variation

	Test #1			Test #2			Test #3		
No.	L_o **(μm)**	L_f **(μm)**	**% Stretch**	L_o **(μm)**	L_f **(μm)**	**% Stretch**	L_o **(μm)**	L_f **(μm)**	**% Stretch**
1	2821.7	2823.2	0.05	3970.4	3970.4	0.00	4681.7	4681.5	0.00
2	2771.3	2816.7	1.64	2926.2	2944.1	0.61	3033.3	3023.5	-0.32
3	2467.2	2481.4	0.58	2306	2307.8	0.08	3164.5	3158.4	-0.19
4	2462.6	2489.9	1.11	3226.6	3226.6	0.00	3366.9	3338.7	-0.84
5	1168.1	1175.3	0.62	3359.4	3390	0.91	3170.6	3160.1	-0.33
6	1256.1	1245.9	-0.81	1786.4	1786.4	0.00	1553.9	1571.4	1.13
7	1526.2	1509.6	-1.09	1418.6	1422.6	0.28	1795.6	1806.3	0.60
8	1352.1	1341.3	-0.80	1104.6	1104.9	0.03	1592.1	1604.2	0.76
9	3540.9	3563.8	0.65	1126.8	1130	0.28	1602.8	1608.9	0.38
		Average	0.22		Average	0.24		Average	0.13
		SD	0.94		*SD*	0.32		*SD*	0.63
		V	4.37		*V*	1.33		*V*	4.81

Average resulting values:

Average % Stretch	**0.20**
SD	**0.06**
V	**0.30**
Range	**0.11**

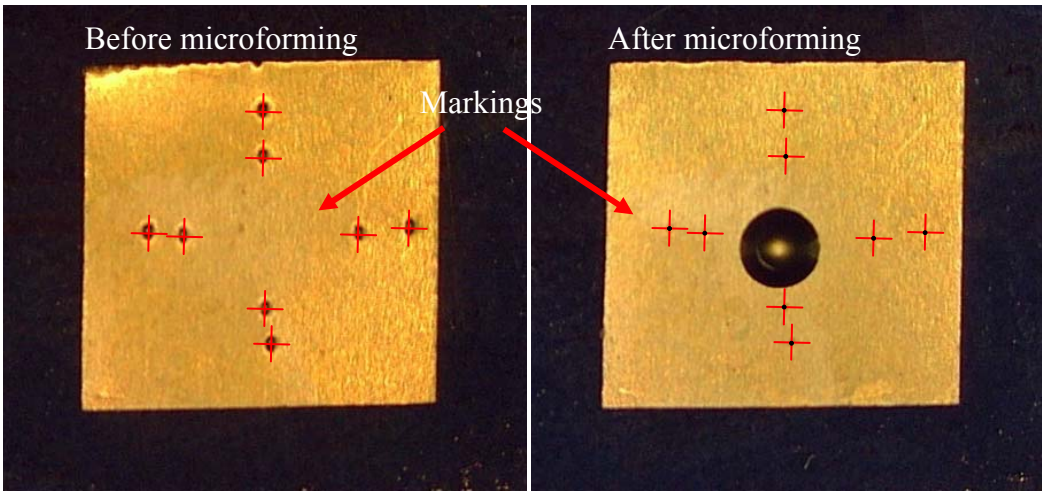

Figure IV- 1 Designated markings for measurement of stretchability before and after forming

APPENDIX V: PROCEDURE FOR MICROFORMING THIN SHEETS

1. Samples were cut into a 9x9 mm squares after air blowing it for cleaning purposes.
2. Sample was clamped between the die halves and tightening was applied by screw power.
3. The die was placed on the v-grooves of the kinematic coupling module so it would demonstrate the six point contact between the die and fixture.
4. Thin sheet surface, or zero point, was then determined by the control system and process parameters (percent force drop, speed, and depth) were entered into the controlling program before starting the test.
5. After performing the test, the die was taken out and Sample was removed from the die.

APPENDIX VI: PROCEDURE FOR ELECTROLYTIC POLISHING AND ETCHING OF *CuZn30* AND *Al1100* THIN SHEETS

Procedure for thin sheet polishing of *CuZn30* and *Al1100*:
The process was done on a LectroPol-5 electrolytic etching module provided by Struers with custom mixed electrolytes. The procedure was the following:

1. Sample was cut into a piece bigger than 1cm^2 in area and then cleaned by alcohol and air blown to dry.
2. The required electrolyte was inserted into the container slot. The mixed electrolytes were E5 for brass and A2 for aluminum.
3. The required voltage and current were set automatically from the default process menu and the pump flow was adjusted to slightly surface on the mask orifice.

4. The sample was placed on top of the provided 1cm^2 mask before setting the anode on top of the sample and then the test was started.
5. After the polishing process, the sample was dipped into water for cleaning and then air blown to dry.

Procedure for electrolytic etching of *CuZn30*:

The process was done on a LectroPol-5 electrolytic etching module provided by Struers with custom mixed electrolytes. The procedure was the following:

1. Sample was cut into a suitable size and cleaned using alcohol and then air blown for drying.
2. The required electrolyte (D2) was inserted into the container slot.
3. The required voltage and time were set manually as 2.5V and 20 seconds respectively, and the pump flow was adjusted to slightly surface on the mask orifice.
4. The sample was placed on top of the provided 1cm^2 mask before setting the anode on top of the sample and then the test was started.
6. After the etching process, the sample was dipped into water for cleaning and then air blown to dry.

Procedure for electrolytic etching of *Al1100*:

The process was done on a Bueler®'s Electromet 4 polisher consisting of an Electropolisher power supply as well as an Electropolisher cell module. The procedure was the following:

1. Sample was cut into a suitable size and cleaned using alcohol and then air blown to dry.
2. Sample was placed on top of the cell module and the pump was turned on to adjust the solution level which has to reach the bottom surface of the tested sample.
3. The test time and voltage were adjusted as 1 minute and 18V respectively with 60% pump speed
4. The pump was turned on and the test was started by pushing the start button.
5. After the mentioned duration, the etching process was conducted and the pump was turned off. The sample was then removed and washed by water then dried by using an air gun.

APPENDIX VII: STATISTICAL DATA FOR GRAIN SIZE MEASUREMENT OF *CuZn30* THIN SHEETS

Table VII-1 Grain size measurement of 25µm CuZn30

No.	Test #1			Test #2			Test #3		
	Line length (µm)	Crossed boundaries	Grain size (µm)	Line length (µm)	Crossed boundaries	Grain size (µm)	Line length (µm)	Crossed boundaries	Grain size (µm)
1	112.4	15	7.5	133.4	16	8.3	108.2	16	6.8
2	86.4	12	7.2	112.7	14	8.1	110	13	8.5
3	154.2	19	8.1	91.1	10	9.1	116.3	18	6.5
4	98.2	12	8.2	65	7	9.3	97.6	9	10.8
5	107.7	16	6.7	76.3	8	9.5	98.8	12	8.2
6	91.7	13	7.1	83.1	9	9.2	99.5	11	9.0
7	142.7	22	6.5	119.7	16	7.5	117.9	11	10.7
8	117.4	17	6.9	99.5	13	7.7	92.8	12	7.7
9	59	8	7.4	61.4	7	8.8	65	10	6.5
10	52.6	6	8.8	50.6	5	10.1	54.2	6	9.0
		Ave. Grain size	**7.4**		Ave. Grain size	**8.8**		Ave. Grain size	**8.4**

Table VII-2 Grain size measurement of 50µm CuZn30:

No.	Test #1			Test #2			Test #3		
	Line length (µm)	Crossed boundaries	Grain size (µm)	Line length (µm)	Crossed boundaries	Grain size (µm)	Line length (µm)	Crossed boundaries	Grain size (µm)
1	221.1	13	17.0	194.6	14	13.9	213.8	14	15.3
2	203.1	14	14.5	172.2	12	14.4	192.3	12	16.0
3	212.3	14	15.2	199	14	14.2	210.7	14	15.1
4	123.6	9	13.7	114.3	7	16.3	130.9	10	13.1
5	149.6	11	13.6	124.2	8	15.5	132	9	14.7
6	123.3	9	13.7	108	7	15.4	121.2	9	13.5
7	182	13	14.0	180	11	16.4	199.3	15	13.3
8	210.9	18	11.7	170.4	10	17.0	195.2	16	12.2
9	78.8	9	8.8	66.8	8	8.4	67.1	5	13.4
10	91.6	7	13.1	71.4	6	11.9	73.9	6	12.3
		Ave. Grain size	**13.5**		Ave. Grain size	**14.3**		Ave. Grain size	**13.9**

Table VII-3 Resulting grain size and statistical parameters:

Thickness	d_1	d_2	d_3	d_{ave}	*SD*	*V*
***CuZn30*-25µm**	7.4	8.8	8.4	8.2	0.72	8.79
***CuZn30*-50µm**	13.5	14.3	13.9	13.9	0.40	2.88

- d: Average grain size
- d_{ave}: Average value of three measurements
- SD : Standard deviation
- V : Coefficient of variation

APPENDIX VIII: PROCEDURE FOR THIN SHEET MARKING BY PHOTOLITHOGRAPHY TECHNIQUE

The photolithography process was conducted in a clean room with a highly sensitive environment to ensure the proper application of photoresist. The procedure was the following:

1. A specimen (substrate) was cut to the required square area to fit under the photomask.
2. Specimen was cleaned with acetone and alcohol then air-blown.
3. Specimen was heated at 110°C for about 1 minute to dry surface.
4. Specimen was placed on a CEE (Cost Effective Equipment) spin coater machine and the photoresist was applied in the form of drops on top of the specimen's surface, then it was spun at 4000rpm for 30seconds.
5. Step 4 was repeated if PR was not evenly distributed.
6. Specimen was removed and bake at 110°C for 1 minute.
7. Specimen was placed inside the vacuum chamber of a Karl Suss (MJB3) photolithography machine.
8. The photomask was placed and aligned with the thin sheet specimen.
9. Ultra violet rays were beamed at the specimen for 9 seconds through the photomask.
10. After UV exposure, specimen was backed at 110°C for 1 minute.
11. For developing of exposed photoresist, specimen was immersed in an AZ 400K commercial developer by Clariant (1:4 water) for 50 seconds to 1 minute.
12. Substrate was then dipped in water for final cleaning and air blown to dryness.

REFERENCES

1. M. Geiger, M. Kleiner, R. Eckstein, N. Tiesler and U. Engel, "Microforming", CIRP Annals - Manufacturing Technology, 2001, v 50, n 2, pp 445-462.
2. M. Heckele & W. Schomburg, "Review on micro molding of thermoplastic polymers", Journal of Micromechanics and Microengineering, (2004), v 14, pp 1-14.
3. K.F. Ehmann, D. Bourell, M. Culpepper, R.E. DeVor, T. Hodgson, T. Kurfess, M. Madou, K. Rajurkar, "An international assessment of micro-manufacturing research technology", Processing and Fabrication of Advanced Materials XIV With Frontiers in Materials Science, 2005, pp 211-224.
4. R. Williams; S. Melkote; W. Sun, Y. Huang, B. Kinsey, D. Yao, "Recent advances in micro/meso-scale manufacturing processes", Proceedings of IMECE2005, American Society of Mechanical Engineers, Manufacturing Engineering Division, MED, v 16-2, 2005, pp 863-884.
5. M. Geiger, U. Engel, F. Vollertsen, R. Kals, A. Messner, "Metal forming of microparts for electronics", Production Engineering, v 2, 1994, pp 15-18.
6. M. Geiger, A. Messner, U. Engel, R. Kals, F. Vollertsen, "Design of micro-forming processes – fundamentals, material data and friction behavior", Proceedings of the 9th International Cold Forging Congress, Solihull, England, 1995, pp 155-164.

7. M. Geiger, F. Vollertsen and R. Kals, “Fundamentals on the manufacturing of sheet metal microparts”, CIRP Annals - Manufacturing Technology, v 45, n 1, 1996, pp 277-282.
8. M. Geiger, A. Messner, U. Engel, “Production of microparts – Size effects in bulk metal forming, similarity theory”, Production Engineering, v 4, 1997, pp 55-58.
9. T. A. Kals and Ralf Eckstein, “ Miniaturization in sheet metal working”, Journal of Materials Processing Technology, v 103, n 1, 2000, pp 95-101.
10. L.V. Raulea, A.M. Goijaerts, L.E. Govaert, F.P.T. Baaijens, “Size effects in the processing of thin metal sheets”, Journal of Materials Processing Technology, v 115, 2001, pp 44-48.
11. J. Gau, C. Principe, J. Wang, “An experimental study on size effects on flow stress and formability of aluminum and brass for microforming”, Journal of Materials Processing Technology, v 184, 2007, pp 42-46.
12. U. Engel, A. Messner, N. Tiesler, “Cold forging of micro parts”, Proceedings of the 1st ESAFORM Conference on Materials Forming, Sophia Antipolis, France, 1998, pp 77-80.
13. N. Tiesler and U. Engel, ‘Microforming – effects of miniaturization, Proceedings of the Eighth International Conference on Metal Forming, 2000, pp 355-360.
14. N. Tiesler, “Microforming - Size effects in friction and their influence on extrusion processes”, Wire, v 52, n 1, February, 2002, pp 34-38.
15. N. Krishnan, J. Cao, B. Kinsey, S. Parasiz, M. Li, “ Investigation of deformation characteristics of micropins fabricated using microextrusion”, Proceedings of

IMECE2005, American Society of Mechanical Engineers, Manufacturing Engineering Division, MED, v 16-1, 2005, pp 341-348.

16. N. Krishnan, J. Cao, K. Dohda, "Microforming: Study of friction conditions and the impact of low friction/high strength die coatings on the extrusion of micropins", Proceedings of IMECE2005, American Society of Mechanical Engineers, Manufacturing Engineering Division, MED, v 16-1, 2005, pp 331-340.
17. J. Cao, N. Krishnan, Z. Wang, H. Lu, W. Liu, A. Swanson, "Microforming: Experimental investigation of the extrusion process for micropins and its numerical simulation using RKEM", Transactions of the ASME, v 126, 2004, pp 642-652.
18. F. Vollertsen, Z. Hu, H. Schulze Niehoff and C. Theiler, " State of the art in micro forming and investigations in micro deep drawing", Journal of Materials Processing Technology, v 151, n 1-3, 2004, pp 70-79.
19. F. Vollertsen, H. Schulze Niehoff and Z. Hu, "State of the art in microforming", International Journal of Machine Tool & Manufacture, v 46, 2006, pp 1172-1179.
20. J. F. Michel and PP Picart, " Size effects on the constitutive behavior for brass in sheet metal forming", Journal of Materials Processing Technology, v 141, 2003, pp 439-446.
21. H. Hoffman and S. Hong, " Tensile test of very thin sheet metal and determination of flow stress considering the scaling effect", CIRP Annals - Manufacturing Technology, v 55, n 1, 2006, pp 263-266.
22. S. Mahabunphachai and M. Koç, "Fabrication of micro-channel arrays on thin metallic sheet using internal fluid pressure: Investigations on size effects and

development of design guidelines", Journal of Power Sources, v 175, 2008, pp 363-371.

23. Y. Saotome, K. Yasuda, and H. Kaga, "Microdeep drawability of very thin sheet steels", Journal of Materials Processing Technology, v 113, n 1-3, 2001, pp 641-647.
24. Y. Saotome and T. Okamoto, "An in-situ incremental microforming system for three-dimensional shell structures of foil materials", Journal of Materials Processing Technology, v 113, n 1-3, 2001, pp 636-640.
25. H. Justinger and G. Hirt, "Analysis of size-effects in the miniaturized deep drawing process", Key Engineering Materials, v 344, Sheet Metal, 2007, pp 791-798.
26. J. Gau, C. Principe, M. Yu, " Springback behavior of brass in micro sheet forming", Journal of Material Processing Technology, v 191, 2007 , pp 7-10.
27. Y. Saotome, T. Hatori, T. Zhang, A. Inoue, "Superplastic micro/nano-formability of $La_{60}Al_{20}Ni_{10}Co_5Cu_5$ amorphous alloy in the supercooled liquid state", Materials Science and Engineering, v A304-306, 2001, pp 716-720.
28. Y. Saotome, K. Itoh, T. Zhang, A. Inoue, "Superplastic nanoforming of Pb-based amorphous alloy", Scripta Materialia, v 44, 2001, pp 1541-1545.
29. Y. Saotome and H. Iwazaki, "Superplastic extrusion of microgear shaft of 10μm in module", Microsystems Technology, v 6, 2000, pp 126-129.
30. Y. Saotome and H. Iwazaki, "Superplastic backward microextrusion of microparts for micro-electro-mechanical systems", Journal of Materials Processing Technology", v 119, 2001, pp 307-311.

31. S. Son, M. Kim, K. Park, W. Lee, “Micro forming characteristic of Al5083 superplastic alloy”, Proceedings - 9th Russian-Korean International Symposium on Science and Technology, KORUS-2005, v 1, 2005, pp 556-559.
32. M.S. Yeh, H.Y. Lin, H.T. Lin, C.B. Chang, “Superplastic micro-forming with a fine grained Zn-22Al eutectoid alloy using hot embossing technology”, Journal of Materials Processing Technology, v 180, 2006, pp 17-22.
33. T. Furushima and K. Manabe, “Experimental and numerical study on deformation behavior in dieless drawing process of superplastic microtubes”, Journal of Materials Processing Technology, v 191, 2007, pp 59-63.
34. T. Furushima and K. Manabe, “Experimental study on multi-pass dieless drawing process of superplastic Zn–22%Al alloy microtubes”, Journal of Materials Processing Technology, v 187–188, 2007, pp 236–240.
35. J. Ocaña, M. Morales, C. Molpeceres, O. García, J. Porro, J. García-Ballesteros, “Short pulse laser microforming of thin metal sheets for MEMS manufacturing”, Applied Surface Science, v 254, 2007, pp 997-1001.
36. G. Cheng, D. Pizada, Z. Ming, “Microstructure and mechanical property characterizations of metal foil after microscale laser dynamic forming”, Journal of Applied Physics, v 101, 063108, 2007, pp 1-7.
37. B. Eichenhueller, E. Egerer, U. Engel, “Microforming at elevated temperature – forming and material behavior”, International Journal of Advanced Manufacturing Technology, v 33, 2007, pp 119-124.
38. S.P. Keeler, “Determination of forming limits in automotive stamping”, Sheet Metal Industries, v 42, n 461, 1965, pp 683-691.

39. S.P. Keeler and W.A. Backofen, “Plastic instability and fracture in sheets stretched over rigid punches”, ASM Transactions, v 56, n 1, 1963, pp 25-48.
40. Z. Marciniak and K. Kuczynski, “Limit strains in the processes of stretch-forming sheet metal”, Int. J. Mech. Sci., v 9, 1967, pp 609-620.
41. Z. Marciniak, K. Kuczynski and T. Pokora, “Influence of the plastic properties of a material on the forming limits diagram for sheet metal in tension”, International Journal of Mechanical Sciences, v 14, 1973, pp 789-805.
42. K. Yamaguchi and P.B. Mellor, “Thickness and grain size dependence of limit strains in sheet metal stretching”, International Journal of Mechanical Sciences, v 18, 1975, pp 85-90.
43. R. Mahmudi, “Forming limits in biaxial stretching of aluminium sheets and foils”, Journal of Materials Processing Technology, v 37, 1993, pp 203-216.
44. M. Aghaie-Khafri and R. Mahmudi, “Optimizing homogenization parameters for better stretch formability in an Al-Mn-Mg alloy sheet”, Materials Science Engineering, v 399, 2005, pp 173-180.
45. F. Stachowicz, “Effect of grain size, thickness and prestrain on the forming limits of 63-37 brass sheets”, Metalurgija, v 3, 1998, pp 179-182.
46. Annual Book of ASTM Standards, “E112-96: Standard Test Methods for Determining Average Grain Size”, v 3.01, July, 2003, pp 256-281
47. Robert E. Reed-Hill and Reza Abbaschian, “Physical Metallurgy Principles”, Thomson-Engineering, Third edition, 1991.
48. George E. Dieter, “Mechanical Metallurgy”, McGraw Hill, Third Edition, 1986.

49. A.B. Haberfield and M.W. Boyles, Laboratory determined forming limit diagrams, Sheet Metal Industries, v 50, 1973, pp 400, 402-405, 411.

50. J.H. Schmitt and J.M. Jalinier, "Damage in sheet metal forming—II. Plastic instability", Acta Metallurgica, 1982, vol. 30, pp 1799-1809.

51. Annual Book of ASTM Standards, "Standard Test Method for Ball Punch Deformation of Metallic Sheet Material", ASTM E643-84, v 03.01, ASTM, 2000.

52. http://www.hsi-inc.com, June 5th, 2006.

53. http://www.cooperinstruments.com, June 5th, 2006.

54. http://www.copper.org, January 15th, 2005.

55. American Society for Metals, "Metals Handbook, Desk Edition", Second Edition, American Society for Metals, v 2, 1998, pp 427, 512.

56. http://www.aluminum.org, November 20th, 2007.

57. http://www.4m-net.org, June 5th, 2006.

58. P. Bley, W. Menz, W. Bacher, K. Feit, M. Harmening, H. Hein, J. Mohr, W.K. Schomburg, W. Stark, "Application of LIGA process in fabrication of three-dimensional mechanical microstructures", 4th International Symposium on MicroProcess Conference, Kanazawa, Japan, 1991, pp 384-389.

59. K. Dunke, H.D. Bauer, W. Ehrfeld, J. Hobfeld, L. Weber, G. Horcher, G. Muller, "Injection-molded fiber ribbon connectors for parallel optical links fabricated by LIGA technique", Journal of Micromechanics and Microengineering, v 8, 1995, pp 146-157.

60. Annual Book of ASTM Standards, “Standard Practice for Temper Designations for Copper and Copper Alloys—Wrought and Cast”, ASTM B 601-99a, v 02.01, ASTM, Jan 2000.
61. Annual Book of ASTM Standards, “Standard Practice for Heat Treatment of Wrought Aluminum Alloys”, ASTM B918 - 01, v 02.02, ASTM, Jan 2003.
62. A. Nadai, “Plasticity; A Mechanics of the plastic state of matter”, McGraw-Hill Book Co., New York and London, 1931.
63. A. Nadai, “Theory of flow and fracture of solids”, v 1, McGraw-Hill Book Company, New York, 1950.
64. T. Naka, F. Yoshida, M. Ohmori, “ Flow Stress and ductility of brass with various Zn-content range of strain rate”, Zairyo/Journal of the Society of Materials Science, Japan, v 44, n 500, 1995, pp 591-596.
65. M. Suery, B. Baudelet, " Flow stress and microstructure in superplastic 60/40 brass”, Journal of materials Science, v 8, 1973, pp 363-369.
66. N. Shuaib, M. Khraisheh, O. Rawashdeh, “Size effects on strain limits of thin *CuZn30* brass sheets”, Proceedings of the 2nd International Conference on Micro Manufacturing, Clemson, SC, 2007, pp 140-144.
67. http://www2.dupont.com, June 10th, 2008.
68. http://www.teflon.com, June 10th, 2008.
69. R. Pearce, “A users’ guide to forming limit diagrams”, Sheet Metal Industries, December, 1971, pp 943-949.
70. S.S. Hecker, “Cup test for assessing stretchability”, Metals Engineering Quarterly, v 14, n 4, Nov, 1974, pp 30-36.

71. S.S. Hecker, “Simple technique for determining forming limit curves”, Sheet Metal Industries, November, 1975, pp 671-676.

72. A.K. Gosh and S. S. Hecker, “Failure in thin sheets stretched over rigid punches”, Metallurgical Transactions A, v 6A, 1975, pp 1065-1074.

73. J. Cao, N. Krishnan, L.F. Mori, and H. Espinosa, “ Experimental investigation of the size effects observed in the extrusion of micropins”, Proceedings of the 1st International Conference on Micro Manufacturing, Urbana-Champaign, IL, 2006, pp 126-131.

74. N. Krishnan, J. Cao and K.F. Ehmann, “Microforming: Study of grain size and friction effects in the extrusion of micropins”, Proceedings of the 4th International Workshop on Microfactory IV, Shanghai, China, October, 2004.

75. T. Sobis, U. Engel, M. Geiger, “A theoretical study of wear simulation in metal forming processes”, Journal of Material Processing Technology, n 34, 1992, pp 233-240.

76. International Standard ISO 12004, “Metallic materials, guidelines for the determination of forming-limits diagrams”, International Organization for Standardization, 1997 ISO 12004:1997(E)

77. http://www.gom.com/EN/measuring.systems/aramis/system/system.html

78. U. Engel, “Tribology in microforming”, Wear, v 260, n 3, 2006, pp 265-273.

79. R. Eckstein, M. Geiger, U. Engel, “ Specific characterization of micro sheet metal working”, Proceedings of SheMet, September 1999, pp 529-536.

80. D.V. Wilson, A.R. Mirshams, W.T. Roberts, “An experimental study of the effect of sheet thickness and grain size on limit-strains in biaxial stretching”, International Journal of mechanical Sciences, v 25, n 12, 1983, pp 859-870.
81. G. Sachs and K. Van Horn, “Practical Metallurgy”, American Society for Metals, 1951.
82. M. Gad-el-Hak, “The MEMS Handbook”, CRC Press, 2002.
83. C. Wang and K. Zhang, “Superplastic microforming of Zn-Al22 alloy ribs”, Journal of Materials Science & Technology, v 20, n 2, 2004, pp 236-238.
84. J.P. Wulfsberg, S.E. Hilpert, A. Ostendorf, K. Samm, “Fundamentals of laser-assisted microforming”, Proceedings of the 1st Colloquium of DFG Priority Program Process Scaling, Bremen, October, 2003, pp 1-8.
85. J.P. Wulfsberg and M. Terzi, “ Investigation of laser heating in microforming applying sapphire tools”, CIRP Annals-Manufacturing Technology, v 56, n 1, 2007, pp 321-326.
86. G. Kim, J. Ni, R. Mayor, H. Kim, “An experimental investigation on semi-solid forming of micro/meso-scale features”, Transactions of the ASME, v 129, April, 2007, pp 246-251.
87. W.J. Kim, S.J. Yoo, H.K. Kim, “Superplastic microforming of Mg-9Al-1Zn alloy with ultrafine-grained microstructure”, Scripta Materialia, v 59, 2008, pp 599-602.
88. M. Suery and B. Baudelet, “Flow stress ad microstructure in superplastic 60/40 brass”, Journal of Materials Science, v 8, 1973, pp 363-369.

89. J. Pilling and N. Ridley, “Superplasticity in crystalline solids”, The Institute of Metals, 1989.

90. K. Manabe and O. Shimomura, “ Effect of temperature and drawing speed on warm deep drawing characteristics of AZ31 magnesium alloy sheet”, Journal of Japan Institute of Light Metals, v 56, n 10, 2006, pp 521-526.

91. W.W. Wood, “Combined effects of high velocity and temperature on sheet metal formability”, Proceedings of the International Production Engineering Research Conference, 1963, pp 311-319.

92. K. Brun and R. Kurz, “Measurement uncertainties encountered during gas turbine driven compressor field testing”, Transactions of the ASME, v 123, January, 2001, pp 62-69.

93. R.B. Abernethy, R.P. Benedict, R.B. Dowdell, “ASME measurement uncertainty”, Journal of Fluids Engineering, Transactions of the ASME, v 107, n 2, 1983, pp 161-164.

94. R.B. Abernethy and R.P. Benedict, “Measurement uncertainty: A standard methodology”, Instrumentation in the Aerospace Industry, v 30, 1984, pp 411-420.

95. R.P. Benedict, “How to handle errors in measurement”, Instrumentation in the Aerospace Industry, v 30, 1984, pp 411-420.

96. Nasr A. Shuaib and Marwan K. Khraisheh, “Method and Apparatus for Characterizing Microscale Formability of Thin Sheet Materials”, U.S. Patent 12/177,968 filed June 2008. (Patent pending)

VITA

Nasr AbdelRahman Shuaib

Date and Place of Birth

- June 6th, 1978 / Madison, WI

Education

- Bachelor's degree in Mechanical Engineering, University Khartoum, Khartoum, Sudan, 2002.

Experience

- Teaching Assistant (August 2007- May 2008) (Mechanical Engineering Department -University of Kentucky, Lexington, Kentucky, USA)
- Research Assistant (August 2004- December 2008) (Mechanical Engineering Department -University of Kentucky, Lexington, Kentucky, USA)
- Best™ Dairy Products Co., Khartoum, Sudan (January-June 2004)
- International Center for Quality, Khartoum, Sudan (January-December 2003)

Awards & Honors

- Recipient of the GAANN Fellowship for assistance in areas of national need by the Department of Education (January 2005- July 2007)
- Member of the Delta Epsilon Iota Academic Honor Society (January 2008 – Present)

Technical Publications and Conference Papers

- N. A. Shuaib, M. K. Khraisheh, O. A. Rawashdeh, "Size effects on strain limits of thin *CuZn30* brass sheets", Proceedings of the 2nd International Conference on Micro Manufacturing, Clemson, SC, 2007, pp 140-144.
- F.K. Abu-Farha, N.A. Shuaib, M.K. Khraisheh, K.J. Weinmann, "Limiting Strains of Sheet Metals Obtained by Pneumatic Stretching at Elevated Temperatures", Annals of the CIRP, 2008, In Press.

Unique Contributions

- Nasr A. Shuaib and Marwan K. Khraisheh, "Method and Apparatus for Characterizing Microscale Formability of Thin Sheet Materials", U.S. Patent 12/177,968, filed June 2007.